

LATTICE SIMULATIONS OF THE SU(2)-MULTI-HIGGS PHASE TRANSITION

A Thesis Submitted to the
College of Graduate Studies and Research
in Partial Fulfillment of the Requirements
for the degree of Master of Science
in the Department of Physics and Engineering Physics
University of Saskatchewan
Saskatoon

By
Mark B. Wurtz

©Mark B. Wurtz, March 2009. All rights reserved.

PERMISSION TO USE

In presenting this thesis in partial fulfilment of the requirements for a Postgraduate degree from the University of Saskatchewan, I agree that the Libraries of this University may make it freely available for inspection. I further agree that permission for copying of this thesis in any manner, in whole or in part, for scholarly purposes may be granted by the professor or professors who supervised my thesis work or, in their absence, by the Head of the Department or the Dean of the College in which my thesis work was done. It is understood that any copying or publication or use of this thesis or parts thereof for financial gain shall not be allowed without my written permission. It is also understood that due recognition shall be given to me and to the University of Saskatchewan in any scholarly use which may be made of any material in my thesis.

Requests for permission to copy or to make other use of material in this thesis in whole or part should be addressed to:

Head of the Department of Physics and Engineering Physics
162 Physics Building
116 Science Place
University of Saskatchewan
Saskatoon, Saskatchewan
Canada
S7N 5E2

ABSTRACT

The Higgs boson has an important role in the theoretical formulation of the standard model of fundamental interactions. Symmetry breaking of the vacuum via the Higgs field allows the gauge bosons of the weak interaction and all fermions to acquire mass in a way that preserves gauge-invariance, and thus renormalizability. The Standard Model can accommodate an arbitrary number of Higgs fields with appropriate charge assignments. To explore the effects of multiple Higgs particles, the $SU(2)$ -multi-Higgs model is studied using lattice simulations, a non-perturbative technique in which the fields are placed on a discrete space-time lattice. The formalism and methods of lattice field theory are discussed in detail. Standard results for the $SU(2)$ -Higgs model are reproduced via Monte Carlo simulations, in particular the single-Higgs phase structure, which has a region of analytic connection between the symmetric and Higgs phases. The phase structure of the $SU(2)$ -multi-Higgs model is explored for the case of $N_H \geq 2$ identical Higgs fields. There is no remaining region of analytic connection between the phases, at least when interactions between different Higgs flavours are omitted. An explanation of this result in terms of enhancement from overlapping phase transitions is explored for $N_H = 2$ by introducing an asymmetry in the hopping parameters of the Higgs fields.

ACKNOWLEDGEMENTS

Thank you to my supervisor Tom Steele, who helped me through the good times and the tough times. Thank you to our colleague Randy Lewis, who helped us make our way through the lattice of confusion.

For Mom, Dad, and Ward. Thank you for raising me, guiding me, and being there to look up to.

CONTENTS

Permission to Use	i
Abstract	ii
Acknowledgements	iii
Contents	v
List of Figures	vii
1 Quantum Field Theory	1
1.1 Introduction	1
1.2 Lagrangian Field Theory	2
1.3 Gauge Theories	4
1.3.1 Group Generators	5
1.3.2 Local Symmetry Transformations	7
1.3.3 Phases Along Paths	8
1.4 The Path Integral	9
1.4.1 Introduction to the Path Integral	9
1.4.2 Field Theory Path Integral	10
1.4.3 The Euclideanized Path Integral	13
2 Lattice Gauge Theory	15
2.1 Lattice Gauge Theory	15
2.2 Monte Carlo Simulation	17
2.2.1 Heatbath Algorithm for SU(2)-Gauge Theory	19
2.2.2 Simulation Results and Benchmarks for SU(2)-Gauge Theory	23
3 Higgs Model on the Lattice	27
3.1 SU(2)-Higgs Model	27
3.1.1 The Higgs and Symmetry Breaking	27
3.1.2 Higgs Lattice Action	32
3.2 Monte Carlo Simulation	34
3.2.1 Heatbath Algorithm for SU(2)-Higgs	35
3.2.2 Overrelaxation Algorithm for SU(2)-Higgs	37
3.2.3 Special Cases	38
3.2.4 Benchmark Simulation Results for the SU(2)-Higgs Model	39
3.2.5 Mapping the Higgs Phase Transition	44
4 Multi-Higgs Phase Transition	51
4.1 SU(2)-Multi-Higgs model	51

4.2	Simulation Results	53
4.2.1	Phase Transition for Symmetric Multiple Higgs Fields	56
4.2.2	Phase Transition for the Asymmetric Two-Higgs Model	66
5	Conclusion	74
	References	75
A	Conventions	80

LIST OF FIGURES

2.1	The Monte Carlo evolution of the average plaquette at $\beta=2.3$ for hot and cold starts on different size lattices.	25
2.2	β dependence of the average plaquette from Monte Carlo simulation (data points) and analytic predictions (denoted by solid lines) on a 16^4 size lattice	26
3.1	The Higgs potential for $\mu_0^2 > 0$ (above) and $\mu_0^2 < 0$ (below). The x and y axes represent the real and imaginary components of the complex field Φ , respectively.	28
3.2	Hot and cold starts of P , ρ^2 , L_ϕ and L_α using the $SU(2)$ -Higgs heatbath update for $\kappa = 0.27$, $\beta = 2.25$ and $\lambda = 0.5$ on a 16^4 lattice.	41
3.3	Hot and cold starts of P , ρ^2 , L_ϕ and L_α using the combined $SU(2)$ -Higgs heatbath-overrelaxation update for $\kappa = 0.27$, $\beta = 2.25$ and $\lambda = 0.5$ on a 16^4 lattice.	41
3.4	κ dependence of $\langle \rho^2 \rangle$ and $\langle L_\phi \rangle$ from Monte Carlo simulations (data points) and analytic predictions (solid lines) for $\beta = \lambda = 0$ on a 16^4 lattice.	42
3.5	κ dependence of $\langle P \rangle$, $\langle \rho^2 \rangle$, $\langle L_\phi \rangle$, and $\langle L_\alpha \rangle$ from a Monte Carlo thermal cycle for $\beta = 2.25$ and $\lambda = 0.5$ on a 16^4 lattice.	42
3.6	observables associated with two metastable states resulting from hot and cold starts for $\kappa = 0.212$, $\beta = 2.0$ and $\lambda = 0.1$ on a 16^4 lattice.	43
3.7	The hysteresis gap $\Delta L_\alpha(\kappa)$ resulting from fast and slow hysteresis cycles at $\beta = 2.2$, $\lambda = 1$ on a 16^4 lattice. Note that 3δ clearly overestimates the statistical fluctuations.	48
3.8	Fast hysteresis runs on a 16^4 lattice.	48
3.9	Slow hysteresis runs on a 16^4 lattice.	49
3.10	The phase diagram for $SU(2)$ -Higgs, resulting from hysteresis runs on a 16^4 lattice. The error bars indicate the uncertainty in the location of the phase transition due to the width of the hysteresis curve.	49
3.11	The maximum of the hysteresis gap from fast and slow hysteresis runs on a 16^4 lattice.	50
4.1	Dependence of $\langle \rho_n \rangle$ and $\langle L_{\phi,n} \rangle$ on κ for each Higgs field at $\beta = 2.25$, $\lambda = 0.5$ for $N_H = 2, 3$ Higgs fields on a 16^4 lattice.	54
4.2	Dependence of $\langle P \rangle$, $\langle \rho_n \rangle$, $\langle L_{\phi,n} \rangle$ and $\langle L_{\alpha,n} \rangle$ on the number of Higgs N_H for $\kappa = 0.2, 0.27$, $\beta = 2.25$, $\lambda = 0.5$ on a 16^4 lattice.	55
4.3	Dependence of $\langle P \rangle$, $\langle \rho_n \rangle$, $\langle L_{\phi,n} \rangle$ and $\langle L_{\alpha,n} \rangle$ on the number of Higgs N_H for $\beta = 1, 2.25, 8, \infty$, $\kappa = 0.4$, $\lambda = 0.5$ on a 16^4 lattice.	55
4.4	Fast hysteresis runs for 2 Higgs fields on a 16^4 lattice.	58
4.5	Slow hysteresis runs across for 2 Higgs fields on a 16^4 lattice.	58

4.6	The phase diagram for $SU(2)$ -Higgs, resulting from hysteresis runs for 2 Higgs fields on a 16^4 lattice.	59
4.7	The maximum of the hysteresis gap from fast and slow hysteresis runs for 2 Higgs fields on a 16^4 lattice.	59
4.8	Fast hysteresis runs for 3 Higgs fields on a 16^4 lattice.	60
4.9	Slow hysteresis runs across for 3 Higgs fields on a 16^4 lattice.	60
4.10	The phase diagram for $SU(2)$ -Higgs, resulting from hysteresis runs for 3 Higgs fields on a 16^4 lattice.	61
4.11	The maximum of the hysteresis gap from fast and slow hysteresis runs for 3 Higgs fields on a 16^4 lattice.	61
4.12	The phase diagram for $SU(2)$ -Higgs, resulting from hysteresis runs for 5 Higgs fields on a 12^4 lattice.	62
4.13	The maximum of the hysteresis gap from fast and slow hysteresis runs for 5 Higgs fields on a 12^4 lattice.	62
4.14	The phase diagram for $SU(2)$ -Higgs, resulting from hysteresis runs for 10 Higgs fields on a 12^4 lattice.	63
4.15	The maximum of the hysteresis gap from fast and slow hysteresis runs for 10 Higgs fields on a 12^4 lattice.	63
4.16	Fast hysteresis cycles of the gauge-invariant link for $N_H = 1, 2, 3, 10$ Higgs fields on a 16^4 lattice.	64
4.17	Metastability of the gauge-invariant link at selected transition points for $\lambda = \infty$ on a 16^4 lattice.	64
4.18	Qualitative sketch of the $SU(2)$ -Higgs phase structure in (β, λ, κ) parameter space for $N_H = 1, 2, 3$. The shaded area represents regions of strong first-order phase transition. The unshaded area represents regions which may be either a weak first-order or second-order phase transition. Note that the hole in the phase diagram for $N_H = 1$ is not present for $N_H \geq 2$ and thus the Higgs and symmetric phases are completely separated.	65
4.19	Fast hysteresis runs of Higgs 1 for 2 Higgs fields with asymmetric hopping parameters $\kappa_2 = 2\kappa_1$ on a 12^4 lattice.	68
4.20	Slow hysteresis runs of Higgs 1 for 2 Higgs fields with asymmetric hopping parameters $\kappa_2 = 2\kappa_1$ on a 12^4 lattice.	68
4.21	Phase diagram of Higgs 1 for 2 Higgs fields with asymmetric hopping parameters $\kappa_2 = 2\kappa_1$ on a 12^4 lattice.	69
4.22	Maximum hysteresis gap of Higgs 1 for 2 Higgs fields with asymmetric hopping parameters $\kappa_2 = 2\kappa_1$ on a 12^4 lattice.	69
4.23	Fast hysteresis runs of Higgs 2 for 2 Higgs fields with asymmetric hopping parameters $\kappa_2 = 2\kappa_1$ on a 12^4 lattice.	70
4.24	Slow hysteresis runs of Higgs 2 for 2 Higgs fields with asymmetric hopping parameters $\kappa_2 = 2\kappa_1$ on a 12^4 lattice.	70
4.25	Phase diagram of Higgs 2 for 2 Higgs fields with asymmetric hopping parameters $\kappa_2 = 2\kappa_1$ on a 12^4 lattice.	71
4.26	Maximum hysteresis gap of Higgs 2 for 2 Higgs fields with asymmetric hopping parameters $\kappa_2 = 2\kappa_1$ on a 12^4 lattice.	71

4.27	Overlapping of phase diagrams for 2 Higgs fields with asymmetric hopping parameters $\kappa_2 = 2\kappa_1$ on a 12^4 lattice. The upper phase line corresponds to Higgs 1 and the lower phase line corresponds to Higgs 2.	72
4.28	Overlapping of phase diagrams for 2 Higgs fields with asymmetric hopping parameters $\kappa_2 = 1.1\kappa_1$ on a 12^4 lattice. The upper phase line corresponds to Higgs 1 and the lower phase line corresponds to Higgs 2.	72
4.29	Phase diagram of Higgs 1 for 2 Higgs fields with asymmetric hopping parameters $\kappa_2 = 10\kappa_1$ on a 12^4 lattice.	73
4.30	Phase diagram of Higgs 2 for 2 Higgs fields with asymmetric hopping parameters $\kappa_2 = 10\kappa_1$ on a 12^4 lattice.	73

CHAPTER 1

QUANTUM FIELD THEORY

1.1 Introduction

The Higgs boson is a hypothetical spin-0 particle, introduced as a way of explaining the origin of mass for all other particles in the standard model of fundamental interactions. The motivation for the Higgs particle is to give particles mass in a way that allows for a renormalizable electroweak theory [1]. This is done through the Higgs mechanism [2], where symmetry-breaking occurs via a non-zero vacuum expectation value (vev) for the Higgs, and the vev effectively gives mass to the other particles. On a discretized space-time lattice, the spontaneous symmetry breaking of the Higgs vacuum manifests itself as a phase transition between the symmetry restoring and symmetry breaking (Higgs mechanism) phases. Currently, the Large Hadron Collider in Cern Switzerland is working towards experiments to test for the existence of the Higgs particle. It is difficult to place experimental constraints on the number of Higgs particles in the Standard Model. For example, an arbitrary number of Higgs fields with conventional quantum numbers (isospin $I = \frac{1}{2}$, hypercharge $Y = \pm 1$) is consistent with experimental observations. The inclusion of multiple Higgs within the Standard Model is the simplest extension of the minimal Higgs sector, in particular the minimal supersymmetric Standard Model [3]. The focus of my thesis research is to study the Higgs phase transition in the $SU(2)$ -Higgs model with multiple Higgs particles using lattice simulation techniques.

In this paper, the foundations of lattice field theory are discussed starting from the perspective of classical Lagrangian field theory and non-Abelian gauge theories, and are developed in a way that is relevant to the lattice. Lattice simulations are

based on the path integral formalism and so the path integral approach to quantization in quantum field theory is discussed in detail. Lattice field theory is a non-perturbative approximation scheme in which space-time is discretized. Quantities in the form of a path integral can then be calculated numerically, using statistical methods, *i.e.* Monte Carlo simulations. The form of the path integral, when transformed to Euclidean space-time, allows for the use of statistical mechanics methods. The derivation of the lattice Lagrangian for non-Abelian gauge theories and the combined gauge-Higgs theory are given. The Monte Carlo methods for the pure $SU(2)$ -gauge theory and the $SU(2)$ -Higgs model are discussed in detail. Simulation results and benchmarks for $SU(2)$ -gauge theory and the $SU(2)$ -Higgs model are presented, which demonstrate that the computer simulations have produced correct results. The $SU(2)$ -Higgs phase structure is mapped using hysteresis curves and a region is found where the phase transition terminates, which is consistent with previous simulation results [4] and the theoretical prediction of an analytic connection between the symmetric and Higgs phases for a single Higgs field in the fundamental representation [5]. When multiple Higgs particles are included, the region of analytic connection disappears and the symmetric and Higgs phases become completely separated by a phase transition. This phenomenon is hypothesized to originate from an enhancement from overlapping phase transitions, as reported for the multi-Higgs three-dimensional $U(1)$ theory [6]. In particular, supporting evidence for this hypothesis is found in the exploration of an asymmetric two-Higgs model as it approaches the symmetric limit of identical quadratic terms (hopping parameters in the discretized theory).

1.2 Lagrangian Field Theory

In non-relativistic quantum mechanics, particles are described by scalar fields that provide a probabilistic description about the behaviour of the particles. Space and momentum are the dynamical variables of the theory, and time describes the evolution of a system. However, this approach lacks the ability to predict the processes of

particle annihilation and creation, which occur for relativistic particles through the exchange/equivalence of energy and mass. A relativistic quantum theory should be based on the interactions of particles with other particles, and thus the interaction of their fields should be built into the theory. For a relativistic quantum theory, the fields become the dynamical variables, which leads to a natural formulation of particle interactions. The approach to develop quantum field theory in this paper is to start from a classical Lagrangian and move into the path integral formulation.

A first step in developing a theory of fields is to derive the dynamical equations of motion and conservation laws in terms of the fields. The principle of least-action is retained as a fundamental concept, which is used to derive the Euler-Lagrange equations for fields, and also Noether's theorem (For standard discussions see [7, 8]). The Lagrangian is generalized to the Lagrangian density so that it can be written as a function of the fields ϕ and their 4-derivatives, where the fields themselves depend on space-time. The action S can now be written as the integration of the Lagrangian density \mathcal{L} over space-time,

$$S = \int d^4x \mathcal{L}(\phi, \partial_\mu \phi, x^\mu). \quad (1.1)$$

The Euler-Lagrange equation follows from taking the extremum of the action with respect to first order variations in the fields $\phi(x) \rightarrow \phi'(x) = \phi(x) + \delta\phi(x)$, the derivatives of the fields, and the space-time coordinates $x^\mu \rightarrow x'^\mu = x^\mu + \delta x^\mu$,

$$\delta S = \int_R d^4x \left\{ \left[\frac{\delta \mathcal{L}}{\delta \phi} - \partial_\mu \left(\frac{\delta \mathcal{L}}{\delta(\partial_\mu \phi)} \right) \right] \delta\phi + \partial_\mu \left(\frac{\delta \mathcal{L}}{\delta(\partial_\mu \phi)} \delta\phi + \mathcal{L} \delta x^\mu \right) \right\} = 0. \quad (1.2)$$

The integration of the 4-divergence can be rewritten as the integration over the surface of the integration region. By setting the variations in the fields and the coordinates to zero on the boundary of the region of integration, *i.e.* the fields have fixed boundary conditions, the surface term will equal zero,

$$\int_R d^4x \partial_\mu \left(\frac{\partial \mathcal{L}}{\partial(\partial_\mu \phi)} \delta\phi + \mathcal{L} \delta x^\mu \right) = \oint_{\partial R} d^3\sigma_\mu \left(\frac{\partial \mathcal{L}}{\partial(\partial_\mu \phi)} \delta\phi + \mathcal{L} \delta x^\mu \right) = 0. \quad (1.3)$$

Because the variations of the field inside R are arbitrary, the integrand of the remaining part of Eq. (1.2) must equal zero. This gives the Euler-Lagrange equations,

$$\frac{\partial \mathcal{L}}{\partial \phi} - \partial_\mu \left(\frac{\partial \mathcal{L}}{\partial(\partial_\mu \phi)} \right) = 0. \quad (1.4)$$

The fixed surface variations leave the Lagrangian invariant up to a 4-divergence. To derive Noether's theorem, variations are used that are arbitrary on the boundary but that leave the Lagrangian invariant $\mathcal{L} \rightarrow \mathcal{L}$, which implies that the action is also invariant $\delta S = 0$. Such a transformation is also called a symmetry. Since the Lagrangian is invariant, the Euler-Lagrange equations still hold for these different boundary conditions. The result is Eq. (1.3) but for arbitrary symmetry transformations. Because the region R is now arbitrary with respect to the variations the integrand of Eq. (1.3) is zero, which gives Noether's theorem,

$$\partial_\mu \left(\frac{\partial \mathcal{L}}{\partial (\partial_\mu \phi)} \delta \phi + \mathcal{L} \delta x^\mu \right) = \partial_\mu J^\mu = 0. \quad (1.5)$$

The 4-divergence of J^μ is zero, and it is therefore a conserved current. A conserved physical quantity can be calculated for any infinitesimal transformation of the fields or coordinates that preserves the Lagrangian.

The next step is to obtain the Lagrangian for a spinless relativistic field. The dynamical equation of motion can be motivated using¹ $p^2 = E^2 - \vec{p}^2 = m^2$, and the methods of first quantization, $\vec{p} \rightarrow -i\vec{\nabla}$, $E \rightarrow i\frac{\partial}{\partial t}$. This gives the Klein-Gordon equation,

$$(\partial^2 + m^2) \phi = 0. \quad (1.6)$$

A Lagrangian for the real Klein-Gordon field that reproduces this equation of motion is

$$\mathcal{L} = \frac{1}{2} (\partial_\mu \phi)^2 - \frac{1}{2} m^2 \phi^2. \quad (1.7)$$

1.3 Gauge Theories

One of the simplest gauge theories is electromagnetism. The Lagrangian for the electromagnetic fields in a vacuum is

$$\mathcal{L} = -\frac{1}{4} F_{\mu\nu} F^{\mu\nu}, \quad (1.8)$$

¹For a list of conventions used see appendix A.

where $F_{\mu\nu}$ is the field strength tensor represented by the four-dimensional curl of the gauge fields A_μ ,

$$F_{\mu\nu} = \partial_\mu A_\nu - \partial_\nu A_\mu. \quad (1.9)$$

Using the Euler-Lagrange equations with A_μ as the dynamical variable we get the equation

$$\partial_\mu F^{\mu\nu} = 0, \quad (1.10)$$

and from the definition of $F_{\mu\nu}$ we obtain the geometric constraint

$$\partial_\lambda F_{\mu\nu} + \partial_\mu F_{\nu\lambda} + \partial_\nu F_{\lambda\mu} = 0. \quad (1.11)$$

Eqs. (1.10) and (1.11) are just the source-free Maxwell equations in a manifestly covariant form.

Quantum Electrodynamics (QED) is the quantum field theory for the electromagnetic force. Particle interactions are manifested through an exchange of photon particles represented by the field A_μ . One of the most important properties of QED is invariance of the Lagrangian under local gauge transformations involving A_μ and the matter fields (*e.g.* electron/positron). QED is classified as an Abelian gauge theory because the gauge transformations are commuting. The weak and strong forces are non-Abelian gauge theories, and contain non-commuting gauge symmetries. Additional vector fields, which describe the force carrying particles of the weak and strong forces, are introduced in a way that preserves and generalizes local gauge invariance.

Three different perspectives for gauge theories will be briefly discussed: group generators, local symmetry transformations, and phases along paths.² The last definition will be used later on in the development of lattice gauge theory.

1.3.1 Group Generators

For non-Abelian gauge theories, the essential form of the Lagrangian remains the same as in Eq. (1.8). However, additional field components are added with the

²The discussion on gauge theories is adapted from Refs. [7, 8, 9].

introduction of a group index (*i.e.* $A_\mu \rightarrow A_\mu^\alpha$, $F_{\mu\nu} \rightarrow F_{\mu\nu}^\alpha$). The different group components of A_μ^α become coupled to one another by adding an additional antisymmetric term to $F_{\mu\nu}^\alpha$

$$F_{\mu\nu}^\alpha = \partial_\mu A_\nu^\alpha - \partial_\nu A_\mu^\alpha + g_0 f^{\alpha\beta\gamma} A_\mu^\beta A_\nu^\gamma, \quad (1.12)$$

where g_0 is the bare coupling constant and $f^{\alpha\beta\gamma}$ are the completely antisymmetric structure constants of the group. The structure constants are related to commutators of the group generators λ^α ,

$$[\lambda^\alpha, \lambda^\beta] = i f^{\alpha\beta\gamma} \lambda^\gamma, \quad (1.13)$$

where λ^α are Hermitian matrices corresponding to a representation of the generators for a unitary group (*e.g.* $SU(N)$). A matrix representation of the vector potential is defined by

$$A_\mu = A_\mu^\alpha \lambda^\alpha. \quad (1.14)$$

Similarly $F_{\mu\nu} = F_{\mu\nu}^\alpha \lambda^\alpha$, the expression for $F_{\mu\nu}$ becomes

$$F_{\mu\nu} = \partial_\mu A_\nu - \partial_\nu A_\mu - i g_0 [A_\mu, A_\nu]. \quad (1.15)$$

The group generators are orthonormalized in the fundamental representation such that

$$\text{Tr} (\lambda^\alpha \lambda^\beta) = \frac{1}{2} \delta^{\alpha\beta}. \quad (1.16)$$

The Lagrangian for non-Abelian gauge theory can now be written as

$$\mathcal{L} = -\frac{1}{4} F_{\mu\nu}^\alpha F_{\alpha}^{\mu\nu} = -\frac{1}{2} \text{Tr} (F_{\mu\nu} F^{\mu\nu}). \quad (1.17)$$

For $SU(2)$, the simplest non-Abelian gauge theory and the one considered in this paper, the group generators in the fundamental representation are the Pauli matrices,

$$\lambda^\alpha = \frac{1}{2} \sigma^\alpha, \quad (1.18)$$

$$\sigma^1 = \begin{pmatrix} 0 & 1 \\ 1 & 0 \end{pmatrix} \quad \sigma^2 = \begin{pmatrix} 0 & -i \\ i & 0 \end{pmatrix} \quad \sigma^3 = \begin{pmatrix} 1 & 0 \\ 0 & -1 \end{pmatrix}, \quad (1.19)$$

$$f^{\alpha\beta\gamma} = \epsilon^{\alpha\beta\gamma}. \quad (1.20)$$

1.3.2 Local Symmetry Transformations

A local symmetry occurs when a modification of the fields in a local region of space-time leaves the action unchanged. Electromagnetism is an Abelian gauge theory, and its Lagrangian is symmetric under the local gauge transformations

$$\phi \rightarrow e^{ig_0\Lambda(x)}\phi, \quad (1.21)$$

$$A_\mu \rightarrow A_\mu - \partial_\mu\Lambda(x), \quad (1.22)$$

where the gauge function $\Lambda(x)$ is an arbitrary function of space-time, and ϕ represents the matter fields interacting with A_μ . A gauge-invariant Lagrangian can be obtained by replacing derivatives of the matter fields ϕ by covariant derivatives of the form

$$D_\mu = \partial_\mu + ig_0A_\mu. \quad (1.23)$$

For non-Abelian gauge theories, generalized gauge transformations are defined for the matter fields and the covariant derivative such that $D_\mu\phi$ transforms in the same way as ϕ ,

$$\phi \rightarrow g\phi, \quad (1.24)$$

$$D_\mu\phi \rightarrow gD_\mu\phi, \quad (1.25)$$

$$D_\mu \rightarrow gD_\mu g^{-1}, \quad (1.26)$$

where $g(x)$ is a mapping of space-time into the gauge group,

$$g(x) = \exp(ig_0\Lambda^\alpha(x)\lambda^\alpha). \quad (1.27)$$

The anti-symmetric field strength tensor $F_{\mu\nu}$ is defined as the commutator of covariant derivative operators, and has a simple transformation,

$$F_{\mu\nu} = -\frac{i}{g_0}[D_\mu, D_\nu], \quad (1.28)$$

$$F_{\mu\nu} \rightarrow gF_{\mu\nu}g^{-1}. \quad (1.29)$$

The Lagrangian in Eq. (1.17) is therefore left gauge invariant. For covariant derivatives of the form $D_\mu = \partial_\mu + ig_0A_\mu$, $F_{\mu\nu}$ is the same as in Eq. (1.15). The corresponding

transformation for the gauge field A_μ can be derived to be

$$A_\mu \rightarrow g A_\mu g^{-1} - \frac{i}{g_0} g \partial_\mu g^{-1}. \quad (1.30)$$

For the gauge group $U(1)$ (*i.e.* an Abelian group) $g(x) = e^{i g_0 \Lambda(x)}$ and we can obtain the transformations for electromagnetism in Eqs. (1.21) and (1.22).

1.3.3 Phases Along Paths

When a particle tranverses a space-time path P , its field acquires an additional phase factor due its interaction with an externally imposed gauge field A_μ ,

$$\phi \rightarrow \exp \left(i g_0 \int_P A_\mu dx^\mu \right) \phi = U(P) \phi. \quad (1.31)$$

For electromagnetic interactions, $U(P)$ is a complex phase rotation. In the Abelian case it is easy to show that for a path P starting at point x and ending at point y , the field $\phi(x)$ has the same gauge transformation as $U(x \rightarrow y)\phi(y)$. This leaves the quantity $\phi^\dagger(x)U(x \rightarrow y)\phi(y)$ gauge invariant. The path-dependent phase factor connects particles at different space-time points in a gauge invariant way. In the more general sense, $U(P)$ can be thought of as a parallel transporter in the gauge group geometry.

For the non-Abelian case we use the analogy with parallel transportation to define the more general phase factor,

$$\frac{dx^\mu}{ds} D_\mu U^\dagger(s) = 0, \quad (1.32)$$

$$U(0) = 1. \quad (1.33)$$

The path is parametrized by $x^\mu(s)$, $s \in [0, 1]$. From Eqs. (1.32) and (1.33) the gauge transformation for $U(s)$ depends only on the end points of the path,

$$U(s) \rightarrow g(0) U(s) g^{-1}(s), \quad (1.34)$$

which leaves $\phi^\dagger(0)U(s)\phi(s)$ gauge invariant. Eq. (1.32) can be written as the differential equation,

$$\frac{dU^\dagger(s)}{ds} + i g_0 \frac{dx^\mu}{ds} A_\mu(s) U^\dagger(s) = 0, \quad (1.35)$$

whose solution with initial condition (1.33) is a path-ordered exponential,

$$U(s) = P \exp \left(ig_0 \int_0^s ds \frac{dx^\mu}{ds} A_\mu \right). \quad (1.36)$$

The path-ordering operation P puts $A(s)$ on the left and $A(0)$ on the right. From Eq. (1.34) it follows that for a closed path C the trace of $U(C)$ is gauge invariant,

$$W(C) = \text{Tr}(U(C)) \rightarrow W(C). \quad (1.37)$$

The quantity $W(C)$ is called a Wilson loop, and its expectation value depends only on the shape of the closed path C .

1.4 The Path Integral

1.4.1 Introduction to the Path Integral

The path integral approach³ to quantum mechanics is an alternative to the canonical formulation (*e.g.* Schrodinger wave equation), and is the basis for calculations in lattice gauge theory. The path integral is a weighted sum over all possible paths of a particle. To construct the path integral in non-relativistic quantum mechanics, consider the expansion of a propagator using complete sets of position basis states at different times $\vec{x}(t_j) = \vec{x}_j$,

$$\begin{aligned} \langle \vec{x}_f, t_f | \vec{x}_0, t_0 \rangle &= \int d^3 \vec{x}_1 \langle \vec{x}_f, t_f | \vec{x}_1, t_1 \rangle \langle \vec{x}_1, t_1 | \vec{x}_0, t_0 \rangle \\ &= \int d^3 \vec{x}_n \cdots d^3 \vec{x}_1 \langle \vec{x}_f, t_f | \vec{x}_n, t_n \rangle \cdots \langle \vec{x}_2, t_2 | \vec{x}_1, t_1 \rangle \langle \vec{x}_1, t_1 | \vec{x}_0, t_0 \rangle, \end{aligned} \quad (1.38)$$

$$t_0 < t_1 < \cdots < t_n < t_f.$$

As the time interval $\delta t = t_{j+1} - t_j$ is made infinitesimal and the number of integrations n goes to infinity, Eq. (1.38) becomes an integration over all possible configurations of some weight factor given by the propagators. For a Hamiltonian of the form

³The following development on the path integral is adapted from Refs. [7, 8].

$H = \frac{\vec{p}^2}{2m} + V(\vec{x})$, which is approximately constant in the infinitesimal interval $t_{j+1} - t_j$, the propagator becomes

$$\begin{aligned}
\langle \vec{x}_{j+1}, t_{j+1} | \vec{x}_j, t_j \rangle &= \langle \vec{x}_{j+1} | e^{-i\hat{H}(t_{j+1}-t_j)} | \vec{x}_j \rangle \\
&= \int \frac{d^3 \vec{p}_j}{(2\pi)^3} \exp \left[i(t_{j+1} - t_j) \left(\vec{p}_j \cdot \frac{\vec{x}_{j+1} - \vec{x}_j}{t_{j+1} - t_j} - H_j \right) \right] \\
&= \left(\frac{m}{2\pi i(t_{j+1} - t_j)} \right)^{\frac{3}{2}} \exp \left[i(t_{j+1} - t_j) \left(\frac{m}{2} \left(\frac{\vec{x}_{j+1} - \vec{x}_j}{t_{j+1} - t_j} \right)^2 - V(\vec{x}_j) \right) \right].
\end{aligned} \tag{1.39}$$

Taking $n \rightarrow \infty$ and $t_{j+1} - t_j \rightarrow 0$ the propagator in Eq. (1.38) becomes

$$\langle \vec{x}_f, t_f | \vec{x}_0, t_0 \rangle = N \int D\vec{x}(t) e^{iS} \equiv Z[\vec{x}(t)], \tag{1.40}$$

where $S = \int_{t_0}^{t_f} dt L(\vec{x}(t))$ is the action, and N is a normalization factor. The integration measure $D\vec{x}(t)$ represents an integration over all possible paths $\vec{x}(t)$ (moving forward in time), for continuous time. In other words, the path integral is an infinite number of time-sliced ordinary integrations over \vec{x} . The integration measure is expressed as

$$D\vec{x}(t) = \lim_{n \rightarrow \infty} \prod_{j=0}^n d\vec{x}(t_j). \tag{1.41}$$

The expectation values of operators can be expressed as path integrals by using the same techniques as before. From Eq. (1.38) the path integral is time ordered. In order to insert operators into the expansion, the product of the operators must also be time ordered,

$$\langle \vec{x}_f, t_f | T \left\{ \hat{Q}(t_m) \cdots \hat{Q}(t_1) \right\} | \vec{x}_0, t_0 \rangle = N \int D\vec{x}(t) Q(t_m) \cdots Q(t_1) e^{iS}. \tag{1.42}$$

1.4.2 Field Theory Path Integral

To establish an analogous path integral for quantum field theory, we will modify Eq. (1.40) by replacing the coordinates with field variables, $\vec{x}(t) \rightarrow \phi(x)$,

$$Z[\phi] = \int D\phi e^{iS} \quad , \quad S = \int d^4x \mathcal{L}(\phi, \partial_\mu \phi). \tag{1.43}$$

As in the canonical approach to relativistic quantum mechanics, the fields become the dynamical variables and the Lagrangian is retained as a fundamental quantity. The integration measure $D\phi$ is defined as

$$D\phi = \prod_x d\phi(x), \quad (1.44)$$

where x spans all of space-time. The sum over all possible trajectories has been replaced by a sum over all field configurations. That is, the path integral is an integration over all values of the fields for an infinite number of space-time slices.

Correlation functions of time ordered field operators are written in the same way as in Eq. (1.42). The correlation function is normalized by dividing by Z , which removes vacuum bubble contributions,

$$\langle 0|T\{\phi(x_m)\cdots\phi(x_1)\}|0\rangle = \frac{\int D\phi \phi(x_m)\cdots\phi(x_1)e^{iS}}{\int D\phi e^{iS}}. \quad (1.45)$$

Adding a source term $J(x)\phi(x)$ to the Lagrangian turns the path integral into a more general quantity called the generating functional,

$$Z[J] = \int D\phi e^{iS(J)}, \quad S(J) = \int d^4x \mathcal{L} + J(x)\phi(x). \quad (1.46)$$

By taking functional derivatives of the generating functional with respect to the source, and then setting the source to zero, $Z[J]$ can generate correlation functions,

$$\langle 0|T\{\phi(x_m)\cdots\phi(x_1)\}|0\rangle = \frac{1}{Z} \frac{1}{i} \frac{\delta}{\delta J(x_m)} \cdots \frac{1}{i} \frac{\delta}{\delta J(x_1)} Z[J] \Big|_{J=0}. \quad (1.47)$$

Correlation functions give the propagation amplitude for m particle scattering processes.

For the free Klein-Gordon Lagrangian $\mathcal{L}_0 = \frac{1}{2}\partial_\mu\phi\partial^\mu\phi - \frac{1}{2}m^2\phi^2 + \frac{1}{2}i\epsilon\phi^2$, the generating functional can be rewritten so that it can be used for finding explicit expressions for the correlation functions,

$$Z_0[J] = \int D\phi \exp \left[i \int d^4x \mathcal{L}_0 + J(x)\phi(x) \right]. \quad (1.48)$$

The $i\epsilon\phi^2$ term is introduced to make the path integral converge, and it also naturally leads to the Feynman propagator. The integral inside the exponential in Eq. (1.48)

can be rewritten using integration by parts and then a change in the field variables,

$$\phi(x) \rightarrow \phi(x) - \int d^4y D_F(x-y)J(y). \quad (1.49)$$

The quantity $D_F(x-y)$ is a Green's function of the Klein-Gordon equation,

$$(\partial^2 + m^2 - i\epsilon)D_F(x-y) = -i\delta(x-y), \quad (1.50)$$

$$D_F(x-y) = \int \frac{d^4p}{(2\pi)^4} \frac{i}{p^2 - m^2 + i\epsilon} e^{-ip \cdot (x-y)}, \quad (1.51)$$

which is also known as the Feynman propagator. Performing the change of variables the generating functional becomes,

$$\begin{aligned} & \int d^4x \frac{1}{2} (\partial_\mu \phi \partial^\mu \phi + m^2 \phi^2 - i\epsilon \phi^2) + J(x)\phi(x) \\ &= \int d^4x -\frac{1}{2} \phi (\partial^2 + m^2 + i\epsilon) \phi + J(x)\phi(x) \\ &\rightarrow \int d^4x -\frac{1}{2} \phi (\partial^2 + m^2 - i\epsilon) \phi + \frac{1}{2} \int d^4x d^4y J(x)D_F(x-y)J(y), \end{aligned} \quad (1.52)$$

$$Z_0[J] = Z_0[0] \exp \left[-\frac{i}{2} \int d^4x d^4y J(x)D_F(x-y)J(y) \right]. \quad (1.53)$$

The generating functional $Z_0[J]$ is now explicitly written in terms of Green's functions. The term that contains the Green's function and the source terms can be separated from the path integral because it is independent of the fields.

A simple example of the usefulness of the generating functional is the two-point function for the free Klein-Gordon field,

$$\langle 0 | T \{ \phi(x_1)\phi(x_2) \} | 0 \rangle = \frac{1}{i} \frac{\delta}{\delta J(x_1)} \frac{1}{i} \frac{\delta}{\delta J(x_2)} \frac{Z_0[J]}{Z_0[0]} \Big|_{J=0} = D_F(x_1 - x_2). \quad (1.54)$$

Eq. (1.54) states that the time-ordered propagation of a particle from point x_1 to point x_2 is given by the Feynman propagator. It gets more interesting if we look at the four-point correlation function,

$$\begin{aligned} \langle 0 | T \{ \phi(x_1)\phi(x_2)\phi(x_3)\phi(x_4) \} | 0 \rangle &= D_F(x_1 - x_2)D_F(x_3 - x_4) \\ &+ D_F(x_1 - x_3)D_F(x_2 - x_4) \\ &+ D_F(x_1 - x_4)D_F(x_2 - x_3). \end{aligned} \quad (1.55)$$

The higher-order correlation functions become the sum of all permutations of the Feynman propagators. This is identical to the result that follows from Wick's theorem, which states that the time ordered product of fields is the sum of all possible contractions (*i.e.* Feynman propagators) of the fields, where a contraction is simply defined as a Feynman propagator. Partial contractions produce vacuum bubbles, which are divided out by the $Z_0[0]$ factor. What we are left with in Eq. (1.55) is a sum of three Feynman diagrams, in which there are no interactions among the particles.

Particle interactions can be introduced by adding an interaction term to the Lagrangian, $\mathcal{L} = \mathcal{L}_0 + \mathcal{L}_{int}$,

$$Z[J] = \int D\phi \exp \left[i \int d^4x \mathcal{L}_0(\phi) + \mathcal{L}_{int}(\phi) + J(x)\phi(x) \right]. \quad (1.56)$$

The interaction term can be separated from the path integral by changing its argument to an operator that is independent of ϕ , $\mathcal{L}_{int}(\phi) \rightarrow \mathcal{L}_{int}(\frac{1}{i} \frac{\delta}{\delta J})$,

$$Z[J] = \exp \left[i \int d^4x \mathcal{L}_{int} \left(\frac{1}{i} \frac{\delta}{\delta J(x)} \right) \right] Z_0[J]. \quad (1.57)$$

This replacement can be performed because ϕ is an eigenvalue of the operator $\frac{1}{i} \frac{\delta}{\delta J}$, when it operates on $e^{iS[J]}$.

By expanding the exponential of the interaction term, and using the form of $Z_0[J]$ in Eq. (1.53), $Z[J]$ becomes a perturbation series. The contributions from the interaction can be formulated to arbitrarily high order by taking functional derivatives of $Z_0[J]$. What we are left with is sum of propagators, which we integrate over, times $Z_0[J]$.

1.4.3 The Euclideanized Path Integral

The path integral formalism bears resemblance to statistical mechanics in which Z is a sum over all configurations of an exponential weight, which is like a partition function, and correlation functions are expressed as derivatives of $Z[J]$ with respect to an external source J . By Wick-rotating the time coordinate, $x^0 = -ix_E^0$, the

integrand of Z becomes identical in form to a Boltzmann weight factor,

$$Z = \int D\phi e^{-S_E} \quad , \quad S_E = \int d^4x_E \frac{1}{2} (\partial_{E\mu}\phi)^2 + \frac{1}{2}m^2\phi^2, \quad (1.58)$$

where S_E is the Euclideanized real Klein-Gordon action. The Euclideanized space-time alters the covariant derivative and so the gauge fields must be Wick rotated in such a way that the gauge theory is preserved [10],

$$A_0 = iA_{E0}, \quad (1.59)$$

$$D_0 = iD_{E0}, \quad (1.60)$$

$$\mathcal{L}_E = \frac{1}{2} \text{Tr} (F_{E\mu\nu}F_E^{\mu\nu}) = -\mathcal{L}, \quad (1.61)$$

$$U(P) = \exp \left(ig_0 \int_P A_{E\mu} dx_E^\mu \right). \quad (1.62)$$

The subscript $_E$ will be dropped from here on.

The path integral may now be re-interpreted as a classical statistical system in which field configurations that minimize the Euclideanized action, *i.e.* the classical field solutions, contribute a large amount to expectation values, while configurations away from the minimal action constitute quantum corrections. Quantization is implemented via the path integral by allowing classical fields to explore all configurations. The dynamics of the field theory are enforced by the weighting of the exponentiated action. This is different from the canonical formulation that treats the fields as operators that satisfy the Euler-Lagrange equation.

CHAPTER 2

LATTICE GAUGE THEORY

2.1 Lattice Gauge Theory

Lattice field theory is an approximation scheme in which space-time is discretized, and the quantum fields become discrete elements on the space-time lattice. The lattice is usually regular with equal lattice spacing a . The lattice approximation allows us to perform numerical path integral calculations, as the partition function becomes a finite number of ordinary integrations. It also provides a regularization scheme that parameterizes ultra-violet divergences, as there are no wavelengths less than two times the lattice spacing in the momentum space formulation.

The gauge fields in lattice theory¹ are represented by elemental links $U_{x\mu}$ of the path dependent phase factor from Eq. (1.36),

$$U_{x\mu} = e^{ig_0 A_\mu(x)a} . \tag{2.1}$$

The link can be represented geometrically by a vector starting at point x and pointing in the μ -direction, and $U_{x\mu}^\dagger$ is a link pointing towards x in the negative $\hat{\mu}$ -direction.

$$U_{x\mu} = x \bullet \xrightarrow{\hat{\mu}} \bullet x + \hat{\mu} \qquad U_{x\mu}^\dagger = x \bullet \xleftarrow{\hat{\mu}} \bullet x + \hat{\mu}$$

The gauge link variable can be used to construct $U(P)$ for any type of path on the lattice.

The next step is to construct a gauge-invariant Lagrangian on the lattice that is equivalent to Eq. (1.17) in the limit $a \rightarrow 0$ [11]. We may gain some intuition by noting that the field strength tensor is a generalized curl of the vector potential, and

¹For standard discussions on lattice gauge theories see Refs. [9, 10]

also that $F_{\mu\nu}$ in Eq. (1.28) is a curvature tensor in the gauge group geometry. This leads us to a guess that the Lagrangian may be formulated as elementary squares constructed from the gauge links,

$$U_{\square} \equiv U_{\mu\nu}(x) \equiv U_{x\mu} U_{x+\hat{\mu}\nu} U_{x+\hat{\nu}\mu}^{\dagger} U_{x\nu}^{\dagger} = \begin{array}{ccc} & \xleftarrow{U_{x+\hat{\nu}\mu}^{\dagger}} & \\ \downarrow U_{x\nu}^{\dagger} & & \uparrow U_{x+\hat{\mu}\nu} \\ & \xrightarrow{U_{x\mu}} & \end{array} \quad (2.2)$$

$$\mathcal{L}_{\square} \equiv \mathcal{L}_{\mu\nu}(x) \equiv \beta \left[1 - \frac{1}{n} \text{Re} \text{Tr} U_{\mu\nu}(x) \right]. \quad (2.3)$$

The dimension of the group matrices is given by n (*e.g.* for $SU(n)$, $\text{Tr}(1) = n$) and β is a normalization constant. The elementary squares, which are commonly called plaquettes, are the smallest possible Wilson loops and are therefore gauge invariant objects on the lattice. To prove that the plaquette variables give us the correct Lagrangian, we must do a little algebra,

$$\begin{aligned} U_{\square} &= e^{ig_0 A_{\mu}(x)a} e^{ig_0 A_{\nu}(x+a\hat{\mu})a} e^{-ig_0 A_{\mu}(x+a\hat{\nu})a} e^{-ig_0 A_{\nu}(x)a} \\ &\approx e^{ig_0 a^2 (\partial_{\mu} A_{\nu} - \partial_{\nu} A_{\mu} + ig_0 [A_{\mu}, A_{\nu}]) + O(a^3)}, \end{aligned} \quad (2.4)$$

$$\begin{aligned} \mathcal{L}_{\square} &\approx \beta \left[1 - \frac{1}{n} \text{Tr} \left(1 - \frac{1}{2} g_0^2 F_{\mu\nu}^2 a^4 + O(a^5) \right) \right] \\ &= \beta \frac{g_0^2}{2n} \text{Tr} (F_{\mu\nu}^2) a^4 + O(a^5). \end{aligned} \quad (2.5)$$

The constant β is now defined to be $\beta = \frac{2n}{g_0^2}$. The term $F_{\mu\nu}^2$ is not an implied sum, *i.e.* $F_{\mu\nu}^2 = F_{\square}^2$ has directional information. To get the correct form for the Lagrangian, the lattice action is defined as the sum over all plaquettes,

$$S \equiv \sum_{\square} \mathcal{L}_{\square} = \sum_x \sum_{\mu > \nu} \mathcal{L}_{\mu\nu}(x), \quad (2.6)$$

$$\mathcal{L}(x) = \sum_{\mu > \nu} \mathcal{L}_{\mu\nu}(x) = \text{Tr} \left(\sum_{\mu > \nu} F_{\mu\nu}^2 \right) a^4 + O(a^5) = \frac{1}{2} \text{Tr} (F_{\mu\nu} F^{\mu\nu}) a^4 + O(a^5). \quad (2.7)$$

As the continuum limit is approached the lattice action becomes identical to the continuum (Euclideanized) action,

$$S_{a \rightarrow 0} = \int d^4x \frac{1}{2} \text{Tr} (F_{\mu\nu} F^{\mu\nu}) + O(a). \quad (2.8)$$

2.2 Monte Carlo Simulation

The lattice formulation makes it possible to compute the path integral numerically. However, because of the very large number of integration variables, it becomes practically impossible to calculate the integrals using a nested summation. The very large number of degrees of freedom suggests that we use statistical methods instead (see [9, 10, 12] for standard discussions). As noted earlier, the Euclideanized form of the path integral is completely analogous to the partition function for a thermodynamic system, and so all of the numerical methods of statistical mechanics can be used to study quantum field theory.

The partition function is a weighted sum over all possible field configurations, and a large portion of the configurations are suppressed by the Boltzmann factor, so only a relatively small number of “important” configurations are needed to approximate the path integral. Monte Carlo simulations randomly generate the most statistically significant field configurations according to the Boltzmann factor. The expectation value of an observable Q can be approximated by the average of a relatively small number of configurations N ,

$$\langle Q \rangle = \frac{\int D\phi Q e^{-S}}{\int D\phi e^{-S}} \approx \frac{1}{N} \sum_{n=1}^N Q_n, \quad (2.9)$$

where Q_n is an observable for the n^{th} -configuration. The factor e^{-S} is taken into account by the probability in which the configurations are generated. Expectation values of any gauge invariant quantity can then be calculated with a statistical error that falls off like $\frac{1}{\sqrt{N}}$.

Monte Carlo algorithms generate a Markov chain of field configurations, that is, the probability for generating each configuration depends on the previous one. The probability to randomly generate a new configuration ϕ_{new} from an old configuration ϕ is given by $P(\phi \rightarrow \phi_{\text{new}})$. The evolution of the Markov chain of configurations behaves like a thermodynamic system, in which equilibrium is established at the desired probability distribution. The equilibrium distribution is given by

$$p_{\text{eq}}(\phi) = \frac{e^{-S(\phi)}}{Z}, \quad (2.10)$$

which means the configurations for calculating expectation values in Eq. (2.9) must be from the equilibrium ensemble. A natural condition for equilibrium is that the configurations stay in equilibrium,

$$p_{\text{eq}}(\phi_{\text{new}}) = \int D\phi P(\phi \rightarrow \phi_{\text{new}})p_{\text{eq}}(\phi). \quad (2.11)$$

This says that the equilibrium distribution is an eigenvector of the updating process. While any initial field configuration can be chosen, the system will eventually reach an equilibrium distribution if the updating algorithm satisfies Eq. (2.11) and ergodicity $P(\phi \rightarrow \phi_{\text{new}}) > 0$. Ergodicity ensures that any new configuration can be obtained from any old one, which can be achieved in one update, several sequential updates, and also by updating parts of the lattice individually. A sufficient (though not necessary) condition that ensures the equilibrium distribution is an eigenvalue of the updating algorithm is that the algorithm satisfies detailed balance

$$e^{-S(\phi)}P(\phi \rightarrow \phi_{\text{new}}) = e^{-S(\phi_{\text{new}})}P(\phi_{\text{new}} \rightarrow \phi). \quad (2.12)$$

Integrating over ϕ and using $\int D\phi P(\phi_{\text{new}} \rightarrow \phi) = 1$ (assuming that a new configuration will always be accepted), Eq. (2.11) is recovered from the detailed balance condition.

The local Metropolis algorithm [13] implements detailed balance by generating a random field variable ϕ_x^{new} and accepting it if the action is lowered [$S(\phi_x^{\text{new}}) \leq S(\phi_x)$] and accepting it with a conditional probability $\exp[S(\phi_x) - S(\phi_x^{\text{new}})]$ if the action is raised [$S(\phi_x^{\text{new}}) > S(\phi_x)$]. The new configuration is generated with a probability distribution $P_G(\phi \rightarrow \phi_{\text{new}})$, which depends on how the generator is implemented, and accepted with probability

$$P_A(\phi \rightarrow \phi_{\text{new}}) = \begin{cases} 1 & \text{if } S(\phi_x^{\text{new}}) \leq S(\phi_x) \\ \exp[S(\phi_x) - S(\phi_x^{\text{new}})] & \text{if } S(\phi_x^{\text{new}}) > S(\phi_x) \end{cases}. \quad (2.13)$$

The total probability of generating ϕ_{new} from ϕ is given by the production $P(\phi \rightarrow \phi_{\text{new}}) = P_G(\phi \rightarrow \phi_{\text{new}})P_A(\phi \rightarrow \phi_{\text{new}})$. If the probability distribution for the generator is reversible, *i.e.* $P_G(\phi \rightarrow \phi_{\text{new}}) = P_G(\phi_{\text{new}} \rightarrow \phi)$, then the detailed balance condition is satisfied. The field variables are updated one at a time because the acceptance

probability would be far too small for practical purposes if the lattice was updated all at once. The update satisfies the local detailed balance condition and local ergodicity. Performing the local update on every field variable on the lattice satisfies detailed balance and ergodicity for the whole system.

The Metropolis method demonstrates how configurations that minimize the action are favoured, and quantum contributions are implemented with an acceptance probability for random changes that increase the action. Also, if the random changes were all accepted, the system would maximize its entropy and the dynamics of the action would not be introduced. The acceptance probability for random changes provides a balance between the high density of states [favours large $S(\phi)$] and the exponential suppression of the Boltzmann factor [favours small $S(\phi)$]. The actual expectation value for S should lay somewhere in the middle ground.

The local heatbath algorithm (see, *e.g.* [9, 14]) generates a field variable ϕ_x^{new} directly with probability

$$P(\phi_x \rightarrow \phi_x^{\text{new}}) = \frac{e^{-S(\phi_x^{\text{new}})}}{Z}, \quad (2.14)$$

which satisfies local detailed balance condition and local ergodicity. It is also easy to see that the local version of the equilibrium condition, Eq. (2.11), is automatically satisfied. The heatbath method generates a field variable that is in equilibrium with its neighbours, whereas the Metropolis method requires a large number of updates or ‘hits’ on a single field variable before it reaches equilibrium. That is, as the number of Metropolis hits approaches infinity, it becomes equivalent to one heatbath update. The heatbath method has the advantage that is more efficient, while the Metropolis method is much easier to implement. For $SU(2)$ -gauge theory the heatbath algorithm is simple enough to implement for practical applications.

2.2.1 Heatbath Algorithm for $SU(2)$ -Gauge Theory

For the $SU(2)$ -gauge heatbath [9, 14], a new link element $U_{x\mu}$ is generated according to the probability distribution

$$dp(U_{x\mu}) \sim e^{-S(U_{x\mu})} dU_{x\mu}, \quad (2.15)$$

where the pure-gauge lattice action is given by the sum of all plaquettes,

$$S = \sum_x \sum_{\mu > \nu} \beta \left[1 - \frac{1}{2} \text{Tr} \left(U_{x\mu} U_{x+\hat{\mu}\nu} U_{x+\hat{\nu}\mu}^\dagger U_{x\nu}^\dagger \right) \right], \quad (2.16)$$

and where the links are $SU(2)$ matrices that can be represented by four real numbers on a 4-dimensional unit sphere,

$$U = a_0 I + i\vec{a} \cdot \vec{\sigma} = \begin{pmatrix} a_0 + ia_3 & a_2 + ia_1 \\ -a_2 + ia_1 & a_0 - ia_3 \end{pmatrix}, \quad (2.17)$$

$$a^2 = a_0^2 + a_1^2 + a_2^2 + a_3^2 = 1. \quad (2.18)$$

It follows that the trace of an $SU(2)$ matrix is automatically real. The Haar measure $dU_{x\mu}$ is invariant under $SU(2)$ transformations and is given by

$$dU = \pi^{-2} d^4 a \delta(a^2 - 1). \quad (2.19)$$

Each link belongs to only 6 plaquettes, so we can ignore the parts of the action that do not contain $U_{x\mu}$. The probability distribution for the new link $U_{x\mu}$ becomes

$$dp(U_{x\mu}) \sim \exp\left(\frac{1}{2}\beta \text{Tr}(U_{x\mu} V_{x\mu})\right) dU_{x\mu}, \quad (2.20)$$

where $V_{x\mu}$ is the sum of the link variables that form a plaquette with $U_{x\mu}$, which are also called staples because they look like incomplete plaquettes (\square),

$$V_{x\mu} = \sum_{\nu \neq \mu} \left(U_{x+\hat{\mu}\nu} U_{x+\hat{\nu}\mu}^\dagger U_{x\nu}^\dagger + U_{x+\hat{\mu}-\hat{\nu}\nu}^\dagger U_{x-\hat{\nu}\mu}^\dagger U_{x-\hat{\nu}\nu} \right) = \sum_{\square=1}^6 U_{\square}. \quad (2.21)$$

Using the property that a sum of $SU(2)$ matrices is proportional to an $SU(2)$ matrix, the sum of staples may be written as,

$$V = \sqrt{\det V} V_0, \quad V_0 \in SU(2). \quad (2.22)$$

The invariant group measure allows us to simplify $dp(U)$ by performing the change of variables

$$U = V_0^\dagger u. \quad (2.23)$$

The group measure remains unchanged [$d(V_0^\dagger u) = du$] and the probability distribution becomes

$$\begin{aligned}
dp(U) &\sim \exp\left(\frac{1}{2}\beta\sqrt{\det V} \operatorname{Tr}(u)\right) du \\
&\sim \exp\left(\beta\sqrt{\det V}a_0\right) \delta(a_0^2 + \vec{a}^2 - 1) da_0 d^3\vec{a} \\
&\sim \exp(\alpha a_0) (1 - a_0^2)^{\frac{1}{2}} da_0 d^2\Omega,
\end{aligned} \tag{2.24}$$

where $\alpha = \beta\sqrt{\det V}$, and $d^2\Omega$ is the solid angle of the vector \vec{a} , which has a length of $\sqrt{1 - a_0^2}$.

The new link U may now be generated as follows: randomly generate a number $a_0 \in [-1, 1]$ with a probability distribution

$$dp(a_0) \sim (1 - a_0^2)^{\frac{1}{2}} \exp(\alpha a_0) da_0, \tag{2.25}$$

and then generate a 3-vector \vec{a} with a totally random direction and length $\sqrt{1 - a_0^2}$. These four random numbers form the random $SU(2)$ matrix

$$u = \begin{pmatrix} a_0 + ia_3 & a_2 + ia_1 \\ -a_2 + ia_1 & a_0 - ia_3 \end{pmatrix}. \tag{2.26}$$

The new link is finally given by the matrix multiplication $U = V_0^\dagger u$.

The real trick is how to generate the random numbers a_0 and \vec{a} according to the probability distribution $dp(U)$. Assuming we have a pseudo-random number generator, we can obtain numbers in any interval with a uniform distribution. To obtain a random number x with a distribution $f(x)$, where $f(x) \geq 0$, an accept/reject procedure can be used. Use the random-number generator to create a trial x ($x_{\min} \leq x \leq x_{\max}$), calculate $f(x)$ and then create a second random number y ($0 \leq y \leq f_{\max}$). If $y < f(x)$ then accept the trial x . Reject the trial x if $y > f(x)$ and repeat the procedure until a number is accepted. The probability of accepting x is proportional to $f(x)$, so the accepted x 's will have the correct statistical weighting. The number a_0 may be created in this way, according to the probability function in Eq. (2.25). The vector \vec{a} can be thought of as a totally random point on a sphere of radius $\sqrt{1 - a_0^2}$, which can easily be created by generating three random numbers, $-1 \leq a_1, a_2, a_3 \leq 1$, and scaling them so that $|\vec{a}| = \sqrt{1 - a_0^2}$.

While using Eq. (2.25) directly in an accept/reject procedure will generate the correct distribution, the function is very strongly peaked because of the exponential, and the acceptance rate will be very low, especially for large α . Since Monte Carlo simulations can be very time consuming, we want to be as efficient as possible. Therefore, an algorithm with a high acceptance rate is desirable, as to minimize the number of computer calculations. The Creutz method [9, 14] is to perform a change of variables which takes the exponential term into account separate from the accept/reject step,

$$z = \exp(\alpha a_0) \tag{2.27}$$

$$dp(z) \sim \left[1 - \left(\frac{\log z}{\alpha} \right)^2 \right]^{\frac{1}{2}} dz. \tag{2.28}$$

A trial z is created in the interval $e^{-\alpha} \leq z \leq e^{\alpha}$, accepted with probability (2.28), and then a logarithm is taken to recover a_0 ,

$$a_0 = \frac{\log z}{\alpha}. \tag{2.29}$$

The probability function in Eq. (2.28) is much more flat and thus offers a better acceptance rate.

The Creutz method offers a huge improvement in the acceptance rate. However, as $\alpha \rightarrow \infty$ the acceptance rate goes to zero by $\sqrt{\frac{\pi}{2\alpha}}$. To overcome this, Kennedy and Pendleton [15] devised an algorithm that has an acceptance rate that goes to one as $\alpha \rightarrow \infty$. However, as $\alpha \rightarrow 0$ the acceptance rate of the Kennedy-Pendleton method goes to zero by $\sqrt{\frac{\pi\alpha^3}{2}}$. The new method is very efficient for large α where Creutz's technique slows down, but it also has a very low acceptance rate for small α where the Creutz method works well. The relative acceptance rates of the two algorithms is given by

$$\frac{R_{KP}}{R_C} = \sqrt{\frac{2\alpha}{\pi}} [1 - \exp(-2\alpha)], \tag{2.30}$$

and is equal to one when $\alpha \approx 1.6849$. However, due to the greater computational complexity of the Kennedy-Pendleton method, the two algorithms have the same

computation time at about $\alpha \approx 8$, as tested on the Fortran 90 compiler. Therefore, to optimize the efficiency of the updater, the Creutz method is used for $\alpha < 8$ and the Kennedy-Pendleton method is used for $\alpha > 8$.

The Kennedy-Pendleton method is significantly more complicated, so only a recipe will be given [15]: generate four random numbers, $x_1, x_2, x_3, y \in [0, 1]$, calculate

$$\delta = -\frac{1}{\alpha} (\log x_1 + \cos^2(2\pi x_2) \log x_3) , \quad (2.31)$$

and accept δ if

$$y^2 \leq 1 - \frac{1}{2}\delta . \quad (2.32)$$

If δ is accepted, then

$$a_0 = 1 - \delta . \quad (2.33)$$

2.2.2 Simulation Results and Benchmarks for SU(2)-Gauge Theory

To simulate on the lattice, an ensemble of field configurations must be generated using the Monte Carlo updater. Each configuration is generated by updating the previous configuration one element at a time, until the entire lattice has been updated. As each field element is updated, the random changes propagate through the lattice, and the system moves towards equilibrium. However, each configuration is related to the previous one, and so several lattice updates may be required before the configurations become statistically uncorrelated. Near a phase transition, a very large number of updates may be required for the system to reach equilibrium. In particular for a first-order phase transition, where there may be metastable equilibria, it will take many updates to move from one phase to the other.

The simplest observable to measure for a pure gauge theory is the average plaquette,

$$P = \frac{1}{6V} \sum_{\square} (1 - \frac{1}{2} \text{Tr} U_{\square}) . \quad (2.34)$$

where V is the lattice volume (*i.e.* the total number of lattice sites). The average plaquette versus the number of Monte Carlo iterations for $SU(2)$ -gauge theory is shown in Fig. 2.1. Two different initial configurations are used: the ordered (cold) start in which all the links are set to unity ($P = 0$), and the random (hot) start in which the links are totally random ($P \approx 1$). After a sufficient number of updates, the different initial configurations reach the same equilibrium value. These results agree with those given by Creutz [9, 14].

The gauge coupling β is analogous to an inverse temperature from the partition function

$$Z = \int DU e^{-6V\beta P}. \quad (2.35)$$

It follows that the expectation value of the average plaquette can be interpreted as the internal energy density of the thermodynamic system,

$$\langle P \rangle = \frac{1}{6V} \frac{\partial}{\partial \beta} \log Z. \quad (2.36)$$

The expectation value of the average plaquette can be calculated as a function of β (recalling that β is a free parameter in the action). For the strong coupling (small β) and weak coupling (large β) regimes the approximate behaviour of the average plaquette with respect to β is known analytically and is given by

$$\text{strong coupling: } \langle P \rangle = 1 - \frac{\beta}{4} \quad (2.37)$$

$$\text{weak coupling: } \langle P \rangle = \frac{3}{4\beta} \quad (2.38)$$

In Fig. 2.2 is a graph of the average plaquette versus β . The β dependence of the average plaquette from Monte Carlo simulations agrees with the strong and weak coupling predictions [9, 14]. For each value of β , 10 updates are performed to thermalize the lattice and then 20 configurations are generated to calculate the expectation value of P (*i.e.* $\langle P \rangle$). The simulation begins with a hot start at $\beta = 0$, and a “cooling run” is performed in which β is iteratively increased. The last configuration from the previous β is used as the initial configuration for the next value of β . The process is then reversed and a “heating run” is done in which β

is iteratively decreased. For pure $SU(2)$ -gauge theory the heating and cooling runs agree. This agreement suggests that no phase transition is present. The separation of the strong and weak coupling regions is characterized by a rapid crossover in the average plaquette [9, 14]. A rapid crossover (also called a smooth or analytic crossover) separates two qualitatively different regions in which there is no phase transition. Some signs of a phase transition are metastable states, a hysteresis curve resulting from heating cycles, and very slow convergence at the transition point.

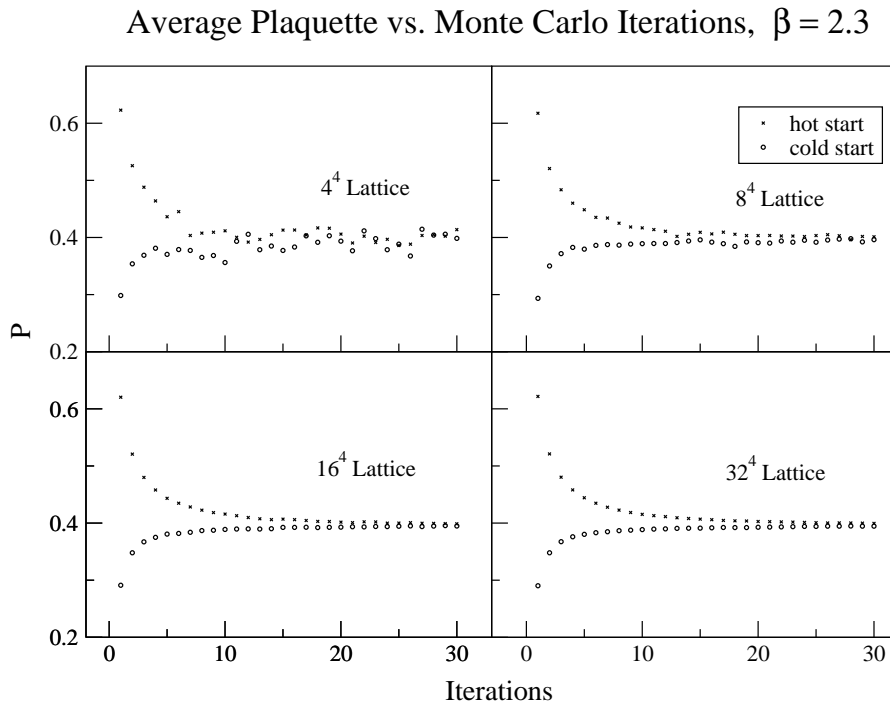


Figure 2.1: The Monte Carlo evolution of the average plaquette at $\beta=2.3$ for hot and cold starts on different size lattices.

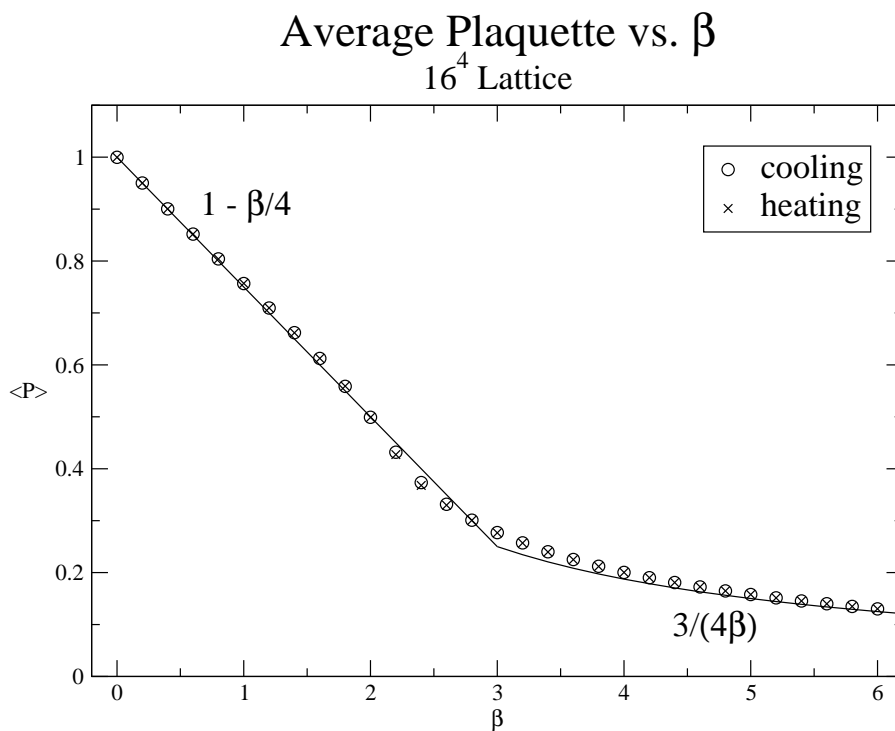


Figure 2.2: β dependence of the average plaquette from Monte Carlo simulation (data points) and analytic predictions (denoted by solid lines) on a 16^4 size lattice

CHAPTER 3

HIGGS MODEL ON THE LATTICE

3.1 SU(2)-Higgs Model

3.1.1 The Higgs and Symmetry Breaking

The Higgs boson is a hypothetical spin-0 particle, introduced as a way of explaining the origin of mass for all particles in the standard model of fundamental interactions. The motivation for the Higgs particle is to give particles mass in a way that allows for a renormalizable electroweak theory. This is done through the Higgs mechanism, where symmetry-breaking results in a non-zero vacuum expectation value (vev) for the Higgs, and the vev effectively gives mass to the other particles. Currently, the Large Hadron Collider in Cern Switzerland is working towards experiments to test for the existence of the Higgs particle. Even though its existence is still in question, the standard form of the Higgs Lagrangian is well known and it is given by the (Euclidean) complex Klein-Gordon Lagrangian plus a 4-point self-interaction,

$$\mathcal{L}_H = \partial_\mu \Phi^\dagger \partial^\mu \Phi + \mu_0^2 \Phi^\dagger \Phi + \lambda_0 (\Phi^\dagger \Phi)^2, \quad (3.1)$$

where Φ is the Higgs $SU(2)$ -doublet, μ_0 is the bare Higgs mass and λ_0 is the bare Higgs self-coupling constant. The interactions with the gauge fields are included in the gauge-invariant Higgs Lagrangian

$$\mathcal{L} = \frac{1}{4} F_{\mu\nu}^\alpha F_\alpha^{\mu\nu} + (D_\mu \Phi)^\dagger D^\mu \Phi + \mu_0^2 \Phi^\dagger \Phi + \lambda_0 (\Phi^\dagger \Phi)^2. \quad (3.2)$$

The $SU(2)$ -Higgs model corresponds to the scalar-field and $SU(2)$ -gauge field portions of the standard model, that is, all of the fermions and other gauge fields are absent.

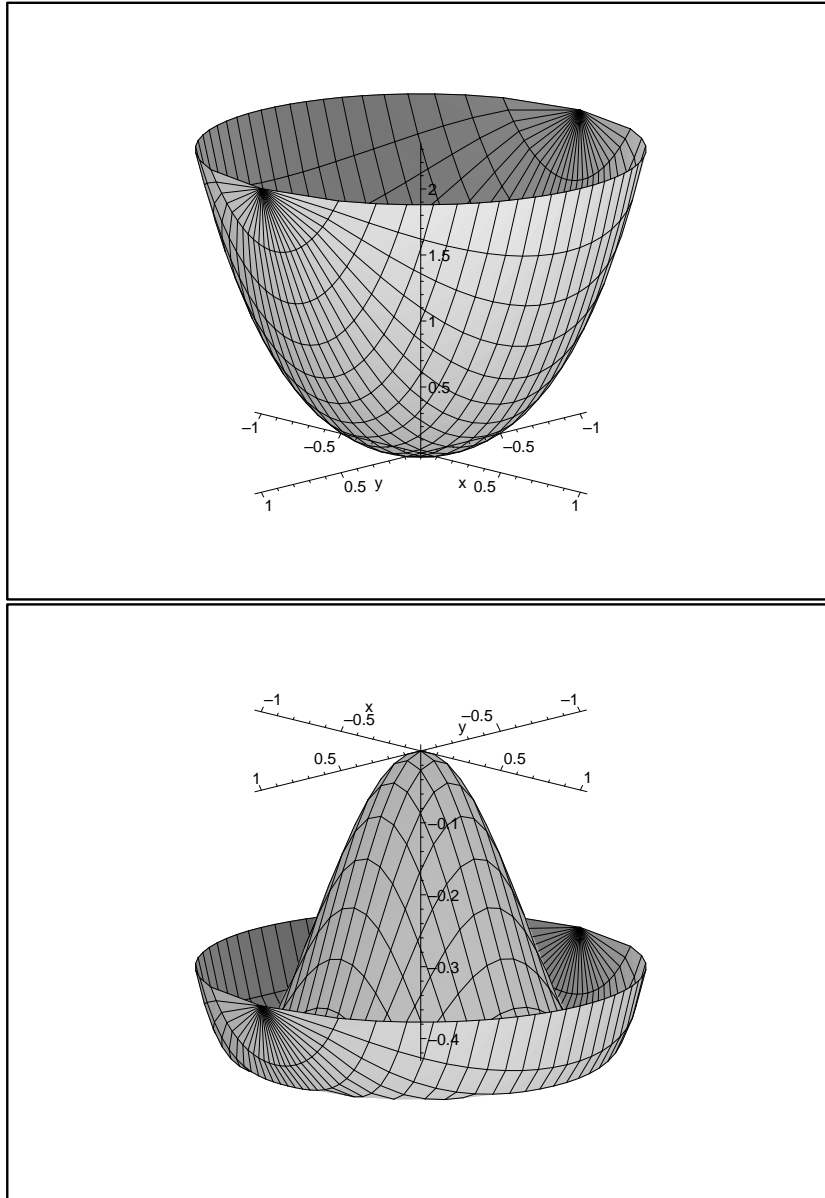


Figure 3.1: The Higgs potential for $\mu_0^2 > 0$ (above) and $\mu_0^2 < 0$ (below). The x and y axes represent the real and imaginary components of the complex field Φ , respectively.

In classical field theory, the symmetry of the vacuum state can be spontaneously broken by the Higgs field.¹ The Higgs potential

$$V(\Phi) = \mu_0^2 \Phi^\dagger \Phi + \lambda_0 (\Phi^\dagger \Phi)^2 \quad (3.3)$$

is invariant under global transformations $\Phi(x) \rightarrow g\Phi(x)$, where g is a unitary group transformation. Fig. 3.1 shows the Higgs potential for the group $U(1)$ where $\Phi = \Phi_1 + i\Phi_2$. The ground state may be found by minimizing the potential V ,

$$\frac{\partial V}{\partial \Phi} = \mu_0^2 \Phi^\dagger + 2\lambda_0 \Phi^\dagger (\Phi^\dagger \Phi) = 0. \quad (3.4)$$

If $\mu_0^2 > 0$, there is a single vacuum state $\langle \Phi \rangle = 0$ which is symmetric under complex rotations. For $\mu_0^2 < 0$, there are degenerate vacua which are not invariant under complex rotations, *i.e.* $\langle \Phi \rangle \neq \langle e^{i\theta} \Phi \rangle$, and

$$|\langle \Phi \rangle| = v = \sqrt{\frac{-\mu_0^2}{2\lambda_0}} \quad (3.5)$$

where v is the non-zero Higgs vev. When the vacuum symmetry is broken, a particular choice of the vacuum results in the appearance of massless Goldstone particles. For example, choosing the vacuum state

$$\langle \Phi \rangle = v \quad (3.6)$$

and writing Φ as

$$\Phi = v + \frac{1}{\sqrt{2}} (\tilde{\Phi}_1 + \tilde{\Phi}_2) \quad (3.7)$$

such that

$$\langle \tilde{\Phi}_1 \rangle = 0, \quad \langle \tilde{\Phi}_2 \rangle = 0, \quad (3.8)$$

results in a massive field $\tilde{\Phi}_1$ and a massless field $\tilde{\Phi}_2$. In general, a spontaneously broken (continuous) symmetry results in a massless Goldstone boson.

The full gauge-Higgs Lagrangian in Eq. (3.2) is invariant under local gauge transformations $\Phi(x) \rightarrow g(x)\Phi(x)$. Breaking a gauge symmetry not only results in a

¹The following discussion on the Higgs mechanism is adapted from Refs. [7, 8].

massless Goldstone boson, but the gauge fields also become massive and the Goldstone boson disappears, “eaten up” by the gauge fields. Considering spontaneously broken $SU(2)$ -gauge theory, the Higgs $SU(2)$ -doublet may be expressed in the form

$$\Phi = g(x) \begin{pmatrix} 0 \\ v + \frac{1}{\sqrt{2}}h(x) \end{pmatrix} \quad (3.9)$$

where $g(x) \in SU(2)$ is an arbitrary gauge transformation, and $h(x)$ is a real valued field with $\langle h(x) \rangle = 0$ that represents the physical Higgs particle. Through the Higgs interaction with the gauge fields, the Higgs vev gives rise to a mass term for the $SU(2)$ -gauge fields,

$$\begin{aligned} (D_\mu \Phi)^\dagger D_\mu \Phi &= \frac{1}{4}g_0^2 \begin{pmatrix} 0 & v \end{pmatrix} \sigma^\alpha \sigma^\beta \begin{pmatrix} 0 \\ v \end{pmatrix} A_\mu^\alpha A^{\mu\beta} + \text{non-quadratic terms} \\ &= \frac{1}{4}g_0^2 v^2 A_\mu^\alpha A^{\mu\alpha} + \text{non-quadratic terms}. \end{aligned} \quad (3.10)$$

The three $SU(2)$ -gauge fields acquire equal mass of $m = \frac{1}{\sqrt{2}}g_0v$. Even though $\mu_0^2 < 0$ is a non-physical mass term, the Higgs field $h(x)$ can still acquire a physical mass,

$$\begin{aligned} \mu_0^2 \Phi^\dagger \Phi + \lambda_0 (\Phi^\dagger \Phi)^2 &= \frac{1}{2} (\mu_0^2 + 6\lambda_0 v^2) h(x)^2 + \text{non-quadratic terms} \\ &= -\mu_0^2 h(x)^2 + \text{non-quadratic terms}, \end{aligned} \quad (3.11)$$

where $m_H^2 = -2\mu_0^2 = 4\lambda_0 v^2$ is the physical Higgs mass (squared). A value of $v = 246\text{GeV}$ has been experimentally measured, but μ_0^2 and λ_0 are currently unknown and thus the Higgs mass m_H remains a free parameter. However, experimental constraints ($114\text{GeV} < m_H < 182\text{GeV}$) have been placed on the Higgs mass using direct production searches and precision electroweak measurements which probe virtual Higgs effects within loop corrections [16, 17].

For $SU(2) \times U(1)$ gauge theory

$$D_\mu = \partial_\mu + i\frac{1}{2}g_0 A_\mu^\alpha \sigma^\alpha + i\frac{1}{2}g_0' B_\mu, \quad (3.12)$$

$$= \partial_\mu + ig_0 A_\mu^\alpha \lambda^\alpha + ig_1 B_\mu \quad (3.13)$$

where A_μ^α and B_μ are the $SU(2)$ and $U(1)$ gauge fields, respectively. The Higgs mechanism results in two massive W^\pm fields with $m_W = \frac{1}{\sqrt{2}}g_0v$, one massive Z_0 field

with $m_Z = \frac{1}{\sqrt{2}}\sqrt{g_0^2 + g_0'^2}v$, and one massless photon field with $m_\gamma = 0$. These are the four force carrying particles of the unified electroweak interaction, and actually consist of a mix of the $SU(2) \times U(1)$ gauge fields. The Higgs mechanism gives the gauge bosons mass in a way that preserves gauge-invariance and thus the theory is renormalizable. The W^\pm and Z_0 particles have observed masses of 80 GeV and 91 GeV, respectively. In this thesis, consistent with the standard approaches in the literature (see *e.g.* [4, 19]), the $SU(2)$ -Higgs model is investigated because the $U(1)$ coupling constant plays a less significant role than the $SU(2)$ coupling. The coupling constants g_0 and g_0' are not significantly different, $g_0' \approx 0.549 g_0$ [17]. However, the lattice coupling constants $\beta_0 = \frac{4}{g_0^2}$, $\beta_1 = \frac{1}{g_1^2}$ are related by $\beta_1 \approx 13.3\beta_0$, and so the $U(1)$ gauge fields are frozen to unity compared to the $SU(2)$ gauge fields. Thus, the $SU(2)$ -Higgs model is a reasonable approximation to full gauge theory.

The Higgs mechanism is also responsible for generating mass for fermions in a gauge invariant way. The left handed nature of the electroweak interaction makes massive fermions violate gauge invariance, which can be remedied by a Yukawa interaction with the Higgs. The fermion mass is given by $m = gv$, where g is the fermion-Higgs Yukawa coupling. It is reasonable to exclude the interactions of the Higgs with fermions on the lattice because the coupling constants are relatively small (except for the top quark).

In lattice simulations it is possible to see evidence of spontaneous symmetry breaking in the form of a phase transition. The vev of the Higgs may be thought of as an order parameter which is zero in the “symmetric phase” and non-zero in the symmetry breaking “Higgs phase”. However, there is no known order parameter for the Higgs phase transition than can be calculated on the lattice [18]. From Eq. (3.9), Φ is gauge dependent and therefore $\langle \Phi \rangle$ always averages to zero when integrating over all gauges. Gauge-invariant quantities such as

$$\langle \Phi^\dagger \Phi \rangle = v^2 + \langle h(x)^2 \rangle , \tag{3.14}$$

where $\langle h(x)^2 \rangle$ constitutes non-zero quantum fluctuations of the physical Higgs, must be used instead. The $\langle \Phi^\dagger \Phi \rangle$ is not an order parameter, but it still offers useful

information about the Higgs phase transition on the lattice.

The Higgs phase transition is peculiar because of its dependence on the parameters of the theory. For some fixed values of the coupling constants, there is a very strong first order transition separating the two phases, while for other values there is no phase transition [4, 19, 20]. For a Higgs field in the fundamental representation, there exists an analytic continuation between the two phases in which one could smoothly move from one phase to the other without ever crossing a phase transition [5]. This analytic connection manifests itself on the lattice as a hole in the phase diagram in which one can move between the symmetric region and Higgs region (by varying the coupling constants) without ever having crossed a phase transition [19]. For this reason the word “phase” is taken with a grain of salt.

3.1.2 Higgs Lattice Action

To put the $SU(2)$ -Higgs model on the lattice, consider the gauge-Higgs Lagrangian

$$\mathcal{L} = \frac{1}{2} \text{Tr} \left[F_{\mu\nu} F^{\mu\nu} + (D_\mu \phi^c)^\dagger D^\mu \phi^c + \mu_0^2 \phi^{c\dagger} \phi^c + \lambda_0 (\phi^{c\dagger} \phi^c)^2 \right], \quad (3.15)$$

where ϕ^c is the continuum Higgs field in the fundamental representation. The Higgs field must be discretized to formulate the gauge-Higgs lattice action [4]. The nearest neighbour approximation is used to rewrite the partial derivative

$$\partial_\mu \phi^c(x) \approx \frac{\phi_{x+\hat{\mu}}^c - \phi_x^c}{a}, \quad (3.16)$$

and the covariant derivative term in the action becomes

$$\begin{aligned} & \int d^4x \frac{1}{2} \text{Tr} \left[(D_\mu \phi^c)^\dagger D_\mu \phi^c \right] \\ & \approx 8a^2 \sum_x \frac{1}{2} \text{Tr} (\phi_x^{c\dagger} \phi_x^c) \\ & \quad - a^2 \sum_{x,\mu} \frac{1}{2} \text{Tr} \left[\phi_{x+\hat{\mu}}^{c\dagger} (1 - ig_0 A_{x\mu} a) \phi_x^c + \phi_x^{c\dagger} (1 + ig_0 A_{x\mu} a) \phi_{x+\hat{\mu}}^c \right] + O(a^4) \\ & \approx 8a^2 \sum_x \frac{1}{2} \text{Tr} (\phi_x^{c\dagger} \phi_x^c) - a^2 \sum_{x,\mu} \text{Tr} \text{Re} (\phi_x^{c\dagger} U_{x\mu} \phi_{x+\hat{\mu}}^c) + O(a^4). \end{aligned} \quad (3.17)$$

The Higgs part of the action is

$$S_H \approx \sum_x \left\{ a^4 \lambda_0 \left[\frac{1}{2} \text{Tr}(\phi_x^{c\dagger} \phi_x^c) \right]^2 + a^2 (8 + a^2 \mu_0^2) \frac{1}{2} \text{Tr}(\phi_x^{c\dagger} \phi_x^c) - a^2 \sum_\mu \text{Tr} \text{Re}(\phi_x^{c\dagger} U_{x\mu} \phi_{x+\hat{\mu}}^c) + O(a^4 \phi^{c2}) \right\}, \quad (3.18)$$

which can be rewritten using the change of variables

$$\phi_x^c = \frac{\sqrt{\kappa}}{a} \phi_x \quad (3.19)$$

$$\lambda_0 = \frac{\lambda}{\kappa^2} \quad (3.20)$$

$$\mu_0^2 = \frac{1 - 2\lambda - 8\kappa}{\kappa a^2}, \quad (3.21)$$

where ϕ_x is the lattice Higgs field, λ is the lattice Higgs (quartic) self-coupling constant, and κ (hopping parameter) is the gauge-Higgs coupling constant. The full $SU(2)$ -Higgs lattice action, up to an irrelevant constant, is given by

$$S = \sum_{\square} \beta \left[1 - \frac{1}{2} \text{Tr} U_{\square} \right] + \sum_x \left\{ \lambda \left[\frac{1}{2} \text{Tr}(\phi_x^\dagger \phi_x) - 1 \right]^2 + \frac{1}{2} \text{Tr}(\phi_x^\dagger \phi_x) - \kappa \sum_\mu \text{Tr}(\phi_x^\dagger U_{x\mu} \phi_{x+\hat{\mu}}) \right\}. \quad (3.22)$$

The lattice Higgs field is a 2×2 matrix satisfying

$$\phi^\dagger = \sigma_2 \phi^T \sigma_2, \quad (3.23)$$

$$\phi = \begin{pmatrix} \phi_0 + i\phi_3 & \phi_2 + i\phi_1 \\ -\phi_2 + i\phi_1 & \phi_0 - i\phi_3 \end{pmatrix} = \rho \alpha, \quad (3.24)$$

where $\phi_m \in \mathbb{R}$ ($m = 0, 1, 2, 3$) are the four real components of the Higgs field, $\rho > 0$ is the Higgs “length”,

$$\rho^2 = \frac{1}{2} \text{Tr}(\phi^\dagger \phi) = \det(\phi) = \phi_0^2 + \phi_1^2 + \phi_2^2 + \phi_3^2, \quad (3.25)$$

and $\alpha \in SU(2)$ is the $SU(2)$ “angular” component of the Higgs field.

3.2 Monte Carlo Simulation

Field configurations for the combined gauge-Higgs system are generated using the heatbath method, because it is more computationally efficient than the Metropolis method, and simple enough for practical use. However, despite its greater efficiency, the Higgs heatbath method still experiences slow convergence to equilibrium and large autocorrelation (statistical dependence of subsequent configurations), especially near a phase transition [21]. This is due, in large part, to the extra radial Higgs degree of freedom ρ , which tends to evolve much more slowly. To overcome this inefficiency an additional update called overrelaxation is implemented in concert with the heatbath.

The idea behind overrelaxation is to move a field variable to a far different location in phase space while resulting in a minimal change in the action, thus creating as large of a change as possible with a very high acceptance rate [22]. The overrelaxation update is often chosen to be deterministic (non-ergodic) and to leave the action invariant (microcanonical). While the equilibrium condition Eq. (2.11) is satisfied, ergodic, canonical updates such as heatbath and Metropolis must be used for the system to converge to equilibrium.

In the deterministic limit, the probability distribution for generating a new field variable ϕ_{new} from an old one ϕ is

$$P_G(\phi \rightarrow \phi_{\text{new}}) = \delta(\phi_{\text{new}} - f(\phi)) , \quad (3.26)$$

where $f(\phi)$ is the proposed update [21]. Inserting this into Eq. (2.11) gives the expression

$$\int d\phi \delta(\phi - f^{-1}(\phi_{\text{new}})) \frac{1}{\left| \frac{df(\phi)}{d\phi} \right|} P_A(\phi \rightarrow \phi_{\text{new}}) e^{S(\phi)} = e^{S(\phi_{\text{new}})} \quad (3.27)$$

(note here that ϕ is treated as a single real variable). The equilibrium condition can be fulfilled by satisfying the detailed balance condition

$$\delta(\phi_{\text{new}} - f(\phi)) P_A(\phi \rightarrow \phi_{\text{new}}) e^{-S(\phi)} = \delta(\phi - f(\phi_{\text{new}})) P_A(\phi_{\text{new}} \rightarrow \phi) e^{-S(\phi_{\text{new}})} \quad (3.28)$$

using the acceptance probability

$$P_A(\phi \rightarrow \phi_{\text{new}}) = \begin{cases} 1 & \text{if } \left| \frac{df(\phi)}{d\phi} \right| \frac{e^{-S(\phi_x^{\text{new}})}}{e^{-S(\phi_x)}} \geq 1 \\ \left| \frac{df(\phi)}{d\phi} \right| \frac{e^{-S(\phi_x^{\text{new}})}}{e^{-S(\phi_x)}} & \text{if } \left| \frac{df(\phi)}{d\phi} \right| \frac{e^{-S(\phi_x^{\text{new}})}}{e^{-S(\phi_x)}} < 1 \end{cases} . \quad (3.29)$$

An additional requirement to satisfy the equilibrium equation is that the update be reversible, *i.e.* $f(f(\phi)) = \phi$, and so the updated variable is a reflection of the old variable. The acceptance rate is optimized by defining the overrelaxation update as a reflection that leaves the action invariant

$$S(f(\phi)) = S(\phi) . \quad (3.30)$$

Using this property, the acceptance probability may be rewritten as

$$P_A(\phi \rightarrow \phi_{\text{new}}) = \begin{cases} 1 & \text{if } \frac{\left| \frac{dS(\phi)}{d\phi} \right|}{\left| \frac{dS(f(\phi))}{df(\phi)} \right|} \geq 1 \\ \frac{\left| \frac{dS(\phi)}{d\phi} \right|}{\left| \frac{dS(f(\phi))}{df(\phi)} \right|} & \text{if } \frac{\left| \frac{dS(\phi)}{d\phi} \right|}{\left| \frac{dS(f(\phi))}{df(\phi)} \right|} < 1 \end{cases} . \quad (3.31)$$

3.2.1 Heatbath Algorithm for SU(2)-Higgs

To simulate the combined gauge-Higgs system the gauge and Higgs fields may be updated separately. The heatbath method for the gauge field requires only a small modification to include the interaction with the Higgs field. As before, the new gauge link $U_{x\mu}$ is generated according to the probability distribution

$$dp(U_{x\mu}) \sim e^{-S(U_{x\mu})} dU_{x\mu} , \quad (3.32)$$

where $S(U_{x\mu})$ is the part of the $SU(2)$ -Higgs lattice action that depends on $U_{x\mu}$, and is given by

$$S(U_{x\mu}) = -\frac{1}{2} \text{Tr} (U_{x\mu} V_{x\mu}) , \quad (3.33)$$

where $V_{x\mu}$ contains all the neighbouring fields that interact with $U_{x\mu}$,

$$V_{x\mu} = 2\kappa\phi_{x+\hat{\mu}}\phi_x^\dagger + \beta \sum_{\square} U_{\square} . \quad (3.34)$$

The gauge link $U_{x\mu}$ may now be updated using the same methods as in the pure gauge theory.

The heatbath update for the Higgs field [23, 24] is implemented by generating the four-real components of ϕ according to the distribution

$$dp(\phi_x) \sim d^4\phi_x \exp \left\{ -\lambda(\rho_x^2 - 1)^2 - \sum_{m=1}^4 (\phi_{xm} - V_{xm})^2 \right\}, \quad (3.35)$$

where $\phi_x = \phi_{xm}\tau_m$, $\tau_m = (I, i\vec{\sigma})$, and V_{xm} is from the nearest neighbour interactions,

$$V_{xm} = \frac{\kappa}{2} \text{Tr} \sum_{\mu=1}^4 \tau_m (\phi_{x+\hat{\mu}}^\dagger U_{x\mu}^\dagger + \phi_{x-\hat{\mu}}^\dagger U_{x-\hat{\mu}\mu}). \quad (3.36)$$

The distribution in Eq. (3.35) may be rearranged so that it is expressed in the form

$$dp(\phi) \sim d^4\phi \exp \left\{ -\lambda \left[\rho^2 - \left(1 + \frac{\xi - 1}{2\lambda} \right) \right]^2 - \sum_{m=1}^4 \xi \left(\phi_m - \frac{V_m}{\xi} \right)^2 \right\}, \quad (3.37)$$

where ξ is an arbitrary parameter that is used to optimize the efficiency of the updating process. The four real components ϕ_m are each generated according to

$$dp(\phi_m) \sim d\phi_m \exp \left\{ -\xi \left(\phi_m - \frac{V_m}{\xi} \right)^2 \right\} \quad (3.38)$$

and the total ϕ is accepted with a conditional probability

$$P_A = \exp \left\{ -\lambda \left[\rho^2 - \left(1 + \frac{\xi - 1}{2\lambda} \right) \right]^2 \right\}. \quad (3.39)$$

The field components ϕ_m may be generated according to the distribution in Eq. (3.38) by borrowing a piece of the Kennedy-Pendleton algorithm [15]. Generate two random numbers $x_1, x_2 \in [0, 1]$ and calculate

$$z_m = \sqrt{\frac{-\log x_1}{\xi}} \cos(2\pi x_2). \quad (3.40)$$

This will generate the distribution

$$dp(z_m) = dz_m \sqrt{\frac{\xi}{\pi}} \exp(-\xi z_m^2), \quad (3.41)$$

and ϕ_m is finally given by

$$\phi_m = z_m - \frac{V_m}{\xi}. \quad (3.42)$$

The parameter ξ is set to maximize the acceptance rate

$$R = \int_{-\infty}^{\infty} d^4\phi \left(\frac{\xi}{\pi}\right)^2 \exp \left\{ \sum_{m=1}^4 \xi \left(\phi_m - \frac{V_m}{\xi}\right)^2 \right\} P_A, \quad (3.43)$$

i.e. $\frac{dR}{d\xi} = 0$, which gives the following equation for ξ

$$\xi^3 + (2\lambda - 1)\xi^2 - 4\lambda\xi - 2\lambda \det(V) = 0. \quad (3.44)$$

In cases where λ and $\det(V)$ are small, the approximation scheme $\xi = 1 + \epsilon$, where $\epsilon = 2\lambda(1 + \det(V)) < 0.1$, may be used to solve Eq. (3.44). If this approximation is invalid, then the exact positive root of Eq. (3.44) is calculated. Also, given $\lambda > 0$ and $\det(V) > 0$ there is only one positive solution for Eq. (3.44).

3.2.2 Overrelaxation Algorithm for SU(2)-Higgs

The overrelaxation update for the $SU(2)$ -gauge field [21, 22] is very simple and is given by the reflection

$$U_{\text{new}} = V_0^\dagger U^\dagger V_0^\dagger, \quad (3.45)$$

where $V_0 \in SU(2)$ is the normalized V from Eq. (3.34), which leaves the action invariant. Since the measure dU is invariant under the reflection, the update is always accepted, *i.e.* $P_A(U \rightarrow U_{\text{new}}) = 1$.

For the overrelaxation of the Higgs field a reflection in ϕ_x that leaves the action invariant is proposed. The part of the action that depends on ϕ_x is given by

$$S(\phi_x) = \lambda (\rho_x^2 - 1)^2 + \rho_x^2 - \phi_x^m V_x^m, \quad (3.46)$$

where V_x^m is given by the nearest neighbour interactions

$$V_x^m = \kappa \sum_{\mu} \text{Tr} \left[\tau^m (\phi_{x+\hat{\mu}}^\dagger U_{x\mu}^\dagger + \phi_{x-\hat{\mu}}^\dagger U_{x-\hat{\mu},\mu}) \right]. \quad (3.47)$$

One approach to overrelaxation is to update the angular and radial components of the Higgs field α , ρ separately [21]. However, a computationally simpler and

more efficient method is to update the ‘‘Cartesian’’ components of ϕ^m parallel and perpendicular to V^m [25]

$$X = \phi^m V_0^m, \quad (3.48)$$

$$Y^m = \phi^m - X V_0^m, \quad (3.49)$$

$$V_0^m = \frac{V^m}{\sqrt{V^n V^n}} = \frac{V^m}{|V|}. \quad (3.50)$$

The action can be rewritten in a more convenient form

$$S(\phi) = \lambda (X^2 + Y^2)^2 + (1 - 2\lambda) (X^2 + Y^2) - |V| X. \quad (3.51)$$

The overrelaxation for the Y^m component is simply the reflection

$$Y_{\text{new}}^m = -Y^m. \quad (3.52)$$

This transformation leaves the action invariant, and is always accepted. The update for the X component is given by the solution to the equation

$$S(X_{\text{new}}) = S(X). \quad (3.53)$$

The reflection X_{new} is the real solution, not equal to X , of the fourth order polynomial given by Eq. (3.53), which can be reduced to a third order polynomial by factoring out the known solution $X_{\text{new}} = X$. From Eq. (3.31), the probability of accepting X_{new} is given by

$$P_A(X \rightarrow X_{\text{new}}) = \min \left\{ 1, \frac{\left| \frac{dS(X)}{dX} \right|}{\left| \frac{dS(X_{\text{new}})}{dX_{\text{new}}} \right|} \right\}. \quad (3.54)$$

If the update is rejected, then $X_{\text{new}} = X$. The final value of the Higgs variable resulting from the overrelaxation is given by

$$\phi_{\text{new}}^m = Y_{\text{new}}^m + X_{\text{new}} V_0^m = (X + X_{\text{new}}) V_0^m - \phi^m. \quad (3.55)$$

3.2.3 Special Cases

For some special values of the input parameters β, κ and λ the heatbath and overrelaxation updates may need to be modified, or simplifications may be made to improve

computational efficiency. In the case where $\beta = \infty$ the gauge fields are fixed to unity and no update is needed for gauge fields. If $\beta = \kappa = 0$ then the gauge field heatbath update simply generates random $SU(2)$ -matrices, and no overrelaxation can be performed. If $\kappa = 0$ no overrelaxation is needed for the Higgs field. If $\lambda = \infty$ the Higgs length is fixed to one ($\phi \in SU(2)$) and the heatbath and overrelaxation techniques for the gauge field may be used for the Higgs field.

3.2.4 Benchmark Simulation Results for the $SU(2)$ -Higgs Model

Simulations of the $SU(2)$ -Higgs model are performed in a very similar way as the pure gauge theory. The Higgs and gauge fields are initially chosen to be either ordered or random, although now the magnitude of the Higgs field ρ must also be initialized. The value of ρ is often initially set to one, although larger values are useful if the simulation is intended to start in the Higgs phase. The order in which the gauge and Higgs fields are updated is not important. For these simulations the gauge field variables for the entire lattice are updated followed by a lattice update for the Higgs field. The heatbath and overrelaxation lattice updates are also performed separately.

Some useful quantities to calculate for $SU(2)$ -Higgs are the average plaquette P (note P is defined differently than in Eq. (2.34)), the Higgs length (squared) ρ^2 , and the gauge-invariant links L_ϕ and L_α

$$P = \frac{1}{6V} \sum_{\square} \frac{1}{2} \text{Tr} U_{\square} \quad (3.56)$$

$$\rho^2 = \frac{1}{V} \sum_x \rho_x^2 \quad (3.57)$$

$$L_\phi = \frac{1}{4V} \sum_{x,\mu} \frac{1}{2} \text{Tr} (\phi_x^\dagger U_{x\mu} \phi_{x+\hat{\mu}}) \quad (3.58)$$

$$L_\alpha = \frac{1}{4V} \sum_{x,\mu} \frac{1}{2} \text{Tr} (\alpha_x^\dagger U_{x\mu} \alpha_{x+\hat{\mu}}) . \quad (3.59)$$

The gauge-invariant link L_ϕ is analogous to an internal energy density for the gauge-Higgs interaction, with κ as a inverse temperature shared by the gauge and Higgs

fields,

$$\langle L_\phi \rangle = \frac{1}{8V} \frac{\partial}{\partial \kappa} \log Z. \quad (3.60)$$

The gauge-invariant link L_α is defined as the normalized gauge-Higgs coupling, and later on will be the primary tool for exploring the Higgs phase transition.

Monte Carlo results from hot and cold starts for P , ρ^2 , L_ϕ and L_α are shown in Fig. 3.2 and Fig. 3.3. The results from Fig. 3.2 were obtained with one heatbath update for each of the gauge and Higgs fields, while Fig. 3.3 was obtained using one heatbath and one overrelaxation for each of the gauge and Higgs fields. The overrelaxation update significantly improves the efficiency of the updating process. The values of λ , β and κ were chosen near a phase transition, so the convergence to equilibrium is slow. The convergence of ρ^2 and L_ϕ shown in Fig. 3.2 and Fig. 3.3 agree with Ref. [4] which was done on a 8^4 size lattice (P and L_α were not shown in Ref. [4]). From here on, one update will consist of one heatbath and one overrelaxation update for each of the gauge and Higgs fields.

At the point $\beta = 0$, $\lambda = 0$ the expectation values of the Higgs length ρ^2 and the gauge-Higgs coupling L_ϕ are analytically solvable [4] and given by

$$\langle \rho^2 \rangle = \frac{14}{3 + 4\sqrt{1 - 28\kappa^2}}, \quad (3.61)$$

$$\langle L_\phi \rangle = \frac{\langle \rho^2 \rangle - 2}{8\kappa}, \quad (3.62)$$

Above $\kappa = \frac{1}{\sqrt{28}}$ (for $\beta = \lambda = 0$) the Higgs length diverges. For arbitrary β and small λ , the large κ behaviour of the Higgs length is given by [4]

$$\langle \rho^2 \rangle \sim \frac{4\kappa}{\lambda}. \quad (3.63)$$

Fig. 3.4 shows simulation results (dots) of the κ -dependence of $\langle \rho^2 \rangle$ and $\langle L_\phi \rangle$, plotted with the analytic predictions (solid lines). For each value of κ the lattice is thermalized with 10 updates and then the expectation value is calculated using the next 20 updates. The last configuration from the previous κ is used as the initial configuration for the next value of κ .

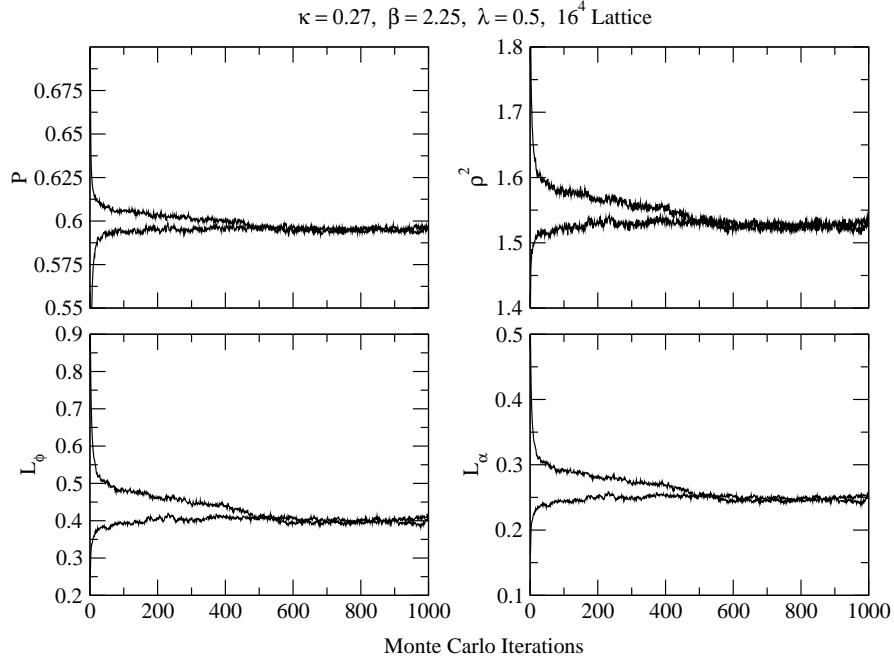


Figure 3.2: Hot and cold starts of P , ρ^2 , L_ϕ and L_α using the $SU(2)$ -Higgs heatbath update for $\kappa = 0.27$, $\beta = 2.25$ and $\lambda = 0.5$ on a 16^4 lattice.

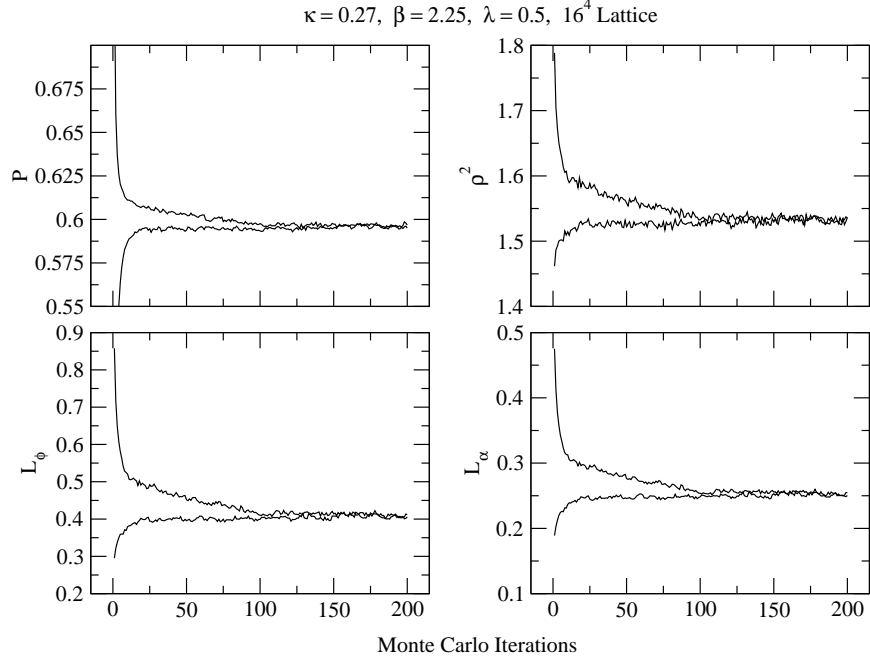


Figure 3.3: Hot and cold starts of P , ρ^2 , L_ϕ and L_α using the combined $SU(2)$ -Higgs heatbath-overrelaxation update for $\kappa = 0.27$, $\beta = 2.25$ and $\lambda = 0.5$ on a 16^4 lattice.

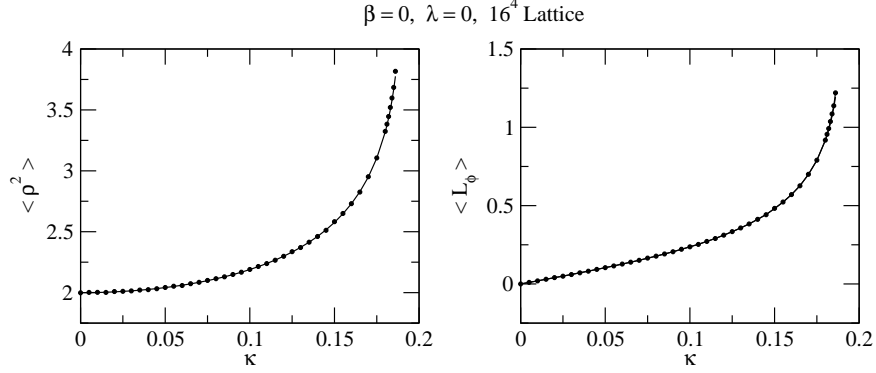


Figure 3.4: κ dependence of $\langle \rho^2 \rangle$ and $\langle L_\phi \rangle$ from Monte Carlo simulations (data points) and analytic predictions (solid lines) for $\beta = \lambda = 0$ on a 16^4 lattice.

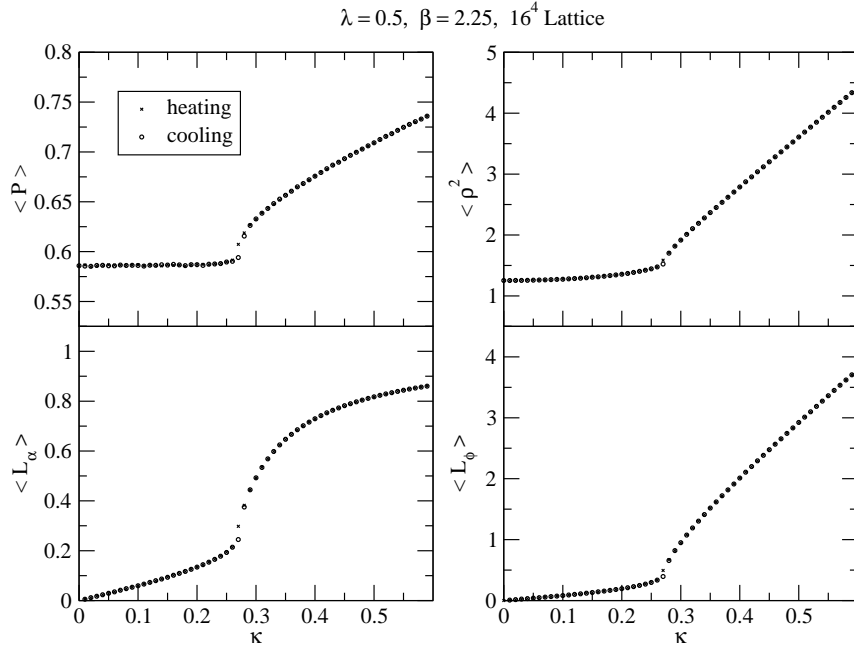


Figure 3.5: κ dependence of $\langle P \rangle$, $\langle \rho^2 \rangle$, $\langle L_\phi \rangle$, and $\langle L_\alpha \rangle$ from a Monte Carlo thermal cycle for $\beta = 2.25$ and $\lambda = 0.5$ on a 16^4 lattice.

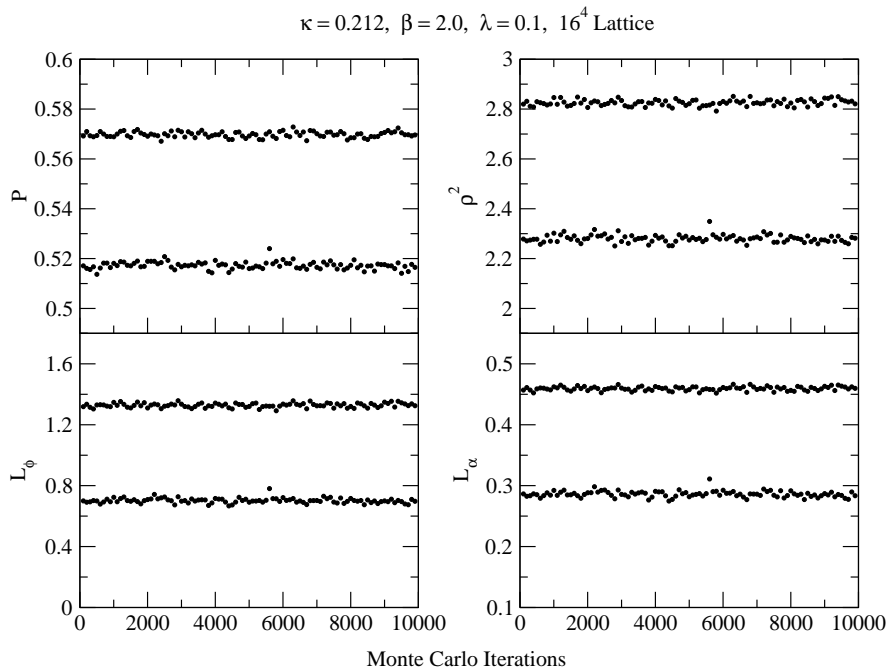


Figure 3.6: observables associated with two metastable states resulting from hot and cold starts for $\kappa = 0.212$, $\beta = 2.0$ and $\lambda = 0.1$ on a 16^4 lattice.

The κ -dependence of $\langle P \rangle$, $\langle \rho^2 \rangle$, $\langle L_\phi \rangle$ and $\langle L_\alpha \rangle$ at $\beta = 2.25$ and $\lambda = 0.5$ is shown in Fig. 3.5 using a thermal cycle. The thermal cycle involves starting at $\kappa = 0$, thermalizing the lattice with 10 updates and then using the next 20 updates to calculate the expectation values, iteratively increasing κ by 0.01 (*i.e.* cooling, since κ is analogous to an inverse temperature) and then repeating the procedure using the last configuration of the previous κ for the initial configuration of the new κ . After a sufficiently large value of κ has been reached the procedure is repeated for decreasing κ (*i.e.* heating). A phase transition between the symmetric and Higgs phase occurs at about $\kappa = 0.27$, where a kink in the observables can be seen at the transition point [4].

At smaller values of λ it is possible to observe two metastable states, indicating the presence of a strong first order phase transition. Fig. 3.6 shows hot and cold starts at $\kappa = 0.212$, $\beta = 2.0$ and $\lambda = 0.1$. The opposite initial configurations converge to different metastable equilibria, which demonstrates that there are two distinct phases at this point in parameter space in agreement with Ref. [4].

3.2.5 Mapping the Higgs Phase Transition

There are two qualitatively different regions in the lattice formulation of the $SU(2)$ -Higgs model which will be referred to as the symmetric phase and the Higgs phase. There is no gauge-invariant order parameter to distinguish between the two phases, however, the symmetric phase may be characterized as a random state of the $SU(2)$ -component of the Higgs field $\alpha \in SU(2)$ and the Higgs phase as an ordered state. The gauge-invariant link $\langle L_\alpha \rangle$ gives a quantitative measurement of the state of the Higgs field. The Higgs phase may also be characterized by large values of the Higgs length $\langle \rho^2 \rangle$, which is a signal of a non-zero vev.

Many basic properties of the phase structure for a single Higgs field in the fundamental representation are well understood, though there is no consensus on a detailed understanding of the nature of the phase transition (PT) across the entire parameter space. For small λ , the PT is demonstrably of first order [20] but the PT strength weakens with increasing λ , complicating the classification of the PT. The most effective approaches used to address this issue are searches for bimodal (“two-peaked”) distributions and lattice scaling dependence on the resulting energy gap [26, 27, 28, 30] or scaling effects within specific heats (susceptibilities) [27, 28, 30, 29, 31]. For example, Ref. [28] concludes that for $\lambda \sim 1$ the PT is first-order for β at and slightly above the terminal point of the phase line, but is unable to ascertain the existence of a tricritical point where the order of the PT would change; it would be called a critical line in (β, κ, λ) space. Since the PT decreases in strength with increasing λ , the $\lambda = \infty$ case presents the greatest challenge in the classification of the PT. Early work [26] suggested a weak first-order PT, but a recent study with large lattices presents evidence for a smooth crossover [31]. Furthermore, the $\lambda = \infty$ model augmented with an additional interaction leads to a line of first-order PTs which decrease in strength as the additional coupling approaches zero [30].

The phase structure of the $SU(2)$ -Higgs theory can be probed by studying the way quantities such as the Higgs length, gauge-invariant link, and average plaquette change with respect to the parameters β , κ , and λ . Sudden changes in the behaviour

(and even discontinuities in the case of first order phase transitions) of these quantities characterize the location and the strength of the phase transition. While a variety of observables could be used to diagnose the Higgs phase transition (dynamical terms in the action are frequently chosen), the gauge-invariant link L_α will be used exclusively for two main reasons. First, it has a bounded range, between -1 and 1 , which sets a natural scale for comparing the strength of the phase transition across the entire parameter space of the theory. Second, it is suitable in the extreme cases where $\lambda \rightarrow \infty$ (where the Higgs length goes to one), and $\beta \rightarrow \infty$ (where the gauge fields go to unity and the average plaquette becomes fixed). Thus in contrast to the Higgs length and average plaquette, the gauge-invariant link provides useful information on the Higgs phase transition for any β and λ .

A typical signature of a phase transition in lattice gauge theories is a hysteresis curve resulting from a cooling/heating (thermal) cycle. This occurs because flattening of the probability distribution near a phase transition slows convergence. The gauge-Higgs coupling constant κ can be thought of as an inverse temperature shared by the Higgs and gauge fields. By iteratively increasing κ after a number of Monte Carlo updates, where the field configurations for the previous κ are used for the start of the new κ , and then iteratively decreasing κ , a hysteresis curve in L_α indicates the presence of a phase transition. The hysteresis curve can then be used to find the approximate location of the phase transition. This approach has the advantage that it is a computationally efficient method to extract information about the phase transition, because it exploits the fact that the system does not thermalize at a phase transition with a small number of updates. This allows efficient exploration of a large region of parameter space for the $SU(2)$ -Higgs model [4, 19], and is also well-suited to the multiple-Higgs case which is the subject of the next chapter.

For given values of β and λ , the location of the PT is initially located by performing a “fast” thermal cycle, increasing κ from 0 to 1 and then decreasing back to 0 in steps of 0.01, performing one update at each value of κ . Ten updates are used to thermalize the lattice at the beginning of the cycle, and again at the maximum value of κ . A hysteresis curve resulting from the thermal cycle is shown in Fig. 3.7. The

difference between the heating and cooling runs of the gauge-invariant link (a.k.a. the hysteresis gap)

$$\Delta L_\alpha(\kappa) = L_\alpha(\kappa_{heating}) - L_\alpha(\kappa_{cooling}) \quad (3.64)$$

is used to calculate the approximate location of the transition $(\kappa_T \pm \sigma_T)_{fast}$. A reliable way to extract information about the location of the phase transition is to simply treat ΔL_α as a distribution and calculate its average and standard deviation with respect to κ

$$\kappa_T = \frac{\int d\kappa \kappa \Delta L_\alpha}{\int d\kappa \Delta L_\alpha}, \quad (3.65)$$

$$\sigma_T = \frac{\int d\kappa (\kappa - \kappa_T)^2 \Delta L_\alpha}{\int d\kappa \Delta L_\alpha}, \quad (3.66)$$

so that σ_T is a measure of the width of the phase transition with respect to κ . The value of κ_T is then refined by narrowing in on the region around the phase transition, $\kappa \in [(\kappa_T - 2\sigma_T)_{fast}, (\kappa_T + 2\sigma_T)_{fast}]$, and performing a “slow” thermal cycle with the same number of updates and steps in κ as before but with correspondingly smaller intervals. The refined location of the PT and its corresponding uncertainty is then $(\kappa_T \pm \sigma_T)_{slow}$. If no signal of a hysteresis is found for the fast cycle, then there is no phase transition and the slow cycle is not performed.

The quantity ΔL_α inherently contains statistical noise, which can be misinterpreted as a hysteresis. To eliminate this problem, the average statistical noise δ is estimated by averaging the absolute difference between subsequent updates

$$\delta = \frac{1}{N} \sum_{n=1}^N |L_\alpha(\kappa_n) - L_\alpha(\kappa_{n+1})|, \quad (3.67)$$

and all $\Delta L_\alpha < 3\delta$ are set to zero. This criteria, albeit arbitrary, was found to be a reliable way of ensuring that statistical fluctuations are not mistaken for a hysteresis signal. Also, 3δ is chosen so that it overestimates statistical fluctuations, as shown in Fig. 3.7, and therefore provides a conservative criterion for identifying a phase transition, *i.e.* no chance of misidentifying statistical fluctuations as a phase transition.

To map the phase transition across parameter space, κ_T is found for different β and fixed λ , and then the process is repeated for a different λ . Figs. 3.8 and 3.9 show a selected set of hysteresis runs for different values of β and λ . Fig. 3.10 shows the phase diagram for the $SU(2)$ -Higgs model, extracted using the fast/slow hysteresis method, which agrees with Ref. [4]. The error bars in Fig. 3.10 are given by σ_T and represent the uncertainty in the location of the phase transition κ_T due to the width of the hysteresis. For large λ and small β there is no hysteresis signal and thus the phase transition becomes an analytic crossover, which is consistent with the prediction of an analytic connection between the symmetric and Higgs regions [5].

The fast and slow thermal cycles may also be used to extract information about the strength of the phase transition. For a strong first-order phase transition, a hysteresis will be present regardless of the number of updates. However, for a second-order or weak first-order (were the two phases are very close together) phase transition, the hysteresis will disappear as the thermal cycle becomes slower. It is therefore possible to obtain additional information on the nature of the phase transition by comparing the fast and slow cycles. In Fig. 3.11, the maximum of the hysteresis gap $\max(\Delta L_\alpha)$ is plotted to demonstrate how the strength of the phase transition changes with β and λ . At small λ , the phase transition is uniform in strength for all β . As λ increases, the phase transition generally becomes weaker. It is interesting to note that (for intermediate λ) the phase transition is strongest around $\beta \approx 1.7$. For larger β (where the Higgs field is weakly coupled to gauge field) the transition becomes second-order or weak first-order. For small beta, the transition weakens and eventually the hysteresis signal disappears (*i.e.* $\Delta L_\alpha < 3\delta$) which indicates that there is no longer a phase transition.

Fast/Slow Cycles and Hysteresis Gap

$\lambda = 1, \beta = 2.2, 16^4$ Lattice

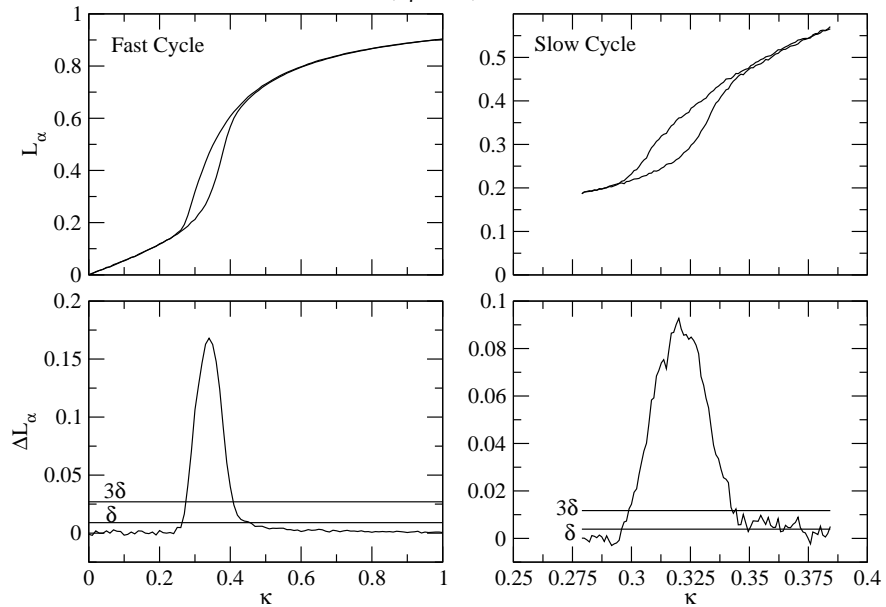


Figure 3.7: The hysteresis gap $\Delta L_\alpha(\kappa)$ resulting from fast and slow hysteresis cycles at $\beta = 2.2, \lambda = 1$ on a 16^4 lattice. Note that 3δ clearly overestimates the statistical fluctuations.

Hystereses: Fast cycles

16^4 Lattice

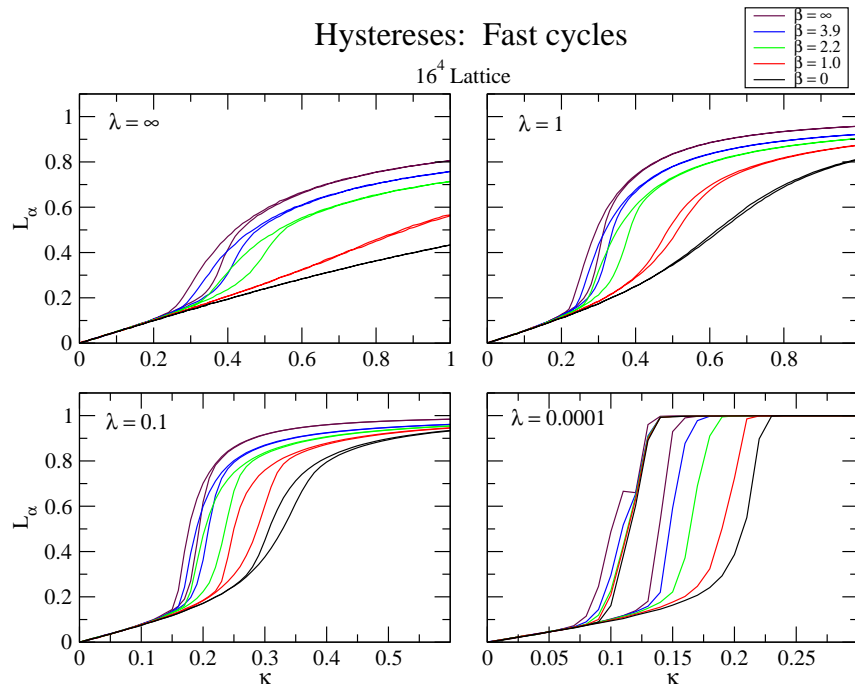


Figure 3.8: Fast hysteresis runs on a 16^4 lattice.

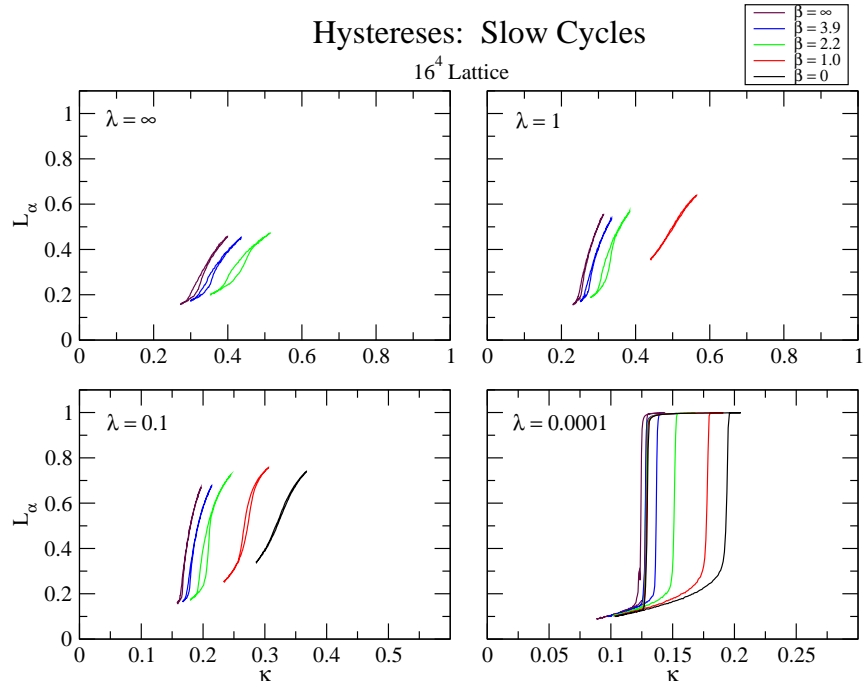


Figure 3.9: Slow hysteresis runs on a 16^4 lattice.

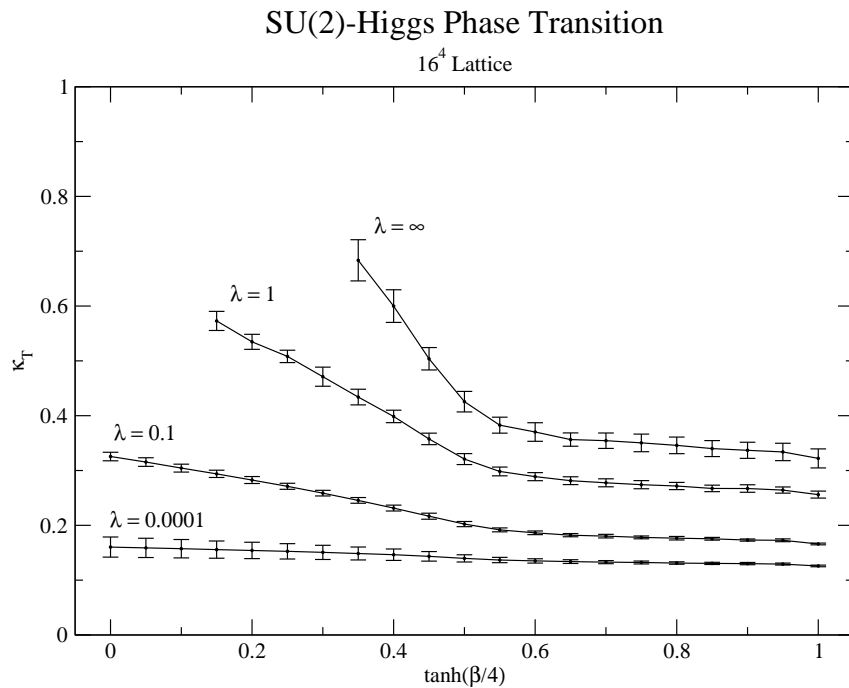


Figure 3.10: The phase diagram for $SU(2)$ -Higgs, resulting from hysteresis runs on a 16^4 lattice. The error bars indicate the uncertainty in the location of the phase transition due to the width of the hysteresis curve.

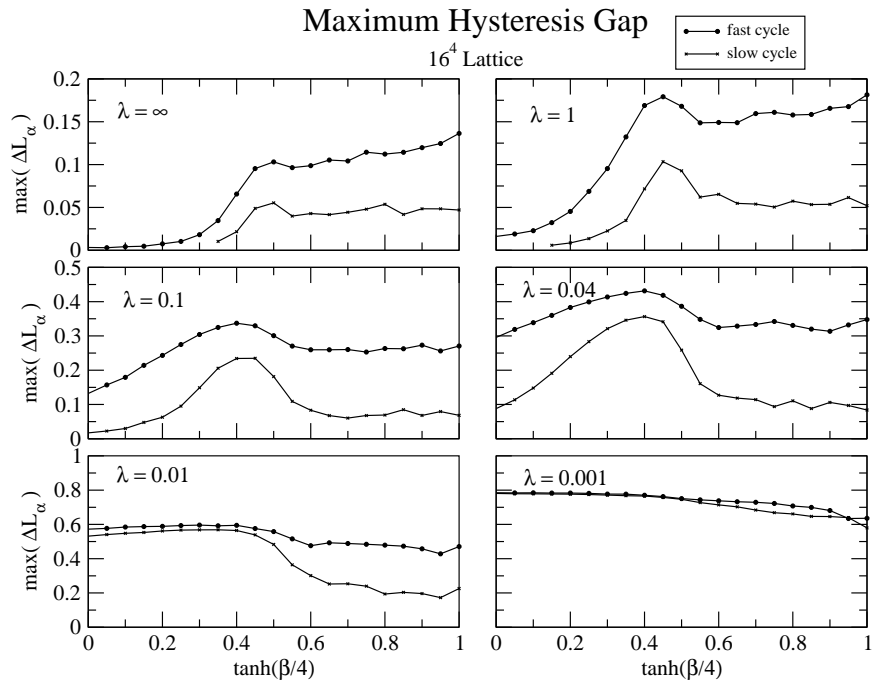


Figure 3.11: The maximum of the hysteresis gap from fast and slow hysteresis runs on a 16^4 lattice.

CHAPTER 4

MULTI-HIGGS PHASE TRANSITION

4.1 SU(2)-Multi-Higgs model

It is difficult to place experimental constraints on the number of Higgs particles in the Standard Model. For example, an arbitrary number of Higgs fields with conventional quantum numbers (isospin $I = \frac{1}{2}$, hypercharge $Y = \pm 1$) is consistent with the experimental observation that

$$\rho = \frac{\sum_{i=1}^{N_H} (I_i(I_i + 1) - \frac{1}{4}Y_i^2) v_i^2}{\sum_{i=1}^{N_H} \frac{1}{2}Y_i^2 v_i^2} = \frac{M_W^2}{M_Z^2 \cos^2 \theta_w} \approx 1, \quad (4.1)$$

where v_i is the vacuum expectation value for each Higgs field and θ_w is the weak mixing angle. Many-Higgs models can generate mass for other particles through symmetry breaking in the same way as single-Higgs models do. The inclusion of multiple Higgs within the Standard Model is the simplest extension of the minimal Higgs sector. In particular, two-Higgs models are a necessary component of the minimal supersymmetric Standard Model [3]. Also, multiple Higgs fields may provide an inexpensive computational laboratory for studying fermions (*i.e.* scalar quarks), which are much more difficult to simulate. The analytic work on the Higgs phase transition, which predicts an analytic connection between the Higgs and symmetric regions, only applies to the case of one Higgs field [5]. Therefore, it is possible that the nature of the Higgs phase transition could be different for the multi-Higgs case. Non-abelian multi-Higgs models have not been studied on the lattice, their phase structure is largely unknown, and they offer new and interesting areas to be explored. This chapter represents the original research of this thesis, and is an extended presentation of [32].

The simplest extension of the $SU(2)$ -Higgs model to include multiple Higgs is where the different Higgs fields do not directly interact with each other (*i.e.* they interact with each other only through the gauge field). In this case, the Lagrangian is given by

$$\mathcal{L} = \frac{1}{2} \text{Tr} \left\{ F_{\mu\nu} F^{\mu\nu} + \sum_{n=1}^{N_H} [(D_\mu \phi_n^c)^\dagger D^\mu \phi_n^c + \mu_{0,n}^2 \phi_n^{c\dagger} \phi_n^c + \lambda_{0,n} (\phi_n^{c\dagger} \phi_n^c)^2] \right\}, \quad (4.2)$$

where N_H is the total number of Higgs fields. Additional terms such as $\frac{1}{2} \text{Tr}(\phi_n^{c\dagger} \phi_n^c \phi_m^{c\dagger} \phi_m^c)$ and $[\frac{1}{2} \text{Tr}(\phi_n^{c\dagger} \phi_m^c)]^2$ ($n \neq m$) where the different Higgs fields directly interact with each other could be included, but the Lagrangian in Eq. (4.2) will be used to simplify the analysis and to observe the effects of simply including additional Higgs fields. The lattice action for the $SU(2)$ -multi-Higgs model is

$$\begin{aligned} S = & \sum_x \sum_{\mu > \nu} \beta \left[1 - \frac{1}{2} \text{Tr} \left(U_{x\mu} U_{x+\hat{\mu}\nu} U_{x+\hat{\nu}\mu}^\dagger U_{x\nu}^\dagger \right) \right] \\ & + \sum_x \sum_{n=1}^{N_H} \left[\lambda_n (\rho_{x,n}^2 - 1)^2 + \rho_{x,n}^2 - \kappa_n \sum_\mu \text{Tr} (\phi_{x,n}^\dagger U_{x\mu} \phi_{x+\hat{\mu},n}) \right]. \end{aligned} \quad (4.3)$$

For simplicity, the lattice quartic couplings are set equal ($\lambda_n = \lambda$ for all n). The hopping parameters are set equal ($\kappa_n = \kappa$ for all n) to study the symmetric multi-Higgs case, and then later an asymmetry ($\kappa_1 \neq \kappa_2$) will be introduced for the two-Higgs case.

The only modification required for the Monte Carlo updating procedure is to sum over all of the Higgs fields in Eq. (3.34), *i.e.* Eq. (3.34) becomes

$$V_{x\mu} = \sum_{n=1}^{N_H} 2\kappa \phi_{x+\hat{\mu},n} \phi_{x,n}^\dagger + \beta \sum_\square U_\square. \quad (4.4)$$

The different Higgs fields must also be updated separately, although the order in which they are updated does not matter because they are not coupled to each other.

4.2 Simulation Results

For multiple Higgs fields, quantities such as the Higgs length and gauge-invariant link may be calculated for each individual Higgs field,

$$\rho_n^2 = \frac{1}{V} \sum_x \frac{1}{2} \text{Tr} (\phi_{x,n}^\dagger \phi_{x,n}) \quad (4.5)$$

$$L_{\phi,n} = \frac{1}{4V} \sum_{x,\mu} \frac{1}{2} \text{Tr} (\phi_{x,n}^\dagger U_{x\mu} \phi_{x+\hat{\mu},n}) \quad (4.6)$$

$$L_{\alpha,n} = \frac{1}{4V} \sum_{x,\mu} \frac{1}{2} \text{Tr} (\alpha_{x,n}^\dagger U_{x\mu} \alpha_{x+\hat{\mu},n}) . \quad (4.7)$$

Fig. 4.1 demonstrates that for the symmetric multi-Higgs case ($\kappa_n = \kappa$, $\lambda_n = \lambda$) the different Higgs fields are indistinguishable from one another, as expected by the symmetry of the discretized Lagrangian. Therefore, for the symmetric case, quantities may be averaged over all Higgs fields, which presumably provides an advantage in reducing statistical errors,

$$\rho^2 = \frac{1}{N_H} \sum_{n=1}^{N_H} \rho_n^2 \quad (4.8)$$

$$L_\phi = \frac{1}{N_H} \sum_{n=1}^{N_H} L_{\phi,n} \quad (4.9)$$

$$L_\alpha = \frac{1}{N_H} \sum_{n=1}^{N_H} L_{\alpha,n} . \quad (4.10)$$

The effect of additional Higgs on the quantities P , ρ^2 , L_ϕ and L_α is shown in Figs. 4.2 and 4.3. Fig. 4.2 demonstrates that additional Higgs fields have little effect when the Higgs fields are in the symmetric phase ($\kappa = 0.2$) and a significant effect near the single-Higgs phase transition point ($\kappa = 0.27$). Since the Higgs fields are not directly coupled with one another, this may be understood through their interactions with the gauge-fields. In the symmetric phase, the Higgs length is small and the Higgs SU(2)-components disordered, thus the gauge-Higgs interaction is small and the additional Higgs fields have little impact on the gauge fields. In the Higgs phase, the Higgs length is large and the Higgs fields ordered (relative to the symmetric phase) and thus the interaction with the gauge field is more significant.

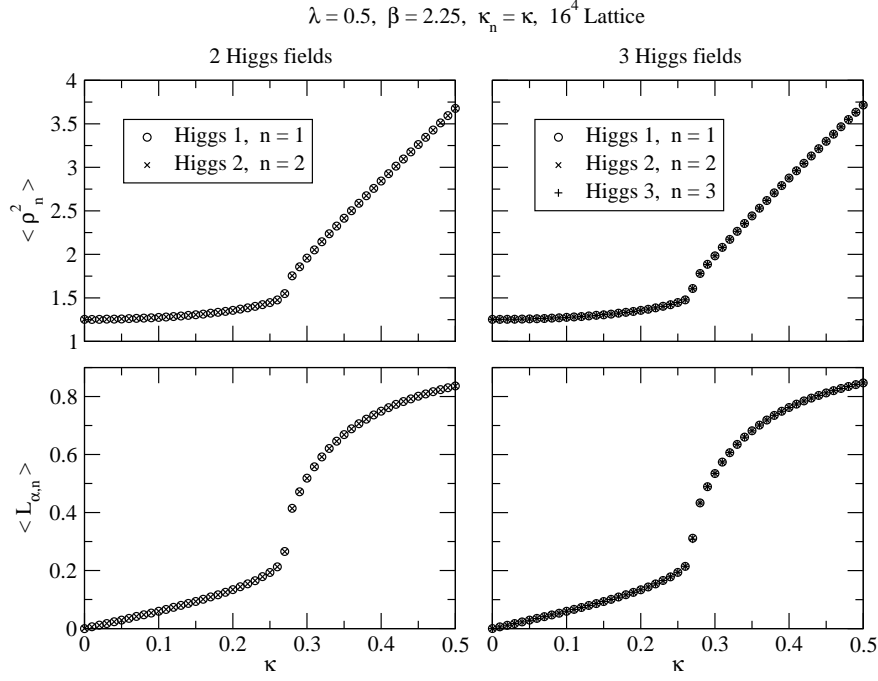


Figure 4.1: Dependence of $\langle \rho_n \rangle$ and $\langle L_{\phi,n} \rangle$ on κ for each Higgs field at $\beta = 2.25, \lambda = 0.5$ for $N_H = 2, 3$ Higgs fields on a 16^4 lattice.

This may be thought of as a cooling of the gauge fields, *i.e.* an effective larger β . In Eq. (4.4) additional Higgs fields have an effect similar to a larger effective value of β . Fig. 4.3 demonstrates the cooling of the gauge fields with increasing numbers of Higgs for $\kappa = 0.4$ (Higgs phase). In other words, as more Higgs fields are added and the system is in the Higgs phase, the system approaches the $\beta = \infty$ limit. For larger value of β , additional Higgs fields have little effect because the gauge fields are already cold, or equivalently, the continuum coupling g_0 between the Higgs and gauge fields is small.

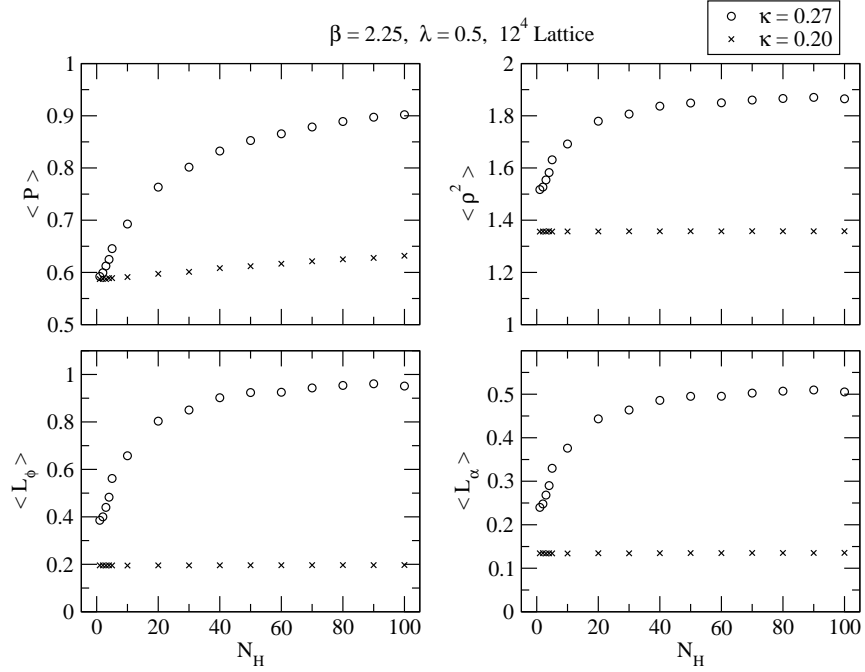


Figure 4.2: Dependence of $\langle P \rangle$, $\langle \rho_n \rangle$, $\langle L_{\phi,n} \rangle$ and $\langle L_{\alpha,n} \rangle$ on the number of Higgs N_H for $\kappa = 0.2, 0.27$, $\beta = 2.25$, $\lambda = 0.5$ on a 16^4 lattice.

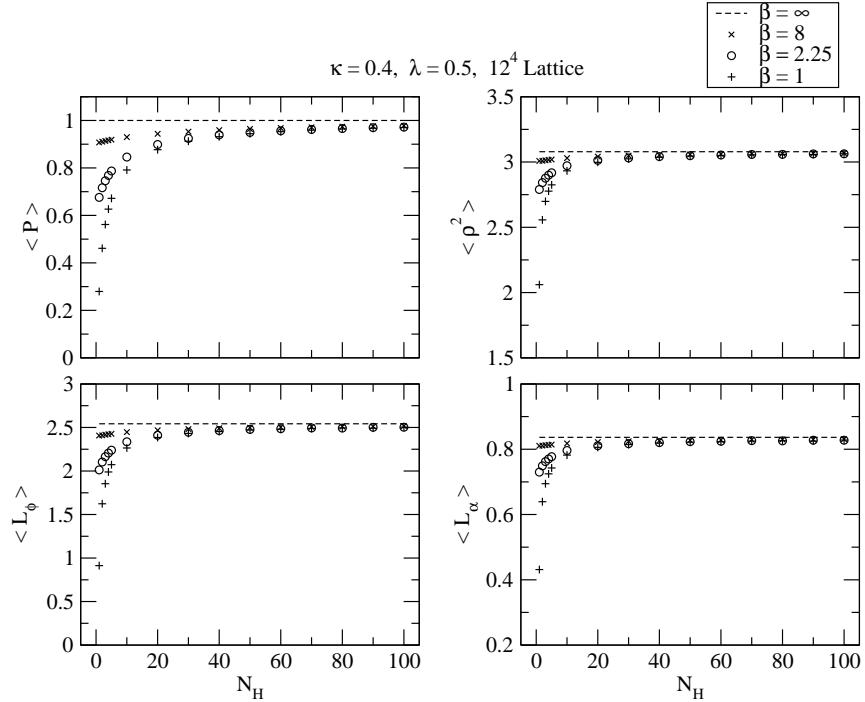


Figure 4.3: Dependence of $\langle P \rangle$, $\langle \rho_n \rangle$, $\langle L_{\phi,n} \rangle$ and $\langle L_{\alpha,n} \rangle$ on the number of Higgs N_H for $\beta = 1, 2.25, 8, \infty$, $\kappa = 0.4$, $\lambda = 0.5$ on a 16^4 lattice.

4.2.1 Phase Transition for Symmetric Multiple Higgs Fields

The hysteresis method that was used to map the phase transition for the single Higgs case is also used for the multi-Higgs case. The gauge-invariant link L_α averaged over all Higgs fields is the quantity used for the hysteresis runs. The most important feature of the symmetric multi-Higgs phase plots shown in Figs. 4.6, 4.10, 4.12 and 4.14 ($N_H = 2, 3, 5, 10$, respectively) is the continuation of the phase transition line down to $\beta = 0$ for all λ .¹ This property is evident from Figs. 4.4, 4.5 ($N_H = 2$), 4.8 and 4.9 ($N_H = 3$) which demonstrate that for $N_H \geq 2$ a hysteresis loop occurs for every value of β and λ . Thus, the hole in the single-Higgs phase diagram, where the Higgs and symmetric phase are analytically connected, does not appear in the symmetric multi-Higgs model where interactions between different flavour Higgs are absent.

For increasing numbers of Higgs, the general progression of the phase transition point is to smaller values of κ_T for fixed β and λ . This is significant in the small β region, but not in the large β region. In the large β region the Higgs fields are weakly coupled to the gauge fields, and thus the indirect interactions between the different Higgs is small. For $\beta = \infty$ ($\tanh(\frac{\beta}{4}) = 1$) the Higgs fields are completely decoupled and thus their behaviour is completely independent of the number of Higgs. The decrease of κ_T in the small β region may be attributed to the cooling of the gauge fields (larger effective β) for increasing numbers of Higgs.

Another interesting effect of multiple Higgs fields is the increasing phase transition strength in the small β , large λ region, for increasing numbers of Higgs. Figs. 4.7, 4.11, 4.13 and 4.15 ($N_H = 2, 3, 5, 10$ respectively) demonstrate the increase of the hysteresis gap, indicating that the region of analytic connection in the single-Higgs case is replaced by a first-order phase transition for sufficient number of Higgs. Fig. 4.16 demonstrates the increasing phase transition strength for increasing numbers of Higgs at $\beta = 0$ and $\lambda = \infty$. Fig. 4.17 demonstrates the existence of long-living metastable

¹Note: Figs. 4.4, 4.5, 4.6, and 4.7 are $N_H = 2$, Figs. 4.8, 4.9, 4.10, and 4.11 are $N_H = 3$, Figs. 4.12, and 4.13 are $N_H = 5$, and Figs. 4.14, and 4.15 are $N_H = 10$.

states at selected transition points, which verifies that a strong first-order phase transition appears in the small β , large λ region. $N_H = 3$ is the smallest number of Higgs fields in which metastable coexisting states were observed at $\beta = 0$ and $\lambda = \infty$.

A qualitative sketch of the phase structure in the 3-dimensional (β, λ, κ) parameter space for $N_H = 1, 2, 3$ is shown in Fig. 4.18. The shaded areas show the regions where the phase transition is unmistakably of first-order. The unshaded areas are regions where it is difficult to ascertain the order of the phase transition, *i.e.* it can not be distinguished between weak first-order or second-order. The striking qualitative observation is that the analytic connection between the Higgs and symmetric phases in the single-Higgs model is not present in the $N_H \geq 2$ symmetric-Higgs models used here. Furthermore, there are progressively stronger first-order phase transitions in the small β , large λ region as N_H increases. It is possible that the addition of direct interactions between the Higgs fields will reveal an analytic connection in a larger parameter space.

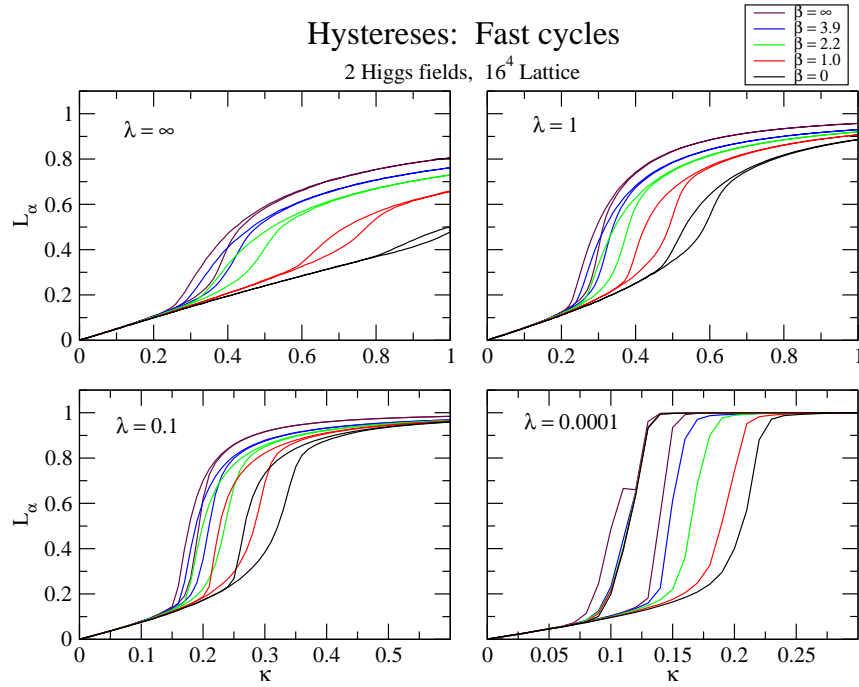


Figure 4.4: Fast hysteresis runs for 2 Higgs fields on a 16^4 lattice.

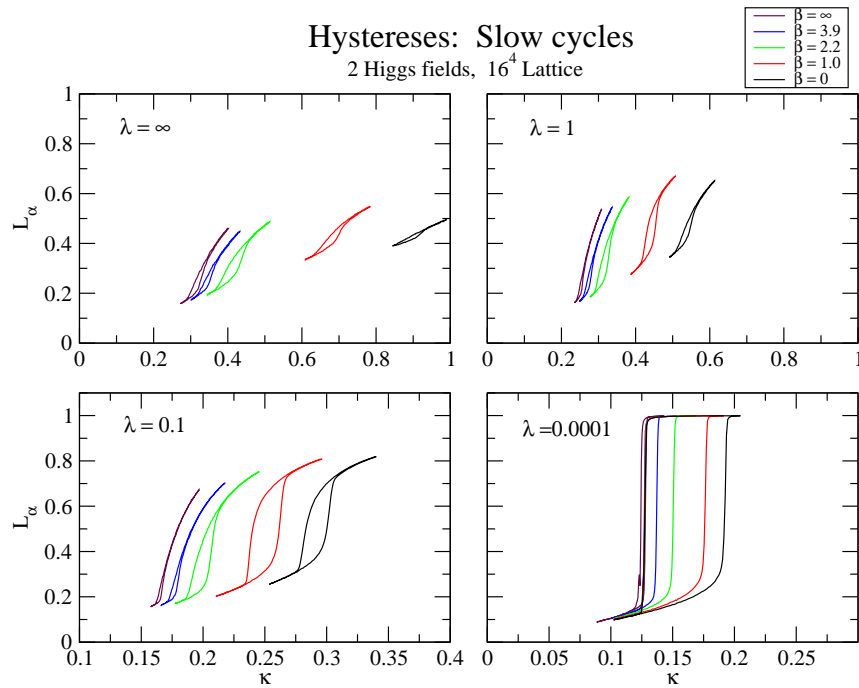


Figure 4.5: Slow hysteresis runs across for 2 Higgs fields on a 16^4 lattice.

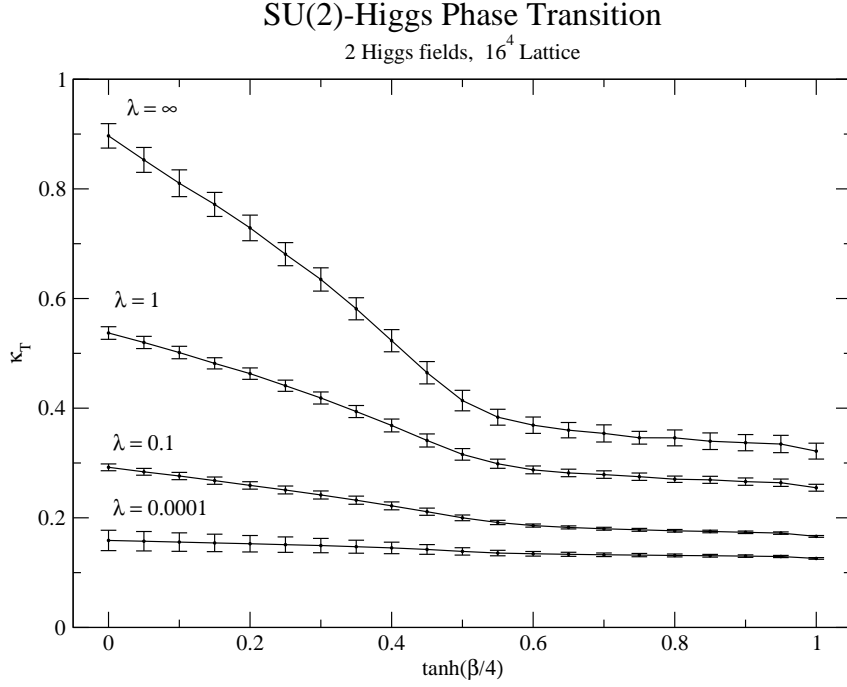


Figure 4.6: The phase diagram for $SU(2)$ -Higgs, resulting from hysteresis runs for 2 Higgs fields on a 16^4 lattice.

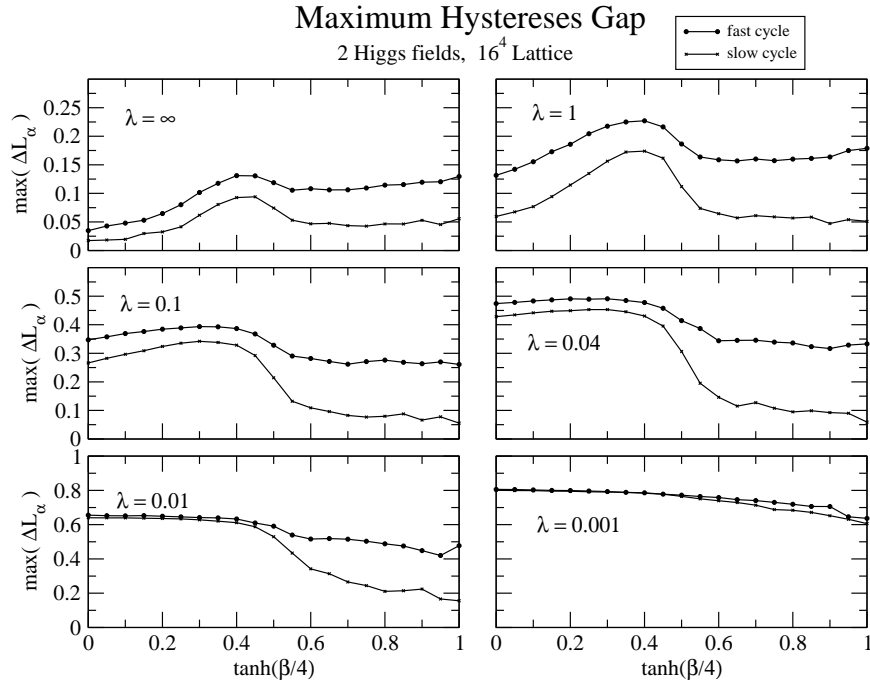


Figure 4.7: The maximum of the hysteresis gap from fast and slow hysteresis runs for 2 Higgs fields on a 16^4 lattice.

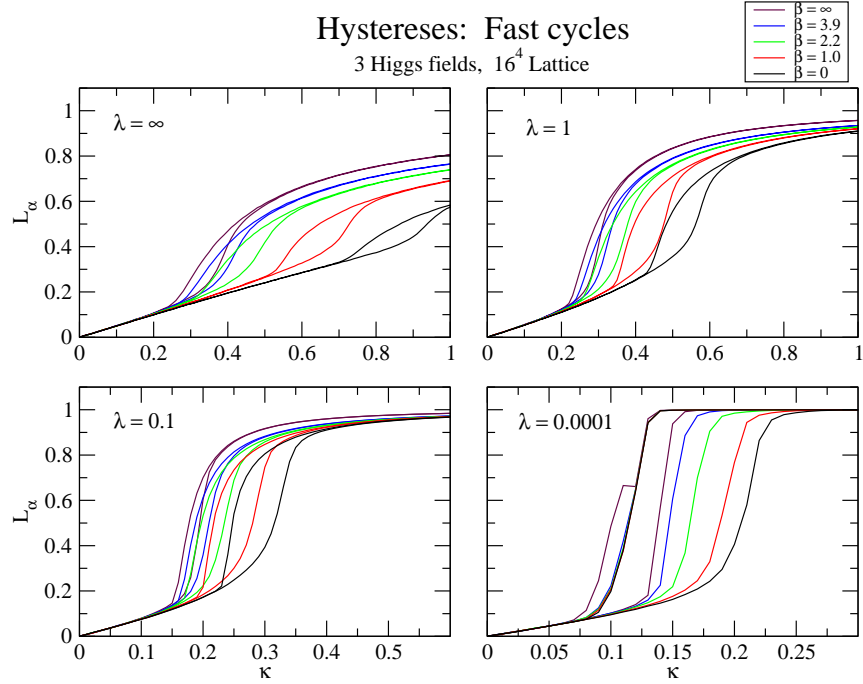


Figure 4.8: Fast hysteresis runs for 3 Higgs fields on a 16^4 lattice.

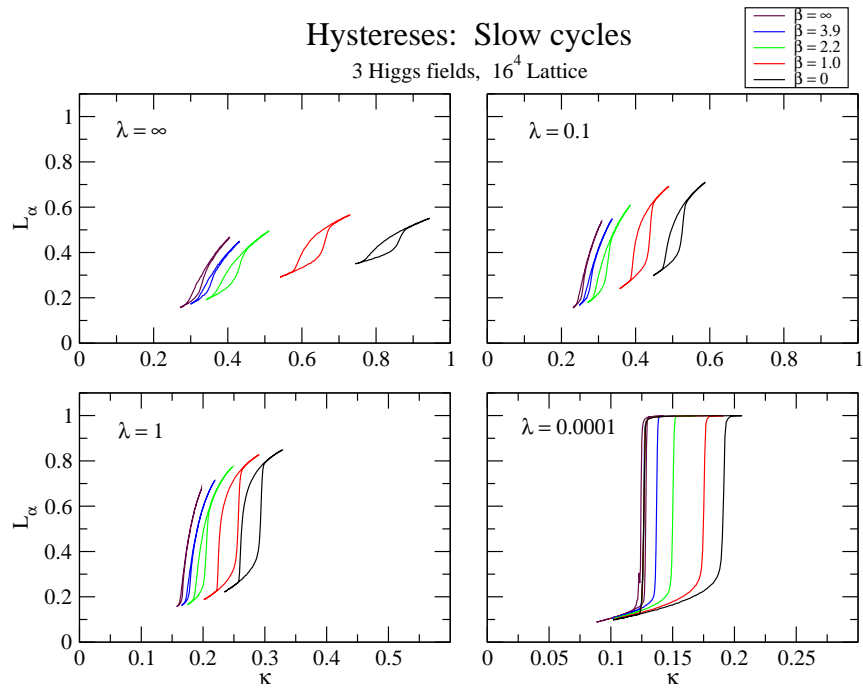


Figure 4.9: Slow hysteresis runs across for 3 Higgs fields on a 16^4 lattice.

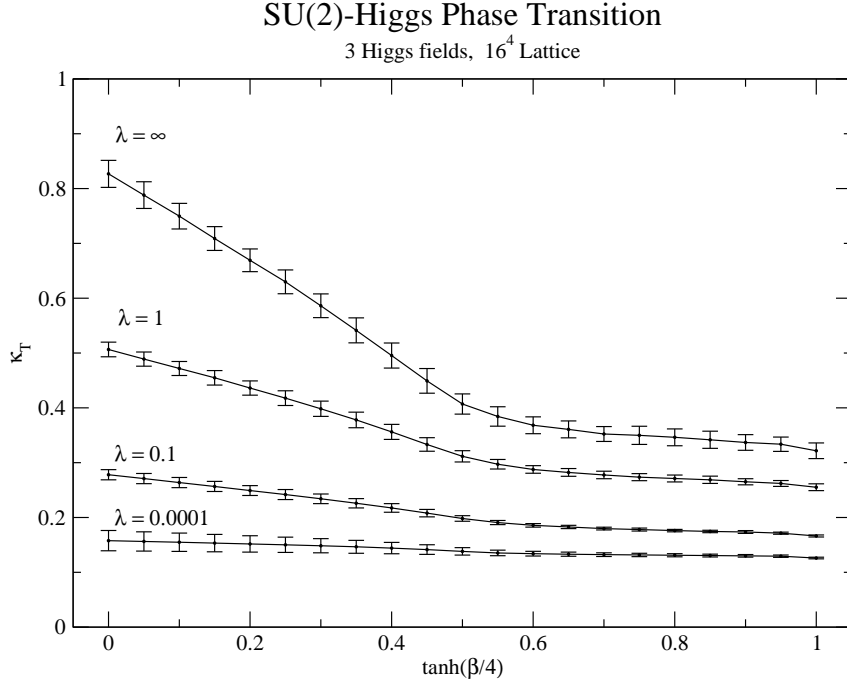


Figure 4.10: The phase diagram for $SU(2)$ -Higgs, resulting from hysteresis runs for 3 Higgs fields on a 16^4 lattice.

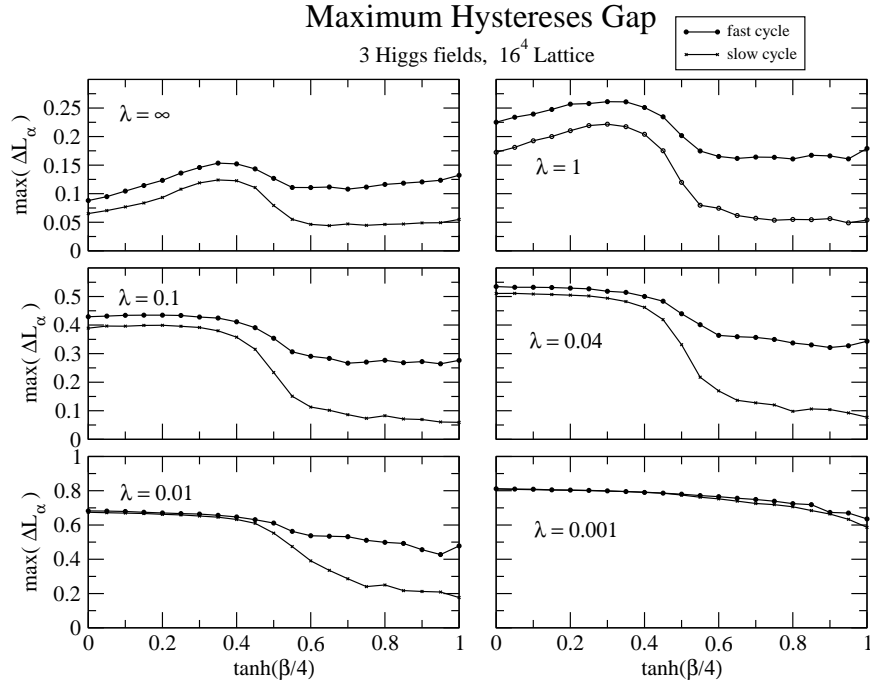


Figure 4.11: The maximum of the hysteresis gap from fast and slow hysteresis runs for 3 Higgs fields on a 16^4 lattice.

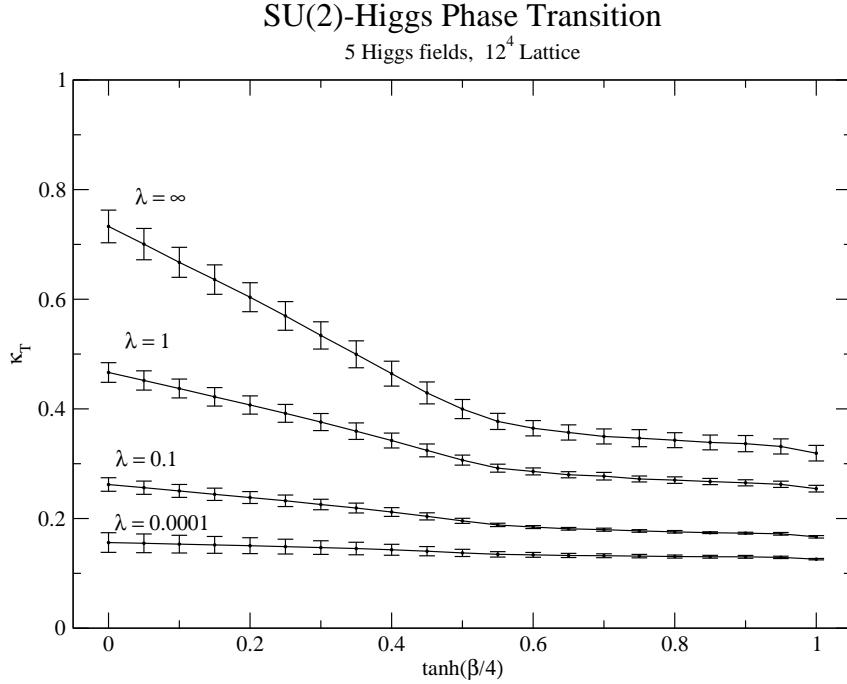


Figure 4.12: The phase diagram for $SU(2)$ -Higgs, resulting from hysteresis runs for 5 Higgs fields on a 12^4 lattice.

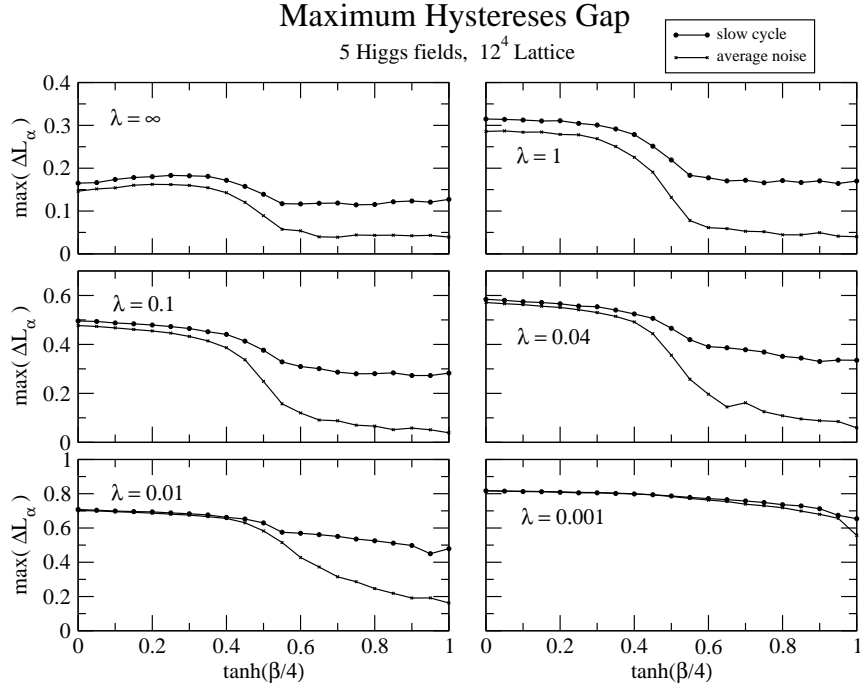


Figure 4.13: The maximum of the hysteresis gap from fast and slow hysteresis runs for 5 Higgs fields on a 12^4 lattice.

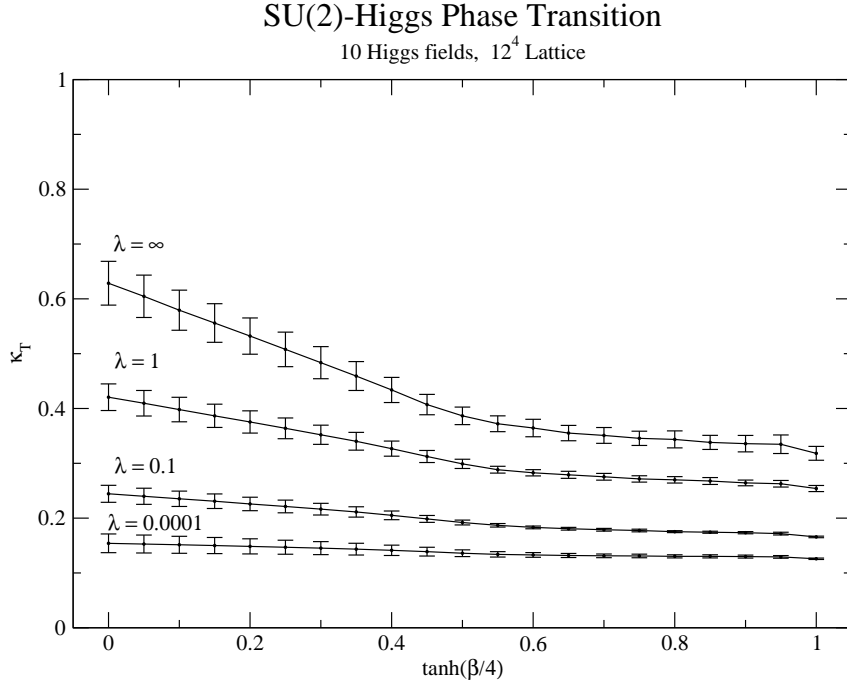


Figure 4.14: The phase diagram for $SU(2)$ -Higgs, resulting from hysteresis runs for 10 Higgs fields on a 12^4 lattice.

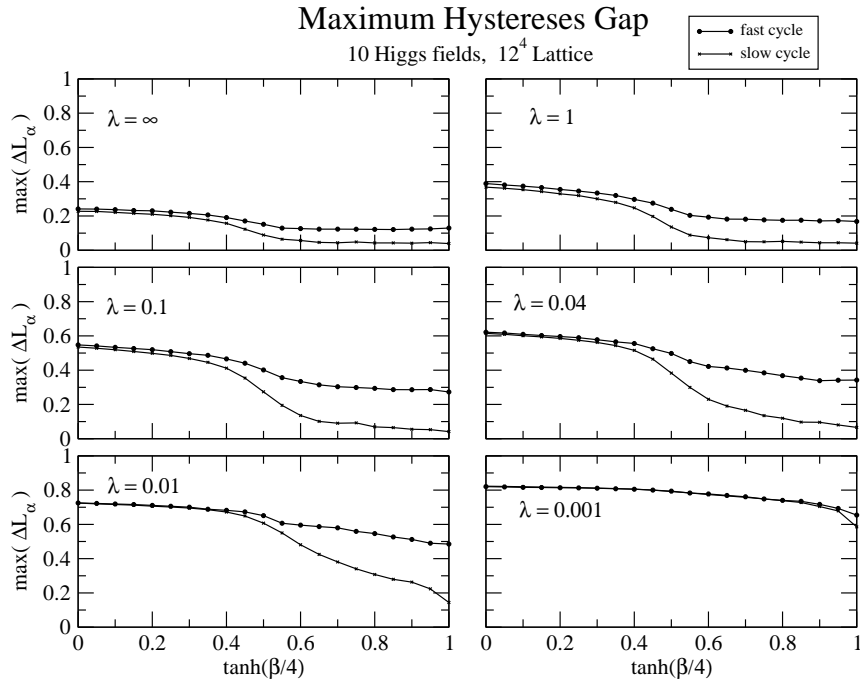


Figure 4.15: The maximum of the hysteresis gap from fast and slow hysteresis runs for 10 Higgs fields on a 12^4 lattice.

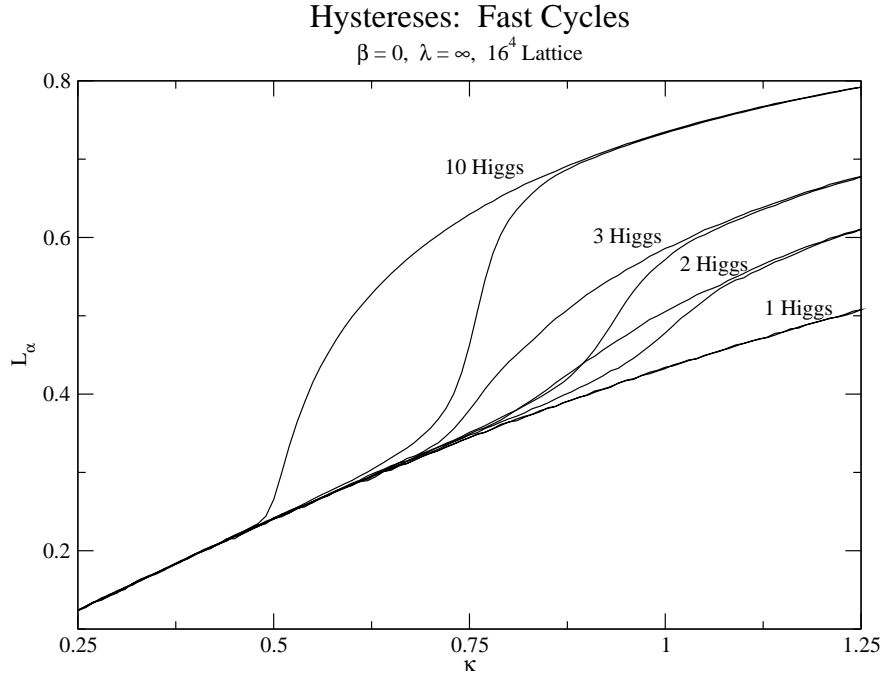


Figure 4.16: Fast hysteresis cycles of the gauge-invariant link for $N_H = 1, 2, 3, 10$ Higgs fields on a 16^4 lattice.

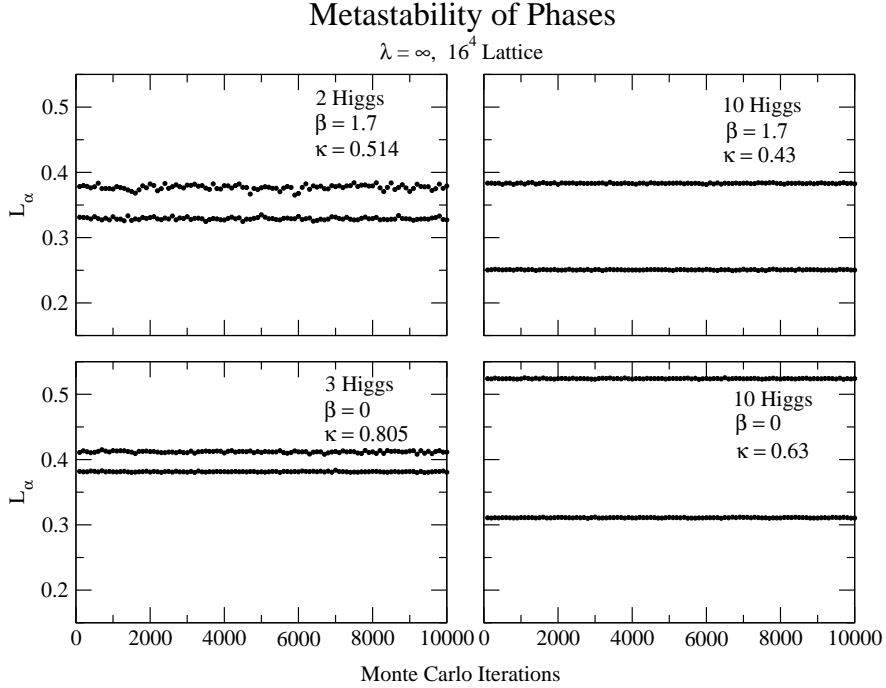


Figure 4.17: Metastability of the gauge-invariant link at selected transition points for $\lambda = \infty$ on a 16^4 lattice.

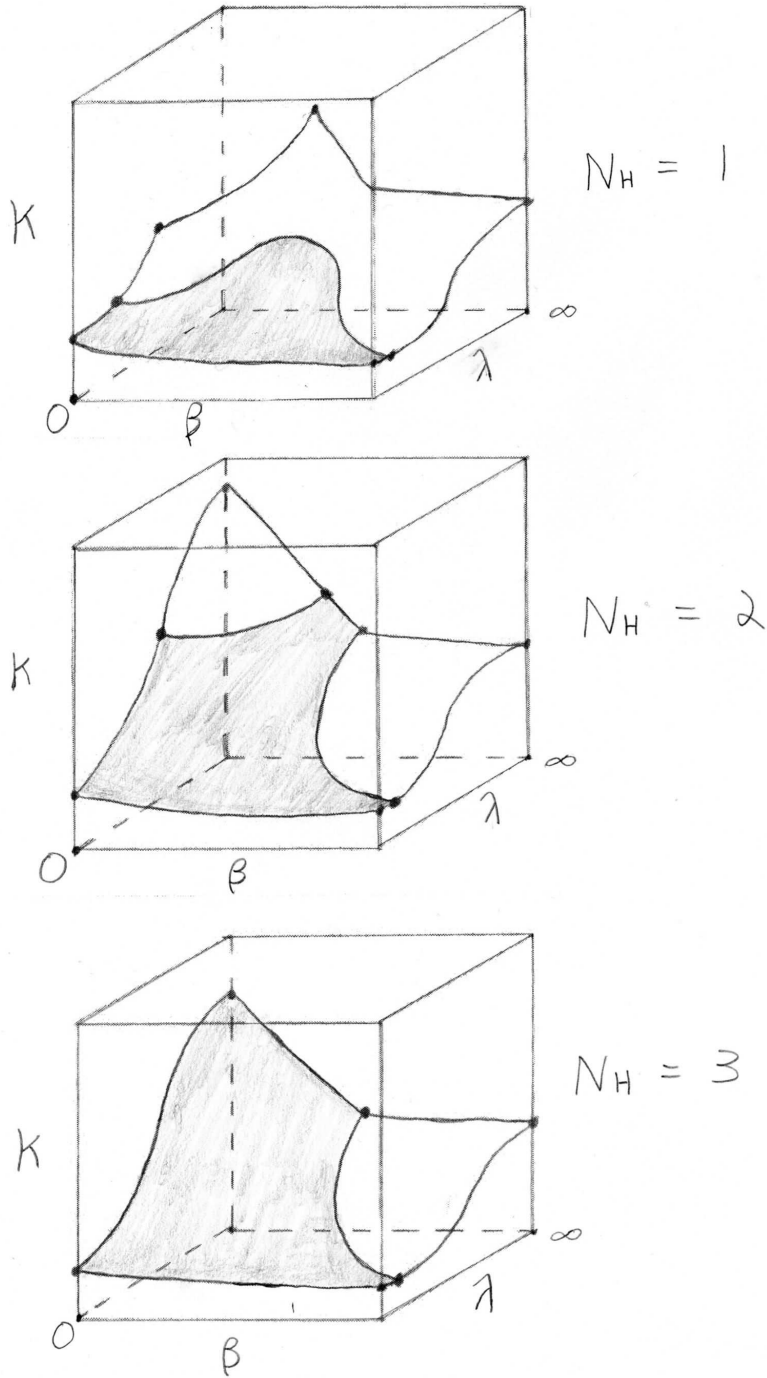


Figure 4.18: Qualitative sketch of the $SU(2)$ -Higgs phase structure in (β, λ, κ) parameter space for $N_H = 1, 2, 3$. The shaded area represents regions of strong first-order phase transition. The unshaded area represents regions which may be either a weak first-order or second-order phase transition. Note that the hole in the phase diagram for $N_H = 1$ is not present for $N_H \geq 2$ and thus the Higgs and symmetric phases are completely separated.

4.2.2 Phase Transition for the Asymmetric Two-Higgs Model

The phase transition of the symmetric $SU(2)$ -multi-Higgs model is enhanced for small β as additional Higgs fields are incorporated into the model. In a study of the three-dimensional $U(1)$ -multi-Higgs model, this enhancement was explained in terms of a mutual reinforcement of overlapping phase transitions using asymmetric hopping parameters [6]. That is, the properties of the phase transition depend on the asymmetry between the different hopping parameters κ_n . To explore the possibility that the enhancement of the 4-dimensional $SU(2)$ -multi-Higgs phase transition originates from overlapping phase transitions, we consider the asymmetric two-Higgs case where $\kappa_1 \neq \kappa_2$.

The hysteresis method is used to obtain the phase transition for two asymmetric Higgs fields. The gauge-invariant link $L_{\alpha,n}$ is different for each of the Higgs fields when $\kappa_1 \neq \kappa_2$, and so the phase transitions of each Higgs field are considered separately. Figs. 4.19, 4.20, 4.23 and 4.24 show the fast/slow hysteresis runs of two Higgs fields with a large (100%) asymmetry $\kappa_2 = 2\kappa_1$. Figs. 4.21 and 4.25 show the phase structure for each Higgs field. Both Higgs fields experience enhancement of their phase transitions, however, the enhancement is weaker for both Higgs fields. Fig. 4.27 shows that an alignment of the two phase transitions occurs in the small β , large λ region of parameter space where the phase lines terminate in the single-Higgs model. Furthermore, in the non-aligned region the lower phase line (corresponding to Higgs 2 with larger κ) closely resembles the single-Higgs case, while the upper phase line (corresponding to Higgs 1 with smaller κ) is similar to a large β single-Higgs system. This behaviour suggests that the first field to enter the Higgs region does so similar to a single-Higgs, and influences the phase transition of the second field by cooling the gauge fields. Fig. 4.26 shows the maximum of the hysteresis gap for Higgs 2, which resembles the single-Higgs case with a small enhancement in the large λ , small β region. Fig. 4.22 demonstrates that the maximum of the hysteresis gap for Higgs 1 resembles the $\beta = \infty$ case for all β . Thus the phase transition for $\kappa_2 = 2\kappa_1$ is like a single-Higgs case for Higgs 2, and a large β case for Higgs 1.

To explore the sensitivity of the enhancement effect on the asymmetry, a moderate (10%) asymmetry where $\kappa_2 = 1.1\kappa_1$ and a very large (900%) asymmetry where $\kappa_2 = 10\kappa_1$ have been studied. Fig. 4.28 shows the phase structure of each Higgs field for $\kappa_2 = 1.1\kappa_1$. At this level of asymmetry the phase lines are much more closely aligned, and the phase structure is almost the same as the symmetric two-Higgs case. Figs. 4.29 and 4.30 show the phase structure for $\kappa_2 = 10\kappa_1$. In this case Higgs 2 is almost identical to a single-Higgs case, and Higgs 1 is almost identical to the $\beta = \infty$ limit.

The interpretation that the enhancement of the Higgs phase transition originates from overlapping phase transitions is examined using asymmetric hopping parameters. For moderate asymmetries, the region in the parameter space of the theory where the phase transition lines overlap corresponds to the region where the enhancement effect occurs. As the asymmetry increases, the phase transition lines are being pulled apart and the enhancement effect is diminished. For a sufficiently large asymmetry, the system approaches the single Higgs limit, the overlapping of the phase transitions disappears and the enhancement effect is completely lost. Thus, the overlapping appears to reinforce the phase transitions and results in the enhancement effect. Fine tuning of the hopping parameters is not required for the overlapping/enhancement effects to occur, indicating that this is a general phenomena that does not require overly restrictive conditions.

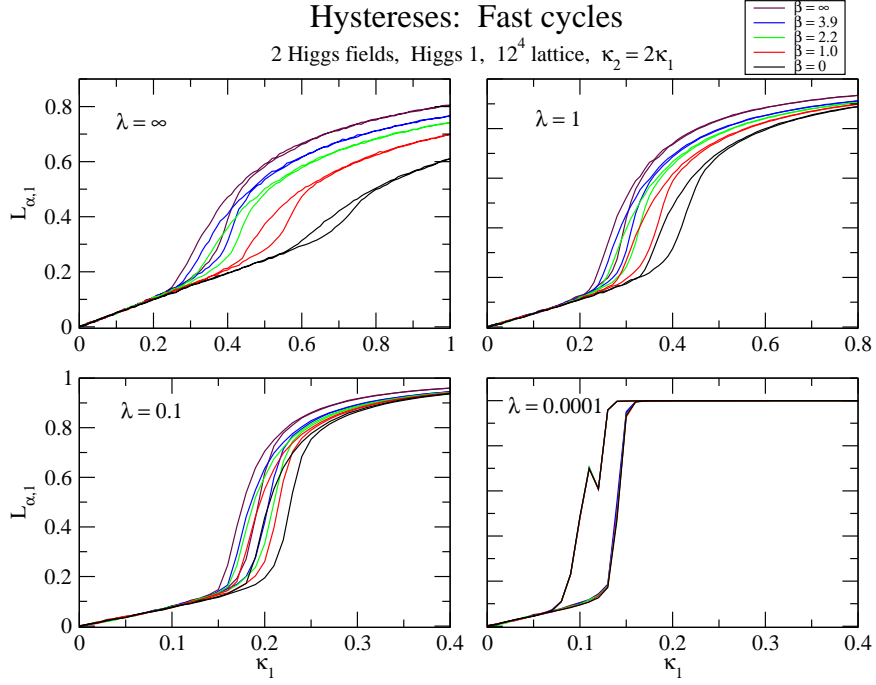


Figure 4.19: Fast hysteresis runs of Higgs 1 for 2 Higgs fields with asymmetric hopping parameters $\kappa_2 = 2\kappa_1$ on a 12^4 lattice.

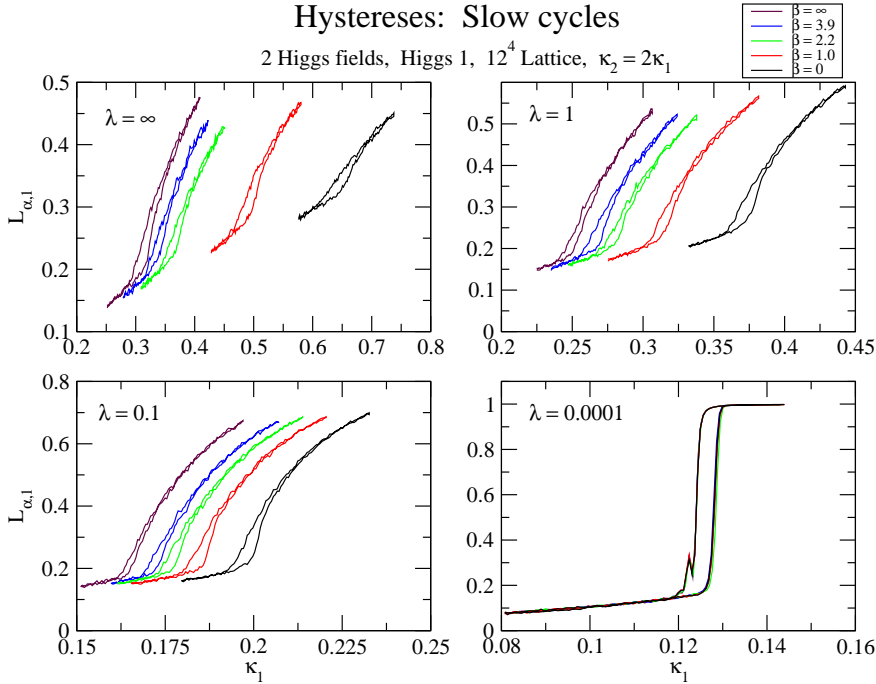


Figure 4.20: Slow hysteresis runs of Higgs 1 for 2 Higgs fields with asymmetric hopping parameters $\kappa_2 = 2\kappa_1$ on a 12^4 lattice.

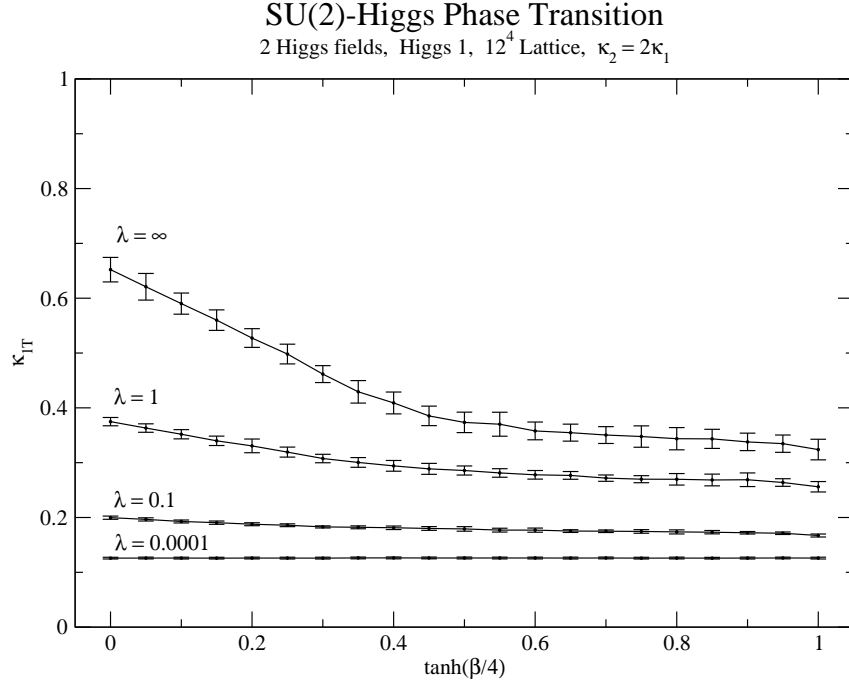


Figure 4.21: Phase diagram of Higgs 1 for 2 Higgs fields with asymmetric hopping parameters $\kappa_2 = 2\kappa_1$ on a 12^4 lattice.

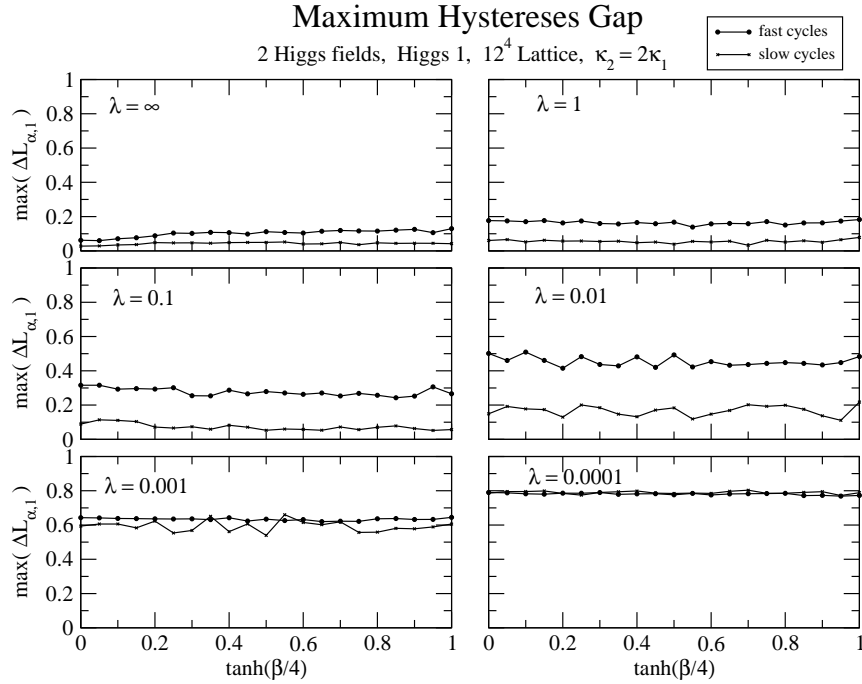


Figure 4.22: Maximum hysteresis gap of Higgs 1 for 2 Higgs fields with asymmetric hopping parameters $\kappa_2 = 2\kappa_1$ on a 12^4 lattice.

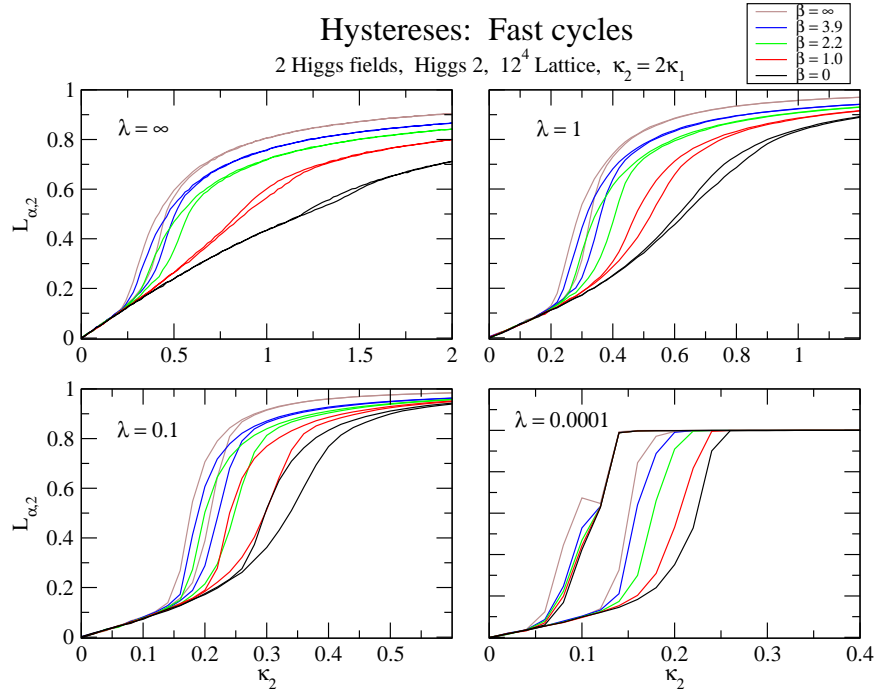


Figure 4.23: Fast hysteresis runs of Higgs 2 for 2 Higgs fields with asymmetric hopping parameters $\kappa_2 = 2\kappa_1$ on a 12^4 lattice.

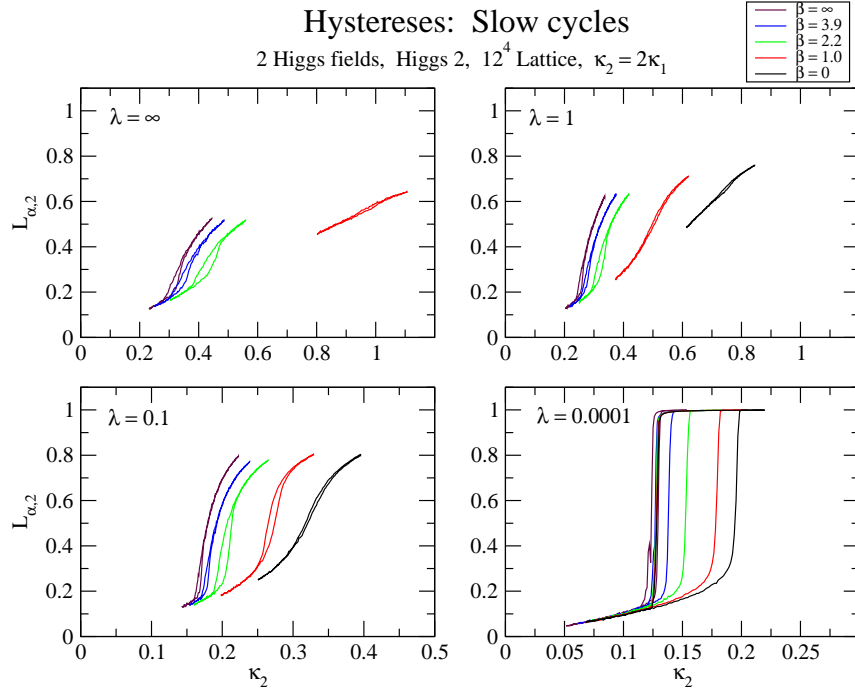


Figure 4.24: Slow hysteresis runs of Higgs 2 for 2 Higgs fields with asymmetric hopping parameters $\kappa_2 = 2\kappa_1$ on a 12^4 lattice.

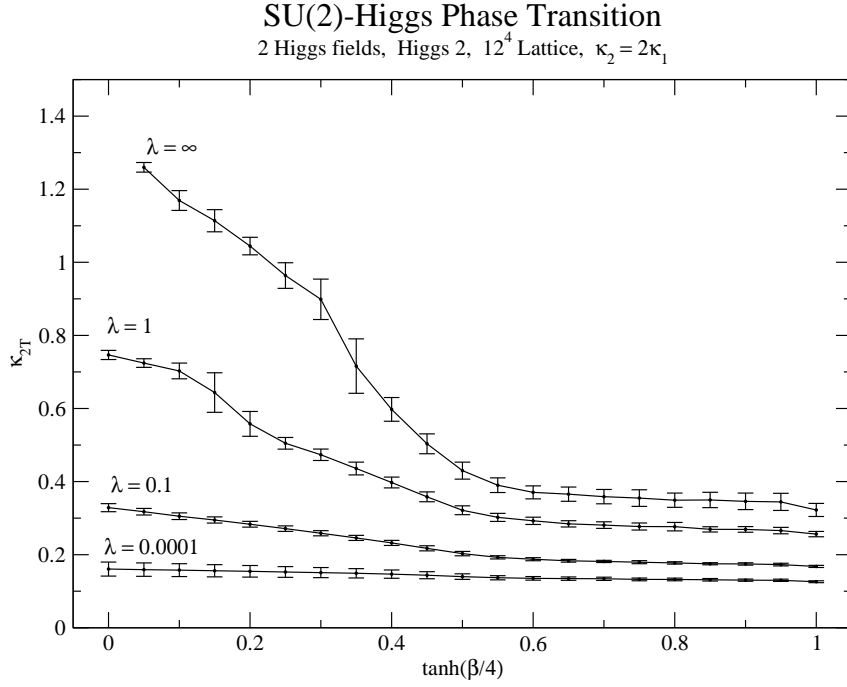


Figure 4.25: Phase diagram of Higgs 2 for 2 Higgs fields with asymmetric hopping parameters $\kappa_2 = 2\kappa_1$ on a 12^4 lattice.

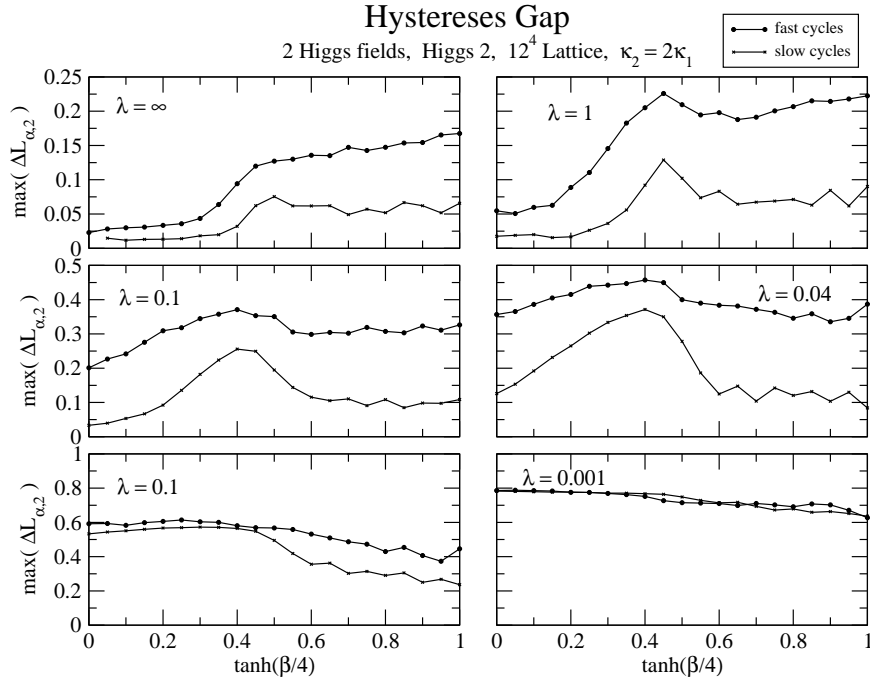


Figure 4.26: Maximum hysteresis gap of Higgs 2 for 2 Higgs fields with asymmetric hopping parameters $\kappa_2 = 2\kappa_1$ on a 12^4 lattice.

SU(2)-Higgs Phase Transition
 2 Higgs fields, 12^4 Lattice, $\kappa_2 = 2\kappa_1$

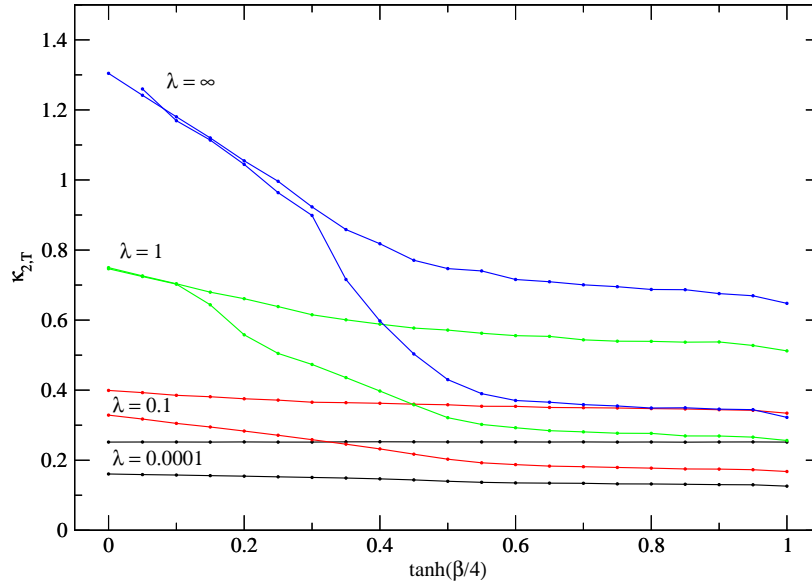


Figure 4.27: Overlapping of phase diagrams for 2 Higgs fields with asymmetric hopping parameters $\kappa_2 = 2\kappa_1$ on a 12^4 lattice. The upper phase line corresponds to Higgs 1 and the lower phase line corresponds to Higgs 2.

SU(2)-Higgs Phase Transition
 2 Higgs fields, 12^4 Lattice, $\kappa_2 = 1.1\kappa_1$

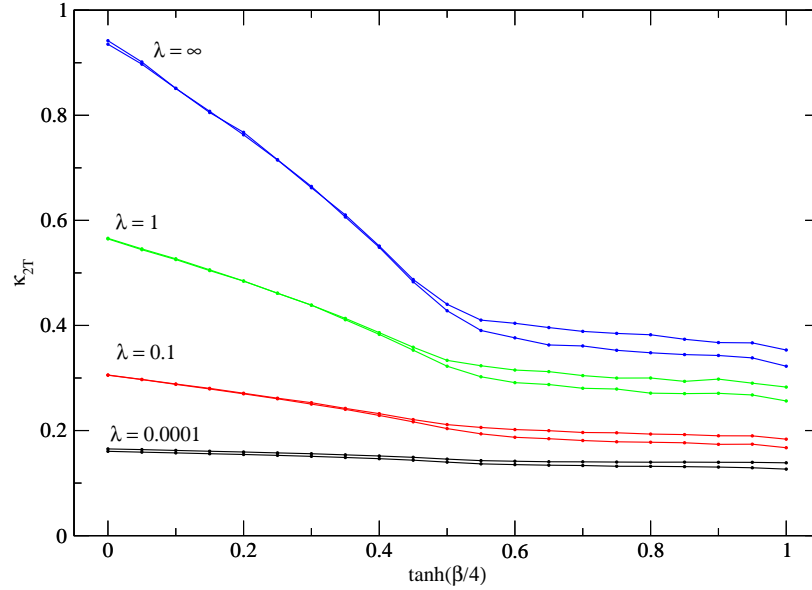


Figure 4.28: Overlapping of phase diagrams for 2 Higgs fields with asymmetric hopping parameters $\kappa_2 = 1.1\kappa_1$ on a 12^4 lattice. The upper phase line corresponds to Higgs 1 and the lower phase line corresponds to Higgs 2.

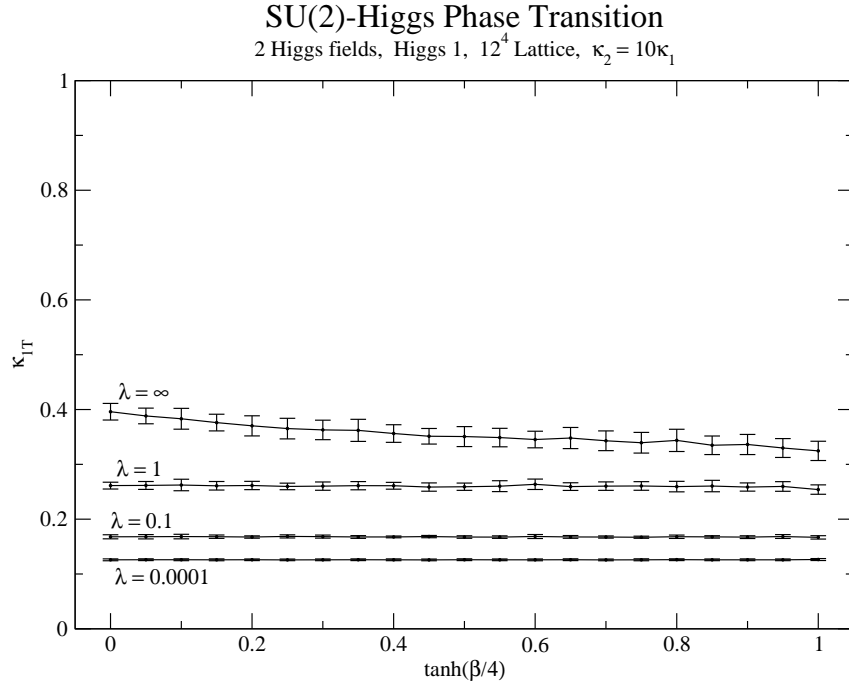


Figure 4.29: Phase diagram of Higgs 1 for 2 Higgs fields with asymmetric hopping parameters $\kappa_2 = 10\kappa_1$ on a 12^4 lattice.

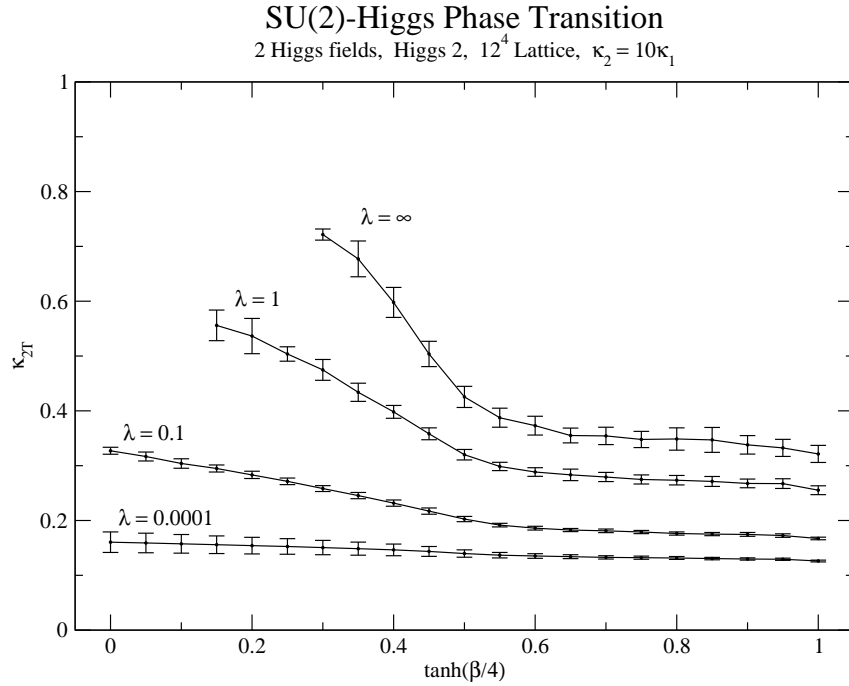


Figure 4.30: Phase diagram of Higgs 2 for 2 Higgs fields with asymmetric hopping parameters $\kappa_2 = 10\kappa_1$ on a 12^4 lattice.

CHAPTER 5

CONCLUSION

The number of Higgs fields has interesting effects on the phase structure of the $SU(2)$ -Higgs model. The region of analytic connection that exists for a single-Higgs model is not present in the $N_H \geq 2$ multi-Higgs model where direct interactions between the different Higgs fields have been omitted. Using lattice simulations, I have shown that a phase transition completely separates the symmetric and Higgs phases for two or more Higgs fields, in marked contrast to the case of a single Higgs fields. For $N_H \geq 3$, the region of analytic connection is completely replaced by a strong first-order phase transition (i.e. metastability is demonstrated) which becomes progressively stronger as the number of Higgs fields increases. It is possible that including extra interactions could reveal an analytic connection between the symmetric and Higgs phases elsewhere in that larger parameter space. That future exploration will allow for an interesting discussion of symmetry breaking.

The enhancement of the phase transition is attributed to the reinforcement of overlapping phase transitions by analyzing the two-Higgs model with asymmetric hopping parameters. A 10% asymmetry of the hopping parameters does not prevent the enhancement effect and the phase transitions overlap in the region of the enhancement. For a 100% asymmetry the Higgs field with with the larger κ experiences a phase transition similar to the single-Higgs case, while the Higgs field with the smaller κ experience a phase transition similar to the large β case as a result of the former Higgs field having a “cooling” effect on the gauge fields. For a sufficiently large asymmetry, the system approaches the single Higgs limit, the overlapping of the phase transitions disappears and the enhancement effect is completely lost.

The inclusion of additional Higgs fields, which are clones of the single-Higgs case,

has revealed non-trivial and unexpected effects on the phase structure of the theory, indicating the possibility of rich and novel phase structures for more elaborate multi-Higgs models. Including direct interactions between the Higgs fields may reveal new phenomena, intricate phase structures, and is left for future work.

BIBLIOGRAPHY

- [1] S.L. Glashow, “Partial-symmetries of weak interactions”, Nucl. Phys. 22 (1961) 579;
S. Weinberg, “A model of leptons”, Phys. Rev. Lett. 19 (1967) 1264;
A. Salam, “Weak and electromagnetic interactions”, in *Elementary Particle Theory; Nobel Symposium No.8*, ed. N. Svartholm (Almqvist and Wiksell, Stockholm, 1968).
- [2] P.W. Higgs, “Broken symmetries, massless particles and gauge fields”, Phys. Lett. 12 (1964) 132;
“Spontaneous symmetry breakdown without massless bosons”, Phys. Rev. 145 (1966) 1156.
- [3] J.F. Gunion, H.E. Haber, Nucl. Phys. B272 (1986) 1; Erratum-ibid.B402 (1993) 567;
J.F. Gunion, H.E. Haber, G.L. Kane, S. Dawson, “The Higgs Hunter’s Guide” (Addison-Wesley, 1990)
- [4] H. Kühnelt, C.B. Lang, G. Vones, “SU(2) gauge-Higgs theory with radial degree of freedom”, Nucl. Phys. B230 [FS10] (1984) 16.
- [5] E. Fradkin, S. Shenker, “Phase diagrams of lattice gauge theories with Higgs fields”, Phys. Rev. D19 (1979) 3682.
K. Osterwalder, E. Seiler, “Gauge field theories on a lattice ”, Ann. Phys. 110 (1978) 440.
- [6] M. Bock, M.N. Chernodub, E.-M. Ilgenfritz, A. Schiller, “An Abelian two-Higgs model of strongly correlated electrons: phase structure, strengthening of phase

- transition and QCD at finite density”, Phys. Rev. B76 (2007) 184502;
- M.N. Chernodub, E.-M. Ilgenfritz, A. Schiller, “Phase structure of an Abelian two-Higgs model and high temperature superconductors”, Phys. Rev. B73 (2006) 100506;
- T.Ono, I.Ichinose, T.Matsui, “Phase Structure and Critical Behavior of Multi-Higgs U(1) Lattice Gauge Theory in Three Dimensions”, Proc. Sci. LATTICE2008 (2008) 252.
- [7] L.H. Ryder, *Quantum Field Theory*, (Cambridge University Press, Cambridge, 1985).
- [8] M.E. Peskin, D.V. Schroeder, *An Introduction to Quantum Field Theory* (Westview Press, 1995)
- [9] M. Creutz, *Quarks, gluons and lattices*, (Cambridge University Press, Cambridge, 1983).
- [10] H.J. Rothe, *Lattice Gauge Theories (Third Edition) An Introduction*, (World Scientific Publishing Co. Pte. Ltd., Singapore, 2005)
- [11] K.G. Wilson, “Confinement of quarks”, Phys. Rev. D10 (1974) 2445.
- [12] I. Montvay, G. Münster, *Quantum Fields on a Lattice*, (Cambridge University Press, Cambridge, 1994)
- [13] N. Metropolis, A.W. Rosenbluth, M.N. Rosenbluth, A.H. Teller, E. Teller, “Equation of State Calculations by Fast Computing Machines”, J. Chem. Phys. 21 (1953) 1087.
- [14] M. Creutz, “Monte Carlo study of quantized SU(2) gauge theory”, Phys. Rev. D21 (1980) 2308.
- [15] A.D. Kennedy, B.J. Pendleton, “Improved heatbath method for Monte Carlo calculations in lattice gauge theories”, Phys. Lett. 156B (1985) 393.

- [16] M.W. Grunewald, “Combined Electroweak Analysis”, J. Phys. Conf. Ser. 110 (2008) 042008.
- [17] C. Amsler, et. al. (Particle Data Group), “Review of Particle Physics”, Phys. Lett. B667 (2008) 1.
- [18] S. Elitzur, “Impossibility of spontaneously breaking local symmetries”, Phys. Rev. D12 (1975) 3978.
- [19] C.B. Lang, C. Rebbi, M. Virasoro, “The phase structure of a non-Abelian gauge Higgs field system”, Phys. Lett. B104 (1981) 294.
- [20] J. Jersák, C.B. Lang, T. Neuhaus, G. Vones, “Properties of phase transitions of the lattice SU(2) Higgs model”, Phys. Rev. D32 (1985) 2761.
- [21] Z. Fodor, K. Jansen, “Overrelaxation algorithm for coupled Gauge-Higgs systems”, Physics Letter B331 (1994) 119.
- [22] M. Creutz, “Overrelaxation and Monte Carlo simulation”, Physical Review D36 (1987) 515.
- [23] Z. Fodor, J. Hein, K. Jansen, A. Jaster, I. Montvay, “Simulating the electroweak phase transition in the SU(2) Higgs model”, Nucl. Phys. B439 (1995) 147.
- [24] B. Bunk, “Monte-Carlo methods and results for the electro-weak phase transition”, Nucl. Phys. B (Proc. Suppl.) 42 (1995) 566.
- [25] K. Kajantie, M. Laine, K. Rummukainen, M. Shaposhnikov, “The electroweak phase transition: a non-perturbative analysis”, Nucl. Phys. B466 (1996) 189.
- [26] W. Langguth, I. Montvay, “Two-state signal at the confinement-Higgs phase transition in the standard SU(2) Higgs model”, Phys. Lett. 165B (1985) 135,
- [27] W. Langguth, I. Montvay, P. Weisz, “Monte Carlo study of the standard SU(2) Higgs model”, Nucl. Phys. B277 (1986) 11.

- [28] W. Bock, H.G. Evertz, J. Jersák, D.P. Landau, T. Neuhaus, J.L. Xu, “Search for critical points in the SU(2) Higgs model”, Phys. Rev. D41 (1990) 2573.
- [29] M. Tomiya, T. Hattori, “A finite size scaling test of an SU(2) gauge-spin system”, Phys. Lett. 140B (1984) 370.
- [30] I. Campos, “On the SU(2)-Higgs phase transition”, Nucl. Phys. B514 (1998) 336.
- [31] C. Bonati, G. Cossu, A. D’Alessandro, M. D’Elia, A. Di Giacomo, “On the phase diagram of the Higgs SU(2) model”, arXiv:0901.4429 [hep-lat].
- [32] M. Wurtz, R. Lewis, T.G. Steele, “Effect of multiple Higgs fields on the phase structure of the SU(2)-Higgs model”, Phys. Rev. D79 (2009) 074501.

APPENDIX A

CONVENTIONS

Fundamental constants: speed of light, and Planck's constant

$$c = \hbar = 1. \tag{A.1}$$

Minkowski space-time metric:

$$g_{\mu\nu} = \begin{pmatrix} 1 & 0 & 0 & 0 \\ 0 & -1 & 0 & 0 \\ 0 & 0 & -1 & 0 \\ 0 & 0 & 0 & -1 \end{pmatrix}. \tag{A.2}$$

Euclidean space-time metric:

$$g_{E\mu\nu} = \begin{pmatrix} 1 & 0 & 0 & 0 \\ 0 & 1 & 0 & 0 \\ 0 & 0 & 1 & 0 \\ 0 & 0 & 0 & 1 \end{pmatrix}. \tag{A.3}$$

Four-vector notation for space-time and momentum-energy, respectively,

$$x^\mu = (x^0 \ x^1 \ x^2 \ x^3) = (t \ \vec{x}), \tag{A.4}$$

$$p^\mu = (p^0 \ p^1 \ p^2 \ p^3) = (E \ \vec{p}). \tag{A.5}$$

Summation convention for repeated space-time and group indices, respectively,

$$A^\mu D_\mu = A_\mu D^\mu = g_{\mu\nu} A^\mu D^\nu = \sum_{\mu=0}^3 \sum_{\nu=0}^3 g_{\mu\nu} A^\mu D^\nu, \tag{A.6}$$

$$A^2 = (A^\mu)^2 = A^\mu A_\mu, \tag{A.7}$$

$$\lambda^\alpha \sigma^\alpha = \sum_\alpha \lambda^\alpha \sigma^\alpha. \tag{A.8}$$